11-19-2015

A Multiscale Systems Model for Advancement of a New Line of Therapy for Osteoporosis

Rena J. Eudy
Univeristy of Connecticut, renae@metrumrg.com

A Multiscale Systems Model for Advancement of a New Line of Therapy for Osteoporosis

Rena Eudy, Ph.D.

University of Connecticut, 2015

Abstract

The osteocyte is a load-sensing bone cell, which plays a pivotal role in the bone modeling process. This process is highly regulated by feedback control and poorly described by isolated *in vivo* or *in vitro* experiments. *In silico* systems models present a way by which experimental and clinical data can be integrated in a mathematical framework so that physiology, pharmacology and disease progression as it relates to bone health, at the level of cell signaling networks up to the tissue level, can can be better understood. The Multiscale Systems Pharmacology Model presented here began as an endeavor to link biological markers and clinical endpoints in a mathematical framework. The goal is to be able to make quantitative inferences around bone physiology, disease progression, and therapeutic modulation of biological targets. This underlying framework has now been extended to include the osteocyte as a source of sclerostin protein, signaling effects of this protein on the Wnt pathway and downstream effects on osteoblasts and osteoclasts. A model of sclerostin inhibition by monoclonal antibodies (mAbs) was developed using data from recent clinical trials, describing the unique mechanism of Wnt pathway modulation for a new treatment for osteoporosis. Techniques for parameter identifiability and optimization were compared and contrasted. Parameters describing mAbs exhibiting target-mediated drug disposition (TMDD) pose identifiability problems, and techniques for establishing identifiability of TMDDs were analyzed. A predictive framework for regional changes in bone mineral density (BMD) was further developed for sclerostin mAbs, and marketed therapies teriparatide and denosumab. Finally, a hazard model of fracture was implemented using lumbar spine BMD, patient baseline char-

acteristics and an additional drug effects as covariates in order to compare efficacy of therapies, their dosing regimens and possible combinations that would elicit the best outcome for patients with osteoporosis. This novel framework is a powerful predictive tool for furthering knowledge of new therapeutic mechanisms in the context of a data-driven, integrated physiological platform.

A Multiscale Systems Model for Advancement of a New Line of Therapy for Osteoporosis

Rena J. Eudy

B.S., University of Virginia, 2007

M.A., Brown University, 2012

A Dissertation

Submitted in Partial Fulfillment of the

Requirements for the Degree of

Doctor of Philosophy

at the

University of Connecticut

2015

APPROVAL PAGE

Doctor of Philosophy Dissertation

A Multiscale Systems Model for Advancement of a New Line of Therapy for Osteoporosis

Presented by

Rena J. Eudy, B.S., M.A.

Major Advisor _____
Marc R. Gastonguay

Associate Advisor _____
Matthew M. Riggs

Associate Advisor _____
Yong-Jun Shin

Associate Advisor _____
Joseph A. Lorenzo

Associate Advisor _____
Kevin S. Brown

University of Connecticut
2015

Dedication, Acknowledgements and Preface

Dedication

To my late husband Joshua Eudy, whose vision and perspective enabled me to endure when I wanted to quit. Whose support came at a costly time but whose knowledge that nothing ever worth doing comes easily was a sustaining force. Your love of what is good and right has changed my perspective and as a result, I have come to better know God as One who is longsuffering and patient. I hope I can be more and more like this everyday. Thank you for being a constant encouragement to me at a crucial time and loving me when I doubted. I miss you.

Ackowledgements

The work presented in this thesis was carried out through the *Department of Biomedical Engineering, University of Connecticut, Storrs, USA*. The University also provided some financial support for the project and for traveling to conferences.

Most of the financial support for my PhD studies and for travel to conferences came from *Metrum Institute, Tariffville, Connecticut, USA*.

I have been blessed to work with and have the support of many people, whom I wish to acknowledge now.

Advisors, **Dr. Marc Gastonguay** and **Dr. Matthew Riggs** for your commitment to take me on as a student and taking the time to guide, teach and train and being an advocate for us in the department, where Pharmacometrics doesn't exist (hopefully, someday)!

My Metrum Colleagues and fellow graduate students, **Dr. Kyle Baron**, **Dr. William Gillespie**, other modeling and statistics experts, **Alanna Ocampo-Pelland** and **Janelle Hajjar**. Kyle spent many hours troubleshooting and developing *mrgsolve* to make it more amenable for bone model applications. Bill did the preliminary hazard model work and had much to do with data structure and additional model development for the fracture model piece. Thanks for your patience, both of you. Alanna and Janelle have been a great support in learning in PK/PD concepts and just in life. You?ve made the PhD process way more fun, ladies. Thank you.

My parents, **Dr. Thomas Burbey** and **Dr. Ingrid Burbey** for your prayers and words of support and stepping up and filling in when you were needed. You are my lifeguards.

My other parents, **Steve** and **Gita Eudy**, because your prayers and words of wisdom mean more to me than you know.

My siblings **Ariel** and **James Scheiner**, **Ryan Burbey**, and **Liz Eudy** for your faithfulness, inspiration and funny text messages and emails that made me smile right when I needed it. It has been my privilege, pleasure and joy to walk alongside all four of you in this life.

My best friends for life **Jessica Si-** , I mean, **Berry**! And **Jennifer Ballou**, your prayers and words of support are invaluable. You have stood beside me, literally, through some of the best and worst of times of my life. You are constant and faithful friends. Thank you doesn't say enough.

And my friends **Stephen Byrne** and **Natalie McMahon**. You came into my life at just the right times to listen to and encourage me. You are a God-send! Thank you for your loyalty and commitment when you didn't even know what you were getting yourself into! ;)

There are many **other friends and family members** that are too many to mention that have sewed into me over these PhD years. I am richly blessed by all of you.

Preface

"The average Ph.D. thesis is nothing but the transference of bones from one graveyard to another."
- Frank J. Dobie.

I like this quote because not only does my PhD dissertation happen to be about bones, but also when thinking about what the author meant by this statement, a lot of ideas come to mind. Some are deeply personal. Some are theological. And yet this quote has a melancholy and sarcastic tone that makes one think that her entire body of work that she's slaved over for years is just another part of the endless life cycle and that there's really 'nothing new under the sun.'

I never would've imagined how personal the graveyard would become to me during the time I was working on my PhD. A year into my schooling, I lost my husband of 2 and half years to the disease of colon cancer, suddenly and unexpectedly. The graveyard was no longer a place where someone who has fulfilled their days lies to rest and where the rest of us remember him as our grandfather or uncle who might have served in a world war or immigrated from Europe so that we could live in a great land. No, it is the thing that stole him I loved the most in the world, far before his time.

Still the phrase 'transference of bones' speaks to me about legacy and to the one still living, the concept of legacy evokes hope and vitality. Joseph, in the bible, was attributed great faith because he gave instructions to his children before he died about the transference of his bones from Egypt to the promised land of Israel. You see, Joseph had a legacy of being a dreamer and through many trials he maintained that God would bring his dreams to pass. Joseph wanted his descendants to see the place where his bones lay and remember that God is the one who brings dreams to pass.

There was a time when receiving a PhD was only a dream- one very far off. I hope that instead of "the average PhD thesis [that] is nothing but" this thesis summarizes an idea of substance and forward-thinking. It encompasses what I have learned during times of success and times of defeat. What I ultimately surmise from this quote is that PhD work is about putting some theories to death (even those you have grown attached to). But it is also about raising other theories and concepts to life (that is, if the data support them!). Both lead to advances for a 'next generation' of dreamers and thesis-writers to use and build upon.

Contents

List of Tables

List of Figures

Acronyms

aBMD areal bone mineral density.

ADC antibody-drug conjugate.

APC-1 adenomatous polyposis coli -1.

BMD bone mineral density.

BMP bone morphogenentic protein.

BSAP bone-specific alkaline phosphatatse.

CTx C-telopeptide.

CV% percent coefficient of variation.

DAISY differential algebra identifiability of systems.

dkk-1 dickkopf.

EAR exact arithmetic rank.

FN femoral neck.

GSK3b glycogen synthase kinase 3 beta.

iv intravenous.

KO knockout.

LRP low-density lipoprotein receptor-related protein.

LS lumbar spine.

mAb monoclonal antibody.

mg milligrams.

MM Michaelis-Menten.

MSPM multi-scale systems pharmacology model.

OB osteoblasts.

OC osteoclasts.

OCY osteocytes.

OPG osteoprotegerin.

P1NP N-terminal propeptide of type 1 collagen.

PD pharmacodynamic.

PK pharmacokinetic.

PL profile likelihood.

pM picomolar.

PTH parathyroid hormone.

QE quasi-equilibrium.

QSP Quantitative Systems Pharmacology.

QSS quasi-steady state.

RANK receptor activator of nuclear factor kappa-B.

RANKL receptor activator of nuclear factor kappa-B ligand.

ROB responding osteoblasts (osteoblast precursor pool).

sFPR1 secreted frizzled-related protein-1.

TGF-b transforming growth factor beta.

TH total hip.

TMDD target mediated drug disposition.

TRACP 5b tartrate-resistant acid phosphatase.

vBMD volumetric bone mineral density.

WIF Wnt inhibitory factor 1.

Chapter 1

Introduction

1.1 Clinical Relevance

Today, an unprecedented number of the general population is living longer and the demand for the health care industry to support a good quality of life is increased proportionally. Because of this longevity, osteoporosis is a large and growing problem because more and more people worldwide are faced with risks of bone fracture. An estimated 34 million Americans have low bone mass, which indicates they are at a high risk for developing osteoporosis [1]. The estimated cost of the disease in the US ranges from $10 to $22 billion in addition to indirect cost associated with reductions of quality of life and productivity.

The gold standard for treatment of osteoporosis is alendronate, part of a class of therapies called bisphosphonates. While effective in significantly increasing bone mineral density (BMD) through an anti-resorptive mechanism, bisphosphonates are not without controversy. Recent studies have shown an increase risk of abnormal fracture in patients on bisphosphonate therapy [2, 3], which has lead to discourse on length of maintenance of these therapies. Because osteoporosis is a chronic metabolic disease this presents quite a problem.

Newer lines of therapy include teriparatide, a parathyroid hormone (PTH) analog with an anabolic mechanism. In contrast to bisphosphonates, anabolic agents increase bone growth by stimulating osteoblast activity, rather than limiting resorption by decreasing osteoclast activity. Unfortunately, teriparatide is limited in its use because it requires a once-per-day subcutaneous injection [4], and func-

tions by replacing areas of older, mineralized bone with new bone of lower mineral content [5]. There remains an unmet clinical need for new therapies for osteoporosis which will improve patient compliance, are more effective in preventing loss of bone density, and will improve fracture rate after several years of active therapy [6].

1.1.1 *Sclerostin in Targeted Bone Remodeling*

Sclerosteosis and Van Buechem are both rare bone diseases that were discovered over 40 years ago [7], characterized by thickening of the skull, facial and jaw bone enlargement and overall increased BMD above age-matched non-affected individuals [8]. While these diseases were identified long ago, it was recently discovered that they were caused by autosomal-recessive loss of function and hypomorphic mutations, respectively, on the SOST gene. The complete loss of SOST expression causes nerve entrapment as a result of bone deformities, and some patients report hearing and vision loss and/or intracranial pressure [9]. Heterozygote carriers of SOST, however, have low circulating sclerostin levels, do not have these symptoms, but do have higher-than-normal bone mass. This finding led to the line of thinking about the potential benefits of dose-dependent sclerostin inhibition for individuals suffering with osteoporosis or other diseases contributing to bone loss. Wnt is implicated in many differentiation pathways in the body, but sclerostin is mainly produced by the osteocyte, so the modulation of sclerostin on Wnt is, for the most part, targeting Wnt signaling in the bone limiting the off-target for non-bone cells. Furthermore, because of it's role in differentiation, Wnt modulation is associated with tumor formation [10], but because osteocytes do not divide, the potential for uncontrolled cell growth leading to tumor formation associated with modified Wnt signaling may be assuaged [11]. The absence of osteosarcoma in patients with van Beuchem disease and sclerosteosis [12, 13] further supports this notion, however oncogenic effects of long term of pharmacological modulation of sclerostin are unknown.

Sclerostin functions by binding to the coreceptor, low-density lipoprotein receptor-related protein (LRP)5/6, competitively inhibiting the binding of Wnt ligands. By preventing Wnt signaling, sclerostin inhibits actions of the canonical Wnt pathway, which includes the formation of the "destruction

complex": Axin, adenomatous polyposis coli -1 (APC-1), and glycogen synthase kinase 3 beta (GSK3b) which phosphorylates β-catenin labeling for ubiquination and destruction [14, 15]. The canonical Wnt pathway is involved in various developmental processes, including osteogenic differentiation of mesenchymal stem cells (MSC). Specifically, β-catenin suppresses MSC differentiation into adipogenic and chondrogenic lineages and promotes an osteoblastic lineage [16]. Sclerostin completes the negative feedback loop at the end of a remodeling event, inhibiting further bone formation. It does this by inhibiting accumulation of β-catenin by acting as a competitive inhibitor of Wnt.

Sclerostin expression is regulated in part by hormones which affect bone metabolism, such as PTH, calcitonin, and glucocorticoids [17]. Patients with primary hyperparathyroidism have significantly lower circulating sclerostin levels and this is consistant with *in vitro* studies demonstrating that PTH inhibits SOST expression [9]. Serum estrogen is inversely associated with serum sclerostin [18], thus estrogens inhibit sclerostin production [19] and estrogen replacement therapy inhibits increases in circulating sclerostin. Conversely, glucocorticoids increase sclerostin expression *in vivo*, and calcitonin up-regulates osteocyte-derived sclerostin expression.

In studies of SOST knockout (KO) animals, increased BMD is seen in trabecular and cortical bone at the peri- and endosteal surfaces [20]. Osteocalcin, a marker of osteoblast growth, is increased in KO mice while the marker of osteoclast growth, tartrate-resistant acid phosphatase (TRACP 5b), was unchanged. This seems to indicate an uncoupling of bone formation and resorption that is atypical of bone growth pathways and osteoporosis-targeting therapies. This KO model has a similar phenotype to that elicited by LRP5 receptor mutations, which also resulted in a increase in osteoblasts without an increase in osteoclast population [21], further supporting the decoupling phenomenon associated with this mechanism.

Consistent with SOST KO models, monoclonal antibodies inhibiting sclerostin administered *in vivo* resulted in increases in BMD of cortical and trabecular bone and vertebral and femoral bone strength [22, 23]. In one study, serum osteocalcin at the trabecular and periosteal surfaces was increased with increasing doses of the inhibitor. Another study showed bone formation markers serum osteocalcin and N-terminal propeptide of type 1 collagen (P1NP) were significantly elevated for the duration of 12-week-long treatment, while the bone resorption marker TRACP 5b remained unchanged

[23].

In healthy post-menopausal (PM) women, a single dose of the sclerostin inhibitor romozozumab

Table 1.1: Sclerostin Inhibitors Currently in Clinical Development

Company	Therapy	Development Stage
Amgen & UCB	monoclonal antibody	Phase 3 clinical trial
Eli Lilly	monoclonal antibody	Phase 2 clinical trial
Novartis	monoclonal antibody	Phase 2 clinical trial
OsteoGeneX	small molecule	Preclinical
Ossify, Inc. (spinoff of OsteoGenex)	Bone graft	Unknown

resulted in dose-dependent increases in lumbar spine and total hip BMD. The largest increases were 5.3% and 2.8%, respectively, above the baseline value in the 10 mg/kg dose cohort after 12 weeks [24]. Consistent with *in vivo* studies, P1NP and osteocalcin increased over 1.5-fold over their baseline values, while serum C-telopeptide (CTx), the bone resorption marker, decreased. In a comparison study of post-menopausal women with low BMD, 210 mg of this mAb dosed once monthly increased BMD at the lumbar spine by 11.3% [25]. Two phase-2 studies were also conducted in wherein blosozumab was dosed in post-menopausal women every 2 weeks or every 4 weeks for a total of 16 weeks [26]. In this study, consistent with the anabolic mechanism, P1NP and osteocalcin were dose-dependently increased, while serum CTx decreased. At the highest dose of 270mg, BMD increased 17.7% at the spine and 6.2% at the total hip. These first in human studies seem to support a mechanism resulting in improved performance compared to existing bone therapies, as increasing formation and sustained or decreased resorption results in a larger anabolic window. The result is a much faster increase in BMD compared to the gold standard therapy for osteoporosis, alendronate. It also surpasses effects seen with teriparatide, the only other anabolic therapy on the market. Table 1.1 lists the sclerostin inhibitors currently being developed by various pharmaceutical companies and table 1.2 describes the development status of leading compounds, romozosumab and blosozumab.

Questions remain about the sustained anabolic effect of this target mechanism, as changes in bone formation markers did not persist and returned to baseline in patients still on active therapy, and

studies longer than a year in duration are not yet reported. The optimal treatment duration for the greatest efficacy with these therapies is unknown. While there were no significant adverse events reported in these relatively short studies, and off-target effects are limited with this mechanism, there is still some concern about cardiovascular safety with longer-term treatment, particularly because Wnt signaling is known to be involved in vascular pathophysiology [27]. These "unknowns" associated with this mechanism of action are opportunities for model development and exploration. Duration of treatment and washout, intermittent treatment, switching between therapies and possible therapeutic combinations are all areas that can be exploration within a modeling platform.

In order to develop a good understanding of what impacts expression of SOST and functions of

Table 1.2: Ongoing Clinical Trials with Romosozumab

Therapy	Trial	Duration	Endpoints	Estimated Completion
Romozosumab and Teriparatide	Phase 3 (STRUCTURE)	12 months	Changes in BMD by DXA and QCT and strength by FEA at total hip	June 2015
Romosozumab 12 mo. followed by denosumab for 24 months	Phase 3 (FRAME)	24 months	Primary: Vertebral fracture incidence Secondary: BMD changes	February 2017
Romosozumab vs Placebo in men with osteoporosis	Phase 3 (BRIDGE)	12 months	Changes in BMD by DXA at LS, FN, and TH	December 2016

the sclerostin protein, it is essential to grasp the function of the cell the produces it. Recently the osteocyte has received more attention from experimental researchers in the area of bone, because it is the longest living bone cell and therefore constitutes more than 90% of all bone cells [28]. The ability of the osteocyte to propagate mechanical signals of loading into chemical signals, make it an important part of the remodeling and repair [29] mechanism. Osteocytes are terminally differentiated osteoblasts, and function to synthesize mineralized matrix and remain trapped therein. They communicate through an system of canaliculi which extend through the matrix and are proximal to circulatory systems, and thus may function as an endocrine organ, directly releasing proteins into the circulation [30].

Through the production of sclerostin, osteocytes control bone formation by two mechanisms: 1.) directly by antagonizing bone morphogenentic protein (BMP) and 2.) indirectly through prevention of Wnt signaling [31], by binding to LRP5 and LRP6. While it is not fully understood cellular signaling involved in resorption activities, the apoptosis of osteocytes is a cue which signals osteoclast recruitment

and increased bone resorption [30]. This is consistent with anti-remodeling properties of estrogens and bisphosphonates, which prevent osteocyte apoptosis. Furthermore, it is known that osteocytes are a major source of receptor activator of nuclear factor kappa-B ligand (RANKL), which also increases resorption activity [32]. Wnt pathway activation in osteocytes has been shown to increase expression levels of osteoprotegerin (OPG) [33]. Taken together, it is clear that osteocyte regulation of cytokines involved in feedback signaling is integral to regulation of remodeling, and therefore understanding how these signals are impacted by therapeutic modulation is imperative.

1.2 Systems Models in the Development of New Therapies

The bone remodeling process is a difficult system to describe at a cellular or molecular level because the cell populations and turnover markers involved are constantly in flux and regulated through multiple control mechanisms. An *in silico* model-based approach is an efficient way to promote understanding of this highly dynamic behavior. Scientists, academic researchers, regulatory and industry representatives desire to understand how new therapies impact biological systems, in order to maximize efficacy and minimize adverse events in patients.

Quantitative Systems Pharmacology (QSP) is somewhat new, or at least newly defined, discipline using physiological modeling to understand how drugs function to affect the system and influence pathophysiology and disease progression. This discipline has targeted the need to make the transition for drugs from discovery to market more efficient and widen the bottleneck caused by late-stage failure in drug development. The goal of this discipline is to use mathematical models to define the input-output relationship between disease and drug activity. Three steps are used in this process: 1.) gather knowledge from literature or preliminary experiments 2.) construct the model, 3.) simulate the outcomes [34]. Not only can this method be used to promote understanding of the underlying biology and improve pathway targeting, it can also be used to impact clinical design via dose and patient selection.

Benefits of applications of QSP to the development of new therapies for osteoporosis are numerous. Mechanistic models promote understanding of how short-term clinical endpoints, like regional

changes in BMD, impact fracture outcomes. Dosing regimens and combination therapies can be investigated in these models to mitigate risks of failure during the long-term clinical trials required for demonstration of efficacy of new therapies on fracture incidence. Recently, a QSP model of bone was used in a clinical pharmacology assessment reviewed by the FDA and influenced a decision to recommend a post-marketing study to test additional dosing regimens in order to avoid hypercalcuria [35]. Investigation of factors (covariates) on relevant outcomes such as turnover markers, BMD changes, and fracture also point to the physiological pathways that have greater impact on these outcomes and may reveal new therapeutic targets.

1.3 Other *in Silico* Models of Bone Physiology and Related Pathways

Pivonka and Komarova [36] issued a thorough review of *in silico* models of bone in 2010, and categorized them into four groups according to the physiological aspects that were the primary focus of each model: 1.) Receptor-ligand interactions and intracellular signaling 2.) Cell dynamics 3.) Tissue-function and 4.) Whole-body calcium homeostasis. Models that fall into these categories are discussed here to highlight the strengths and weaknesses of different modeling approaches, as specifically applied to models of osteocyte function or Wnt signaling.

1.3.1 *Receptor-Ligand Interactions and Intracellular Signaling*

In an attempt to more fully elucidate the roles of different Wnt signal inhibitors Kogan et al. [37] built upon the work of Lee and Mirams [15,38]. This model describes ligand binding (secreted frizzled-related protein-1 (sFPR1) and Wnt inhibitory factor 1 (WIF) binding to Wnt, and dickkopf (dkk-1) binding to LRP, a Wnt co-receptor) and events leading to β-catenin accumulation. This model was validated by two independent published experiments, and provides quantitative measures for the predicted synergistic effects of sFPR1 and dkk-1 on β-catenin accumulation. The aim of this model development project was to suggest potential targets for treatment of cancer, which also involves the Wnt pathway, therefore examining sclerostin-specific targets, like LRP5/6 or other implications of β-

catenin accumulation on bone metabolism was unfortunately not in the scope of this work. The authors also acknowledge that many underlying mechanisms of Wnt pathway have not been elucidated by experimentation; still this work illustrates how mathematical models can generate new hypotheses and be used in generation of new targets, related to Wnt pathway modulation.

1.3.2 *Cell Dynamics*

A cell dynamics model created by Graham and colleagues, defines interactions between discrete bone cell populations and predicts qualitative effects of sclerostin inhibition on bone mass [39]. Descriptive parameters in the model represent effectiveness of paracrine, autocrine and other regulative signaling of bone cells, and the authors used the model to demonstrate how changing expression levels of key proteins, like RANKL, may impact the bone remodeling cycle. A simulation of relative changes in BMD after an increase in osteocyte apoptosis and corresponding inhibition of sclerostin inhibition was demonstrated. Some generalized relationships are defined and sensitivity of parameters due to system perturbation are demonstrated by this model. However, without using experimental data to fit model parameters, it is difficult to make meaningful inferences about parameter estimates and related cellular mechanisms, or to quantify effects of modulation of sclerostin in this qualitative framework.

A semi-empirical cell dynamics model developed by Carew [40] describes the effects of a strain stimuli on bone turnover. The novel aspect of this model is the inclusion of the effect of a physical stimulus on osteocyte response and the modified bone mass and calcium flux that results. The model suggests relative lengths of formation vs. resorption phases under different strain stimuli and possible mechanisms for loss of bone during “strain-free" conditions. One shortcoming of this model is that the structure is mathematically uncoupled; that is, the amount of resorption is fixed for all simulations while formation rate is estimated. In reality, increased strain inhibits osteoclastogenesis and this response is coupled to an increase in osteoblast activity resulting in increased turnover. Also, while there are parameters in the model for key protein binding kinetics, such as receptor activator of nuclear factor kappa-B (RANK), RANKL, OPG and PTH, there is no representation of sclerostin or other proteins and factors important to the osteocyte contribution to the remodeling process. Finally, the model sim-

ulations are unidirectional and do not describe cellular concentrations returning to equilibrium after a remodeling event. Each of these shortcomings were addressed by the authors. Although the model is still semi-empirical, the rate functions were derived from known relationships and the model simulated absolute concentrations consistent with the underlying biology of strain effects on turnover rate.

1.3.3 *Tissue-function*

Another application of systems models of bone addresses the coupled biochemical and biomechanical processes that govern bone remodeling. This is a very important aspect, as bone quality as the combination of geometry, material properties and microstructure [36], is ultimately what influences fracture risk in osteoporosis patients and disease severity. Van Oers et al. (2007) [41] constructed a model examining the mechanosensory role of osteocytes and their influence on osteon size changes during mechanical load. The model describes the relationship between strain magnitude and osteocyte signaling to osteoblasts and -clasts. Signals indicate specific spatial resorbtion and formation of bone. Their model re-enforces the inverse relationship between osteon diameter and strain magnitude, where osteoclasts ultimately determine the size of the osteon and osteoblasts govern the rate and extent of filling of the osteon volume. This model is speculative and qualitative in nature, describing volume/strain components of the biochemical-mechanical relationship of bone remodeling and does not provide any link to specific binding interactions or cellular feedback between osteoclasts and osteoblasts.

Colloca, et al (2014) [42] also constructed a similar model relating the mechanical sensing function of the osteocyte to osteoblast and osteoclast activity in a 3-D finite element model describing longitudinal and transverse stiffness in trabecular bone. The model predictions were compared to stiffness tensors of healthy tissues spanning different ages and states of use. The model predictions were consistent with experimental data. A limitation to this model is that the authors greatly simplified the representation of bone matrix in structure and shape in order to find an analytical solution to the model. There was also no signaling between osteocytes and osteoclasts included in the model, nor any other kind of biochemical messenger pathways or feedback signaling. Finally this model assumed constant lacunar

porosity per volume element of bone matrix in the finite element analysis, when in reality, porosity per volume is dependent on the extent of load-bearing activity specific to a region.

Buenzli (2015) [43] also created a mathematical model describing the embedding process of osteoblasts becoming osteocytes. The model estimates burial rate of osteoblasts based on experimentally derived osteocyte densities and matrix secretory rates are scaled up from *in vivo* data. The model shows that, rather than the density of osteocytes being determined by osteoblast density, there is instead a greater dependency on burial rate of osteoblasts and secretory rate of bone matrix. The model suggests that a large signal derived from multiple osteocytes, likely nonlocal to the embedding site, is required for a negative correlation between burial rate and number of osteocytes in the zone of influence. While several of the model parameters were estimated based on experimental data, the model in its entirety is empirical in nature, while assumptions of the bone mulitcellular unit (BMU) geometry were made and while mechanisms of osteocyte formation remain poorly understood.

1.3.4 *Whole-body Calcium Homeostasis*

Hydroxyapatite of bone serves as a depo for calcium which is released into the blood stream through resorption signals under the control of PTH, calcitonin, sex steroids and thyroid hormones [44]. Kidneys and the intestine also regulate calcium for whole-body processes. Disregulation of whole-body calcium homeostasis is implicated in diseases, such as hyper or hypo-parathyroidism, chronic kidney disease, or other physiological states such as pregnancy or lactation. Therefore, mathematical modeling of calcium homeostasis promotes understanding of how multiple levels of regulation of calcium are affected by disease or physiological state.

Kaiser, et al. (2011) [45] extended a model of interstitial fluid flow through the canaliculus to include movement of calcium to and from the bone tissue and examine how the movement of calcium may affect sheer stress at the osteocyte membrane. This model takes into account fluid flow being governed by electro-osmotic, osmotic and hydraulic effects. The model indicated that for most of the canalicular fluid, the hydraulic gradient governs the flow velocity, but at the boundary layers near a canalicular wall or osteocyte membrane, electro-osmotic and osmotic effects are significant. Shear

stress experienced by the osteocyte is actually affected by a range of chemical gradients relevant to those maintaining calcium homeostasis. These findings provide further explanation for the osteocyte function in sensing mechanical change and translating these to chemical signals. This model assumes simplifications of canalicular geometry and the authors acknowledge lack of understanding of the complex *in vivo* environment of osteocytes, as these model parameter estimates were analytically derived and were not based on experimental data.

In a research area where model applications and scopes vary widely, it is important to identify model qualifications in advance of model selection. Many of these qualities are outlined in Agoram et al. (2014), are used to validate the model discussed in chapter 8. These include:

1. Fit-for-purpose: In the presentation of the model do the authors clearly state model objects and does the model contain all the elements needed to investigate the relevant questions? In efforts to make a model well-representative of the physiology, are there also considerations of model parsimony?

2. Quantitative in nature: Does the model accurately predict directional changes in state variables, as well as magnitude of system dynamics with some level of precision, relative to experimental data?

3. Validation by accepted methods: Were the criteria for choosing the best model established by the authors, and was the model fully validated, preferably by an untested experimental dataset?

While there is a spectrum of mathematical models describing the mechanical role of osteocytes and effects of stress/ strain on chemical signaling [36, 41, 42, 45], these models do not link these signals to full signaling networks which include the RANK/RANKL/OPG axis, transforming growth factor beta (TGF-b) and other sources of feedback. The models lack quantitative descriptions of the system as a whole. Across the spectrum of physiological bone models, there is a missing link between the role of the osteocyte and Wnt pathway modulation required to predict clinical outcomes of new therapies implicated in this pathway. The lack of experimental data linking the Wnt pathway intermediates like β-catenin, axin, APC-1, and other intermediates involved in differentiation pathways, to the feedback

pathways involved in the regulation of bone remodeling, is likely the main reason for the lack of models describing osteocyte function. Much progress has been made in the recent years examining the contribution of the osteocyte to the mechanical and chemical signaling pathways that direct remodeling. The novel aspect of this QSP model is the integration of information gained from experimental data, (information contained in KO mice experiments, *in vitro* data generated from isolated osteocyte cultures) and clinical data to explore hypotheses and help elucidate osteocyte function in the context of therapeutic modulation of sclerostin. This quantitative modeling approach may help to link the biochemical processes to cellular activity to help more clearly define the role of the osteocyte in remodeling.

1.3.5 *The Basis of a Multiscale Systems Pharmacology Model Extension*

In addition to the Pivonoka review, Webster and Muller issued a thorough review of published physiological bone models in 2011 [46]. One of the featured cell populations models was development by Peterson and Riggs in 2010 [47]. The goal of this model was to provide a platform for evaluating longitudinal effects of therapies and disease states on whole body calcium homeostasis by building upon cellular dynamic models of Lemaire, et al. [48], a quantitative model of calcium handling by Raposo, et al. [49] and a model describing relative activities of PTH by Bellido, et al. [50]. While this multiscale model is comprehensive in descriptions of cell dynamics, signaling and calcium homeostasis, it was published at a time when not as much was known about osteocyte biology. In their evaluation of several bone models, Webster and Muller stated, "A major deficiency of the aforementioned mathematical models is that they exclude the role of the osteocyte and neglect the effect of mechanical stimuli on bone formation." The field is in agreement that a quantitative framework describing the osteocyte role in bone remodeling has immediate relevance to the development of these therapies. The addition of the osteocyte to the cell population-type models will be a more complete picture of physiological response to proteins involved in modeling that was previously lacking.

1.4 Project Aims

The goal of this work was to extend the Peterson and Riggs [47] model of whole body calcium homeostasis (henceforth named the multi-scale systems pharmacology model (MSPM)) to create a quantitative framework for simulation of clinical endpoints such as turnover markers, BMD and fracture rate after administration of sclerostin monoclonal antibodies. In doing so the aim is to address the criteria previously outlined for evaluation of the extended systems model.
The relevant questions are:

- Are TMDD models *a priori* identifiable, and if not, which approximations to the model can be used which are identifiable? If so, what are the conditions that lead to *a posteriori* identifiable?
- Does the model accurately describe changes in P1NP and CTx and regional changes in bone mineral density (BMD) seen after sclerostin monoclonal antibody (mAb) administration?
- What is the quantitative role of the osteocyte as it relates to feedback regulation during modeling and remodeling?
- Which dosing regimen with sclerostin inhibitors elicits the greatest increase in BMD in patients with osteoporosis?
- Which model involving changes in lumbar spine (LS) BMD best describes changes in fracture rate from an aggregate dataset?
- In a head-to-head comparison with teriparatide, does the model predict that sclerostin mAb treatment will result in greater increases in BMD and protection from fracture?

Specific aims desgined to answer these questions were:

1. Establish *a priori* identifiability of target mediated drug disposition (TMDD) models and model approximations; estimate pharmacokinetic (PK)/pharmacodynamic (PD) parameters describing sclerostin mAbs and circulating sclerostin using a TMDD model approximation.

- To provide discussion around structural vs. practical identifiability and how lack of identifiability can affect the interpretation of parameter values.
- To discuss methods for establishing model identifiability, namely compare and contrast differential algebra identifiability of systems (DAISY), exact arithmetic rank (EAR) algorithms and likelihood profiling as methods for establishing model identifiability.
- Create and validate a PK/PD model to describe sclerostin mAbs and circulating sclerostin, using data from published Phase1/Phase2 clinical trials with romosozumab and blosozumab.

2. Integrate the PK/PD model into the MSPM and create structural framework for osteocyte and compartments and regional BMD changes after sclerostin mAb administration.
   - Structure osteocyte and estimate parameters linking changes in sclerostin to cellular function.
   - Link osteocyte population to changes in osteoblasts/-clasts by defining effect parameters on the RANK/RANKL/OPG axis.
   - Define structure for total hip, femoral neck, and lumbar spine BMD and estimate parameters describing sclerostin mAbs effects on BMD.
   - Validate the model with an external dataset (reference [51]).
   - Estimate parameters for combination arm (denosumab + teriparatide) to use as a comparator. This also served as another layer of validation for the model.
3. Further develop a time-to-event (TTE) / hazard model of fracture to describe a complete metadata set; use this hazard model of fracture to compare therapies for osteoporosis and investigate parameter modulation effects in the context of sclerostin mAb administration.
   - To systematically construct a metadata set with clinical studies reporting fracture and longitudinal changes in lumbar spine BMD.
   - Develop a TTE / hazard model by testing candidate models with different BMD representations.

- Perform model simulations and sensitivity analyses to investigate drug effects on BMD and probability of fracture.

For this project, the term "multi-scale" refers both to time scales ranging from minutes (e.g. half-life of PTH) to years (BMD changes and fracture risk assessment), and size scales encompassing changes in protein concentrations, cell populations, organ (e.g. parathyroid gland, kidney, bone) functions to clinical measures and outcomes (e.g. BMD and fracture). As a part of future work, linking mechanical stimulation described as the stress/strain dynamics to sclerostin expression and activity (as in [52]), as well as characterizing the role of osteocyte in varying bone architecture would provide a more complete picture of the entire bone remodeling process.

Chapter 2

Methods

2.1 AIM I. Establishing Identifiability of Target-Mediated Drug Disposition Models and Their Approximations (PAPER I, Chapter 7)

Often, unlike small molecules, monoclonal antibodies (mAbs) exhibit non-linear pharmacokinetic behavior. This target mediated drug disposition (TMDD) is caused by high affinity binding of a drug to its target enzyme, receptor or transporter, relative to drug dose and limited number of targets within the drug distribution space [53]. Sclerostin mAbs exhibit this property of non-linearity during the elimination phase, which can be seen in the dose range used in a phase 1 study (fig. 2.1).

Therapeutics exhibiting TMDD can be difficult to model because often the drug's target concentration is not available, and the biological processes described by the full model occur on different time scales [54], making it difficult to identify all parameters in the system. Establishing the *a priori* identifiability of the TMDD model and TMDD model approximations is a novel contribution to the field of pharmacokinetics, in which TMDD models are frequently being used to analyze clinical population data. Identifiability analyses aid in interpretation of model parameters and indicate which parameters may be more or less informed by the experimental data. In the context of MSPM development, TMDD model approximations were also used to develop a PK/PD model linking sclerostin mAb concentration to serum sclerostin.

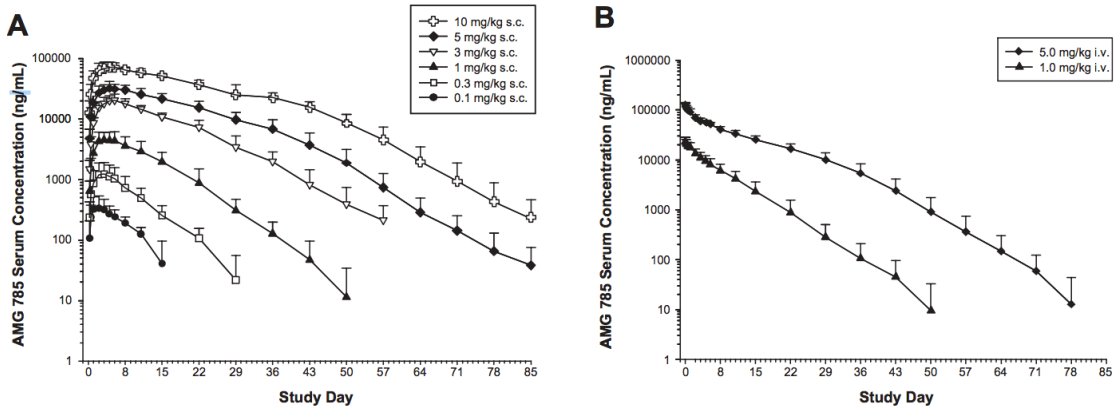

Fig. 1. Serum concentration-time profiles of AMG 785. Profiles shown are following a single subcutaneous (s.c.) dose (*A*) or intravenous (i.v.) dose (*B*) of AMG 785. Data are mean and SD.

Figure 2.1: Serum concentration-time profiles of romozosumab from a phase 1 study. Note the non-linear decline in exposure, typical of mAb elimination kinetics. Used with permission from [24]

Chapter 7 outlines identifiability analyses processes and summarizes results using the exact arithmetic rank (EAR) approach. The differential identifiability of systems (DAISY) approach was also implemented, but limitations to the algorithm prevented analysis of all input/output scenarios implicated in TMDD models, so the EAR approach was relied upon for the final manuscript. DAISY was developed by Saccomani and colleagues [55] and, unlike EAR, which can only establish local identifiability, DAISY can be used to establish global *a priori* identifiability of a system. This algorithm is run as a package within the REDUCE (v3.8) Algebra freeware [56]. It iteratively divides of the set of differential equations by ranked variable sets until a reduced set of minimum rank is reached. A test set of pseudorandom parameter values chosen by the algorithm is evaluated within the reduced system to determine if a unique solution exists.

The following was supplied in the input file:

- a vector, **B**, of inputs, outputs and state variables.
- a vector, **B1**, of unknown parameters. The parameters used in each test case are listed in table 1 (chapter 7).

- a set, **C**, of differential and output equations.
- a seed value, which determines the range of pseudorandom values used for each variable in the reduced system.
- a vector, **IC**, of initial conditions.

  Results are stored in a separate text file.

Initial conditions are not needed in DAISY if global identifiability can be determined without them. If the system is locally identifiable or nonidentifiable without initial conditions, the algorithm re-starts after the reduction step, with this information included. See appendix A for example input/output files for the case of a single-target TMDD when only free drug concentration is available as an input. Because DAISY can only deal directly with pure polynomial forms for the differential equations, the algorithm did not accept the quadratic solution form for free drug concentration, *C*, that is used in quasi-equilibrium (QE) and quasi-steady state (QSS) approximations of TMDD models. However it was used to establish global identifiability of single target, 2-target, and antibody-drug conjugate (ADC) TMDD models.

The profile likelihood (PL) approach, as discussed briefly in chapter 7, can also be used to investigate parameter identifiability of a system, but in a design-dependent way. Because it relies heavily on experimental design, PL alone is not useful to determine whether a system is structurally identifiable, but it can be used to assess impact of study design on *a posteriori* identifiability, once *a priori* identifiability has been determined. Compared with EAR and DAISY, this approach requires the most extensive set-up time and thus was used for comparative purposes, but not to test identifiability of every scenario. NONMEM (v7.3, Icon Development Solutions, Elicott City, MD, USA) was used to implement this approach as maximum likelihood estimation (MLE) is a commonly used algorithm for parameter estimation in this software and is the basis for likelihood profiling. The likelihood describes the probability of the data given the model and parameter values. The maximum likelihood is the highest joint probability of the provided data in a multivariate system. A marginal likelihood profile can be constructed for each parameter by fixing each parameter at a different value above and below the MLE, while reoptimizing all other parameter estimates.

To test for identifiability using this method for a single target TMDD, each variable was fixed at 10 different values within +/- 3 standard errors of the ML estimate. These values are plotted against the minimum objective function value (MOFV) generated in NONMEM, which is approximately proportional to -2log(Likelihood) for each fixed value of the parameter. A perfectly flat profile indicates a structurally non-identifiable parameter. Profiles that identify a unique minimum but exhibit a broad profile within the range of parameter values indicate parameters that are not well supported by the data generated from that experimental design.

Because the PL method requires posing a parameter estimation problem, a real-world example of a TMDD model of the endothelin-receptor antagonist bosentan was analyzed. In the model developed by Mager and Jusko [53], the free target was treated as a time-independent variable and *km* was used instead of *ksyn* and *kdeg* parameters. In order to analyze a full TMDD system, a simulated dataset was generated with parameter estimates and the sampling times from the bosentan study [57] (see appendix A for setup code and example control stream). An exponential inter-individual variance model was applied to *Vc* and *Km* (10% coefficient of variation [CV], each) and a proportional residual error model (15% CV) was also applied to simulate a more realistic study population. A full TMDD parameter set was then re-estimated from this simulated dataset of 16 subjects in each dosing arm. The intravenous (iv) doses simulated were 10, 50, 250, 500 and 950 milligrams (mg).

2.1.1 *PK/PD Model of Sclerostin mAbs (PAPER II)*

As previously described, the plasma concentration profiles of sclerostin mAb exhibit nonlinear clearance and with information about the binding protein (sclerostin) it would theoretically be possible to fit an approximation of a TMDD model. Unfortunately there are no published reports of sclerostin mAb concentration and resulting serum sclerostin levels for the same antibody at the same dose levels. Currently there are published mAb concentration levels in a phase 1 study after single doses of romozosumab and circulating sclerostin profiles from phase1/phase2 studies with single and multiple doses of blosozumab. As a result, the PK and PD models used to describe these profiles were fit sequentially, as described in chapter 8 and concentration profiles from romozosumab were fixed while

estimating the PD parameters, with the exception of *km*, which was re-estimated for blosozumab under the premise that the two antibodies have different binding affinities (see the chapter 8 appendix for additional assumptions).

2.2 AIM II. Implementing PK/PD Model in Bone Model and Determining Model Structure and Parameter Values to Describe Changes in Turnover Markers and BMD (PAPER II, Chapter 8)

The process of implementing osteocytes (OCY) into the MSPM is described in chapter 8. The osteoblast-related compartments were developed initially, followed by the osteoclast-related compartments. The compartments and parameters describing changes in BMD were implemented and estimated last. Other additions to the model included BMD compartments for combination therapy of teriparatide and denosumab, in order to be able to simulate effects seen in the DATA trial, in which the combination arm elicited significantly greater increases in LS BMD, FN BMD and TH BMD after 24 months of active therapy [58]. These additions were built using data from from 27 documented clinical trials with teriparatide [58–75] , denosumab (these are cited in chapter 8) and/or combination therapy.

Parameters were optimized using the R package *minqa* [76] and changes in BMD were simulated using R package *mrgsolve*. To avoid problems with parameter identifiability, only the rate constant for the BMD compartment and the power term on the OC within the BMD equation, were estimated for the combination. The other parameters were fixed to the values of the denosumab BMD compartments. The rationale for this is that the turnover marker profiles for the combination arm resembled those of denosumab, so the assumption is that the same mechanisms of action are at work in the combination arm. The final model was evaluated by sensitivity analysis (shown in appendix A, Figure A.1).

2.2.1 *Optimization Routines*

For a parsimonious model, it is ideal to be able to optimize parameters simultaneously to the endpoints of interest. Although this is not a requirement of a fit-for-purpose systems model, multivariate optimization is highly desired for parameters describing processes that are tightly regulated by feed-

back control, in which there is a high level of dependency between parameters for a given outcome. After the model structure and initial parameter estimates were in place, the parameters $EMAX_{SCLER}$, γ_{Dr}, γ_{OCY}, γ_{OPG},γ_{OB}, $kout_T$, SMAX, and $kout_{TOL}$ were optimized simultaneously to the turnover markers P1NP and CTx.

Multiple optimization routines were explored for this task. Global optimization for large systems models is difficult and this was especially true in this system where P1NP and CTx are highly variable endpoints regulated by feedback control and the available dataset was somewhat sparse. The optimization routes that were explored are summarized in table 2.1. Criteria for optimization method selection were that the method allowed all parameters to move (i.e. avoided falling into local minima over the multivariate parameter space), the method resulted in a lower objective function value than the initial parameter estimates, and that the resulting optimized parameter values resulted in predictions that resembled the clinical data by visual inspection.

Table 2.1: Optimization methods in R

Function	Description	Benefits	Drawbacks
Gradient-based methods			
optim::Nelder [77]	Default optimization method; uses simplex method that does not require gradients	• gives hessian • derivative free	• cannot specify bounds so for difficult problem it can slip into unsolvable variable space
optim::SANN [78]	Stochastic method; searches neighboring regions and calculates acceptance probability using metropolis function.	• derivative free	• very slow
optim::LBFGSB [79]	Quasi-newton method with box-constraints; relies on approximation of inverse hessian and executes a backtracking line search until an acceptable point is found and then it updates the hessian	• allows bounds to be specified	
Rvmmin [80, 81]	Same method as BFGS-B, but updated for efficiency by using masks ie. temporarily fixing parameters	• allows bounds to be specified	
Quadratic Approximation Methods			
minqa::newuoa [76]	Forms a trust-region by models of interpolation and searches within this space for minimum function value	• fast • derivative free • can set trust region radius	• easily falls into local minimum

Continued on next page

Continued from previous page

Function	Description	Benefits	Drawbacks
RsolnP:: solnp [82]	Solves a linearly constrained optimization problem. In the first step, the optimization problem tests a vector of Lagrange multipliers changing with each major iteration and this is subject to a function containing the numerical approximation to the jacobian. In the second step, minor iterations approximate a solution to a quadratic function is found, subject to the same constraints	• takes boundary conditions • gives hessian	• highly constrained by boundary conditions
	Sampling Methods		
MCMCpack:: MCMCmetrop1R [83]	Calls optim first to generate a hessian (the variance-covariance matrix for the Gaussian proposal distribution) as a starting point from which to sample. Then pulls samples from a continuous distribution using a random walk Metropolis algorithm	• user can supply a hessian matrix from a previous optimization step to help speed up algorithm • robust method for difficult problems	• slow
DEoptim [84]	A genetic algorithm which creates a starting population of several vectors of parameter values, based on draws from a uniform distribution defined by specified bounds. This population is transformed based on the strategy selected and the vector most likely to minimize the function is carried forward to the next iteration. New populations are generated and process is repeated until the maximum number of evaluations (specified by the user) is reached	• can be easily parallelized • good for stochastic, noisy functions, or those difficult to differentiate • takes boundary conditions • can specify a starting population, in addition to initial estimates	• does not give hessian • slow

2.3 AIM III. Fracture Model and Simulations (PAPER III, Chapter 9)

A time to event (TTE) / hazard model of fracture was also developed, to be implemented into the bone model and used to explore how therapeutic modulation affects fracture outcome. The primary objective of this part of the project was extend a previously-developed model of fracture to determine the best covariate structure for lumber spine BMD and differentiate the effects of therapy on the the probability of fracture in patients with osteoporosis. The methods for development, results and validation are shown in chapter 9. The final model simulations were performed within the MSPM by linking continuous changes in LS BMD simulated by the systems model, to the TTE model of fracture. The other model covariates required by the TTE model were supplied via an external dataset.

Simulations of regional changes in LS, total hip (TH), and femoral neck (FN) BMD were guided by the STRUCTURE clinical trial that recently completed [85] . To populate baseline characteristics of patients in these studies, patients were resampled from a normal distribution from a subset of the NHANES dataset. Only patients with an osteoporosis diagnosis, age greater than or equal to 55, and with a screening LS BMD of less than 0.83 g/cm^2 were included in the sampling pool. Parameters for the hazard model were sampled from the posterior distribution generated by the model described in chapter 9. 1000 samples were drawn from this posterior and inter-trial random variability was generated for the h0, and BMD parameters by sampling from a multi-variate normal distribution of the estimated random effects for these parameters. These simulations were performed using *mrgsolve* [86].

Chapter 3

Results

3.1 AIM I. Results of Identifiability Analysis for Target-Mediated Drug Disposition (TMDD) Model (PAPER I, Chapter 7) and PK/PD Model for Sclerostin mAbs (PAPER II, Chapter 8)

In the case of a full single-target TMDD, the system was fully globally identifiable under any output scenario, with the exception of the complex only output under iv infusion, and single outputs drug only, target only, or complex only after a subcutaneous dose. The Ritt algorithm performing these steps required unreasonable run times and could not be resolved using this method. All input/output scenarios under the MM approximation were found to be globally identifiable using DAISY, as were all of the TMDD2-target scenarios with the exception of free-drug only input, which was limited by time constraints of the reduction steps, as described. The antibody-drug-conjugate TMDD model is at least locally identifiable if either drug and toxins or target and toxins can be measured and it is globally identifiable only if all species in the model are measurable. Results for this analysis are shown in table 3.1.The results of the likelihood profile analysis of the bosentan study are shown in fig. 3.1 and the code for the analysis is in appendix A.

The final PK/PD model structure and parameter estimates are shown in PAPER II (chapter 8). The visual predictive checks with these parameter estimates are shown in the supplement to PAPER II, figures 4 and 5. The PK and PD dynamics are well-described by the data, within the therapeutic dosing

range (1-5 mg/kg with romosozumab and 150-540 mg blosozumab, single and multiple doses).

Table 3.1: Analysis Results for Antibody-Drug Conjugate TMDD (See Appendix 2 for equations)

Inputs	Outputs	Parameters	Result
iv inf	Drugs & complexes only	*kdeg, kon, koff, kel1, kel2, kelT, kpt, ktp, Vc, ksyn, kint, k2dec*	Non-identifiable: *kelT*
iv inf	Drugs & target or complexes &target	Same as above	Non-identifiable: *kelT*
iv inf	Drugs & toxins or complexes & toxins	Same as above	Locally identifiable[1]
iv inf	Drugs, targets, complexes & toxins	Same as above	Globally identifiable

[1] The system was too complex for the Ritt algorithm within DAISY; the algorithm which performs the reduction steps. The EAR approach was used here, limiting results to nonidentifiable or locally identifiable

3.2 AIM II. Sclerostin-Related Modifications to the Multiscale Systems Pharmacology Model (PAPER II, Chapter 8)

Development and selection of the final model structure for all sclerostin-related components are presented in chapter 8. The step-wise process used to determine the compartmental structure of these effects is outlined in this section.

3.2.1 *Systems Model Equations Describing Compartmental Structure*

Sclerostin Effect on Osteoblast Compartment

1. Increase formation rate of responding osteoblasts (ROB, γ_{Dr}) and formation rate of osteoblasts (OB) (*kb*), by applying a sclerostin effect, normalized to baseline.

$$Dr = kb \cdot \frac{OB_0}{Pic_0} \cdot \left(\frac{\text{SCLER}}{\text{SCLER}_0}\right)^{\gamma_{Dr}} \tag{3.1}$$

$$bigDb = kb \cdot OB_0 \cdot Pic_0/ROB \cdot \left(\frac{\text{SCLER}}{\text{SCLER}_0}\right)^{\gamma_{Db}} \tag{3.2}$$

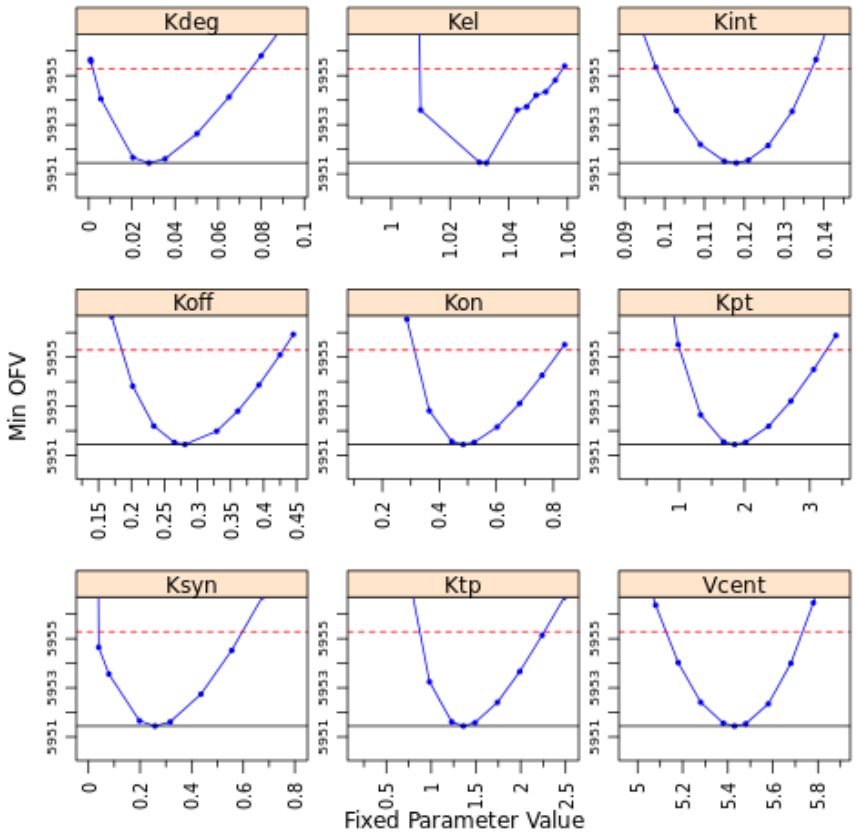

Figure 3.1: Likelihood profiles for single-target TMDD model, showing all parameters to be identifiable

both apply to the equations:

$$\frac{\mathrm{d}}{\mathrm{dt}} ROB = Dr \cdot PicROB \cdot \frac{1}{EST}^{robGAM} - k_{pt} \cdot ROB \tag{3.3}$$

$$\frac{\mathrm{d}}{\mathrm{dt}} OB = \frac{bigDb}{PicOB} \cdot D \cdot FracOBfast \cdot Frackb2 - kbfast \cdot OBfast \tag{3.4}$$

Result: Rapid and large increases in P1NP.

2. Apply an EMAX effect on a precursor pool in order to supply the responding osteoblasts (osteoblast precursor pool) (ROB) compartment with additional substrate and avoid ROB depletion:

$$\frac{\mathrm{d}}{\mathrm{dt}} PREROB = PREROB_{in} \cdot \left(1 - \frac{EMAX \cdot \frac{\mathrm{SCLER}}{\mathrm{SCLER}_0}}{EC_{50} + \frac{\mathrm{SCLER}}{\mathrm{SCLER}_0}}\right) - kout_{PREROB} \cdot PREROB \tag{3.5}$$

$$\frac{\mathrm{d}}{\mathrm{dt}} ROB = Dr \cdot PicROB \cdot \frac{1}{EST}^{robGAM} \cdot \left(\frac{1}{\frac{PREROB}{PREROB_0}}\right) - k_{pt} \cdot ROB1 \tag{3.6}$$

Result: Tmax (time at maximum P1NP concentration) and the slope of the decline in P1NP after the peak was now closer to the concentration curve in the clinical data, but the accumulation phase of the simulations were still not as rapid as in the clinical data.

3. Apply a direct effect on OBfast compartment, using change from baseline (CFB) in sclerostin as a signal.

$$\frac{\mathrm{d}}{\mathrm{dt}} OBfast = \frac{bigDb}{PicOB} \cdot D \cdot FracOBfast \cdot Frackb2 \cdot \left(1 + \frac{EMAX \cdot \mathrm{CFB}_{\mathrm{SCLER}}}{EC_{50} + \mathrm{CFB}_{\mathrm{SCLER}}}\right) - kbfast \cdot OBfast \tag{3.7}$$

Result: Rapid accumulation phase still not achieved.

4. Apply a direct effect on OBfast compartment, using sclerostin normalized to baseline as a signal.

$$\frac{\mathrm{d}}{\mathrm{dt}} OBfast = \frac{bigDb}{PicOB} \cdot D \cdot FracOBfast \cdot Frackb2 \cdot \left(1 + \frac{EMAX \cdot \frac{\mathrm{SCLER}}{\mathrm{SCLER}_0}}{EC_{50} + \frac{\mathrm{SCLER}}{\mathrm{SCLER}_0}}\right) - kbfast \cdot OBfast \tag{3.8}$$

Result: Again, the magnitude of the response can be adjusted by adjusting EMAX, but the accumulation phase was still not as rapid as in the clinical data.

5. Apply a direct effect on OBfast compartment, using a power model of sclerostin normalized to baseline.

$$\frac{\mathrm{d}}{\mathrm{dt}} OBfast = \frac{bigDb}{PicOB} \cdot D \cdot FracOBfast \cdot Frackb2 \cdot \left(\frac{\mathrm{SCLER}}{\mathrm{SCLER}_0}\right)^{\gamma_{Dr}} - kbfast \cdot OBfast \tag{3.9}$$

Result: This had a similar effect as the previous step.

6. Apply pre-cursor pool effect to in-rate and out-rate of ROB; power effect on in-rate precursor pool effect to remove substrate from ROB pool more rapidly.

$$\frac{\mathrm{d}}{\mathrm{dt}}ROB = Dr \cdot PicROB \cdot \frac{1}{EST}^{robGAM} \cdot \left(\frac{1}{\frac{PREROB}{PREROB_0}}\right)^{\gamma_{Dr}} - \frac{PREROB}{PREROB_0} \cdot K_{pt} \cdot ROB1 \tag{3.10}$$

Result: Accumulation slope of P1NP is closer to clinical data, but as soon as the ROB pool is depleted, P1NP declines (see fig. 3.2 and fig. 3.3, panels 3 and 4).

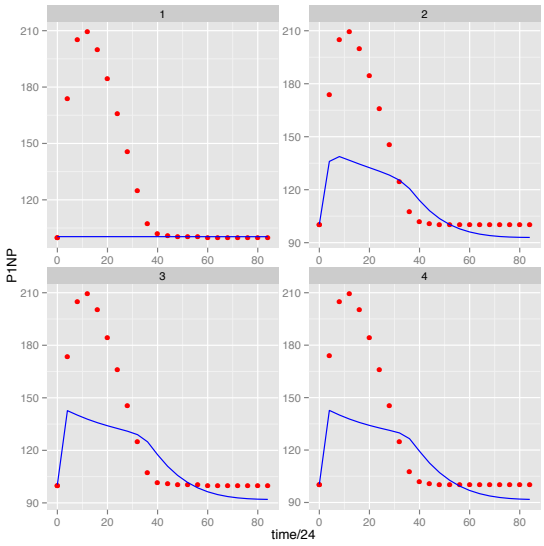

Figure 3.2: P1NP results for different values of γ_{Db} parameters : 0, 0.8,1.5, 2. Red represents clinical data

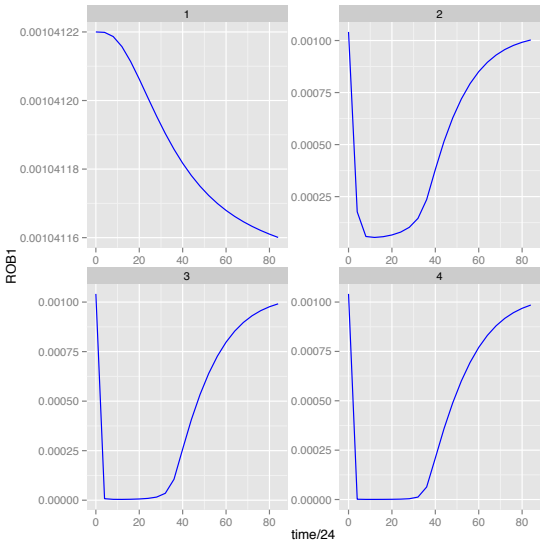

Figure 3.3: ROB results for different values of γ_{Db} parameters : 0, 0.8,1.5, 2. Red represents clinical data

7. Finally, an EMAX model was applied directly onto the OB compartment. This resulted in a superior fit than all other mechanisms that were tried. The structure of the final model was a sigmoid EMAX model propagated through a "translation compartment" to allow for a lag time between peak sclerostin response and peak P1NP response.

$$\frac{\mathrm{d}}{\mathrm{dt}}trans = kin_{trans} \cdot \left(1 + \frac{EMAX_{\mathrm{SCLER}} \cdot \mathrm{SCLER}^{\gamma_{OB}}}{EC_{50,\mathrm{SCLER}}^{\gamma_{OB}} + \mathrm{SCLER}^{\gamma_{OB}}}\right) - kout_{trans} \cdot trans, \tag{3.11}$$

where

$$OB = OBfast \cdot trans + OBslow \quad \& \quad kin_{trans} = kout_{trans} \tag{3.12}$$

P1NP simulations using this model are shown in the appendix of chapter 8.

Sclerostin Effect on Osteoclast Compartment

Next, OC effects were implemented in the model and several modifications were also attempted before arriving at a final model structure.

1. Change "OB effect" applied to the *kin* parameter on the RANKL compartment to an OCY effect:

$$OB_{effect} = \frac{OCY}{OCY_0}^{\gamma_{\text{OCYeffect}}} \tag{3.13}$$

Result: OC activity declined between $\gamma_{\text{OCYeffect}}$ values of 0.1-1, but either did not decline quickly enough or failed to return to baseline.

2. Keep an OB effect (as in the original model) and add an OCY effect on RANKL.

Result: This seemed to have the desired effect if the OB effect was very low (γ_{OBeffect} <0.01) and the OCY effect was relatively high ($\gamma_{\text{OCYeffect}}$ between 0.2-0.3), but still did not have the initial decline in CTx described by the data (see fig. 3.4).

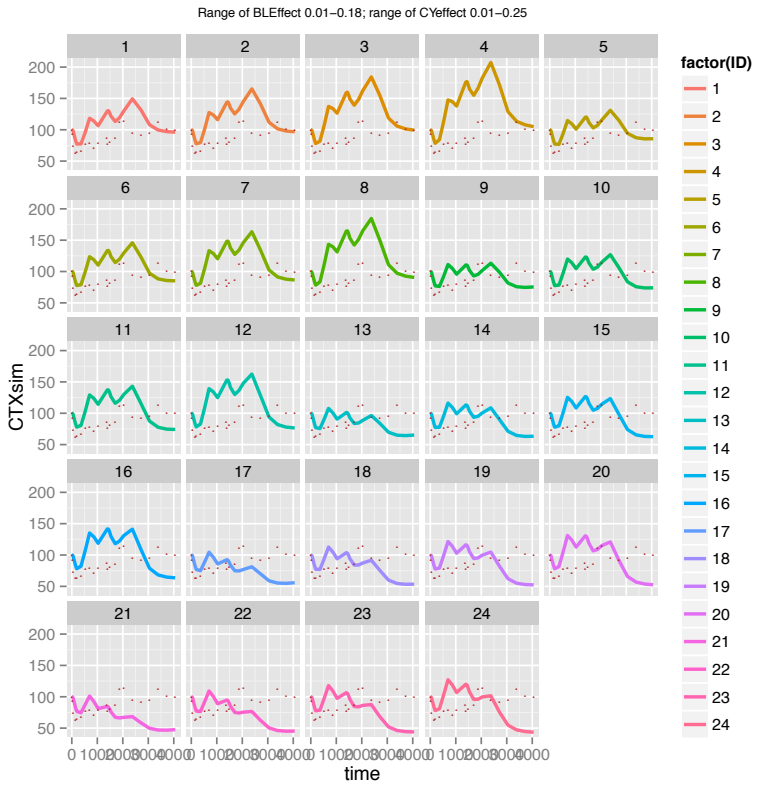

Figure 3.4: Simulations of CTx from a single arm in the clinical dataset show OB and OCY effects on RANKL with a range of test values for the γ parameters. Clinical data from a single treatment arm is shown in red

3. Finally, a sclerostin effect was implemented, in the form of a power model on OPG, as described in chapter 8.

   Result: This had the desired effect of rapidly decreasing OC in the early phase of treatment, but still allowed for recovery at the later phase.

4. EMAX models for the sclerostin effect on OCY and the sclerostin effect on OPG were also tried, but resulted in poor prediction profiles, specifically a 2-phase decline in CTx.

The CTx profiles simulated with the final model structure are shown in the appendix for chapter 8. Final global optimization of parameters was performed after final model structure describing P1NP and CTx profiles was in place. After optimization the parameters related to turnover markers, regional

BMD compartments and parameters were implemented. The optimization methods and BMD portion of the model development for sclerostin-related effects is also described at length in chapter 8.

Model Development for Simulation of Combination Therapy

Further adjustments had to be made to the model so that the OCY effects on RANKL would not interfere with simulations of PTH or teriparatide administration. The steps taken which lead to the final model structure in which sclerostin mAb or teriparatide could be correctly simulated are outlined below.

1. Coupling the anabolic effects together on OCY

$$\text{TERI}_{\text{effect}} = 1 - \text{TERICENT}^{\gamma\, TERI_{SCLER}} \tag{3.14}$$

$$\frac{\text{d}}{\text{dt}} OCY = OB \cdot \text{FRACTION}_{OCY} - OB_{\text{baseline}} \cdot \text{FRACTION}_{OCY} \cdot \text{SCLER}^{\gamma_{OCY}} \cdot \text{TERI}_{\text{effect}} \cdot OCY \tag{3.15}$$

Under the premise that PTH signals to stimulate OCY. There is evidence that increased PTH results in increased expression of OPG and RANKL; perhaps this is signaled through the osteocytes [31, 87].

Result: Magnitude of P1NP and CTx response was still blunted and CTx effect did not decline initially to the extent of the clinical data.

2. Apply PTH effects to areas in the model where sclerostin has an effect, but to varying degrees by supplying different values for $\gamma_{PTH_{Dr}}$,$\gamma_{PTH_{OCY}}$ and $\gamma_{PTH_{OPG}}$.

$$\frac{\text{d}}{\text{dt}} ROB = Dr \cdot PicROB \cdot \frac{1}{EST}^{robGAM} - \text{SCLER}_{\text{effect}}{}^{\gamma_{Dr}} \cdot \left(\frac{PTH}{PTH_0}\right)^{\gamma_{PTH_{Dr}}} \cdot K_{pt} \cdot ROB1 \tag{3.16}$$

$$\frac{\text{d}}{\text{dt}} OCY = OB \cdot \text{FRACTION}_{OCY} - \left(\frac{PTH}{PTH_0}\right)^{\gamma_{PTH_{OCY}}} \cdot OB_{\text{baseline}} \cdot \text{FRACTION}_{OCY} \cdot OCY \tag{3.17}$$

$$\frac{\text{d}}{\text{dt}} \text{OPG} = \text{OPG} \cdot \text{SCLER}_{\text{effect}}{}^{\gamma_{OPG}} \cdot \left(\frac{PTH_0}{PTH}\right)^{\gamma_{PTH_{OPG}}} - k1 \cdot \text{OPG} \cdot \text{RANK} + k2 \cdot \text{COMPLEX} - k0 \cdot \text{OPG} \tag{3.18}$$

Result: Profiles not improved from previous modification.

3. Apply PTH signal only to the in-rate on OCY compartment.

$$\frac{\mathrm{d}}{\mathrm{dt}}OCY = OB \cdot \mathrm{FRACTION}_{OCY} \cdot \left(\frac{PTH}{PTH_0}\right)^{\gamma_{PTH_{OCY}}} - OB_{\mathrm{baseline}} \cdot \mathrm{FRACTION}_{OCY} \cdot OCY \tag{3.19}$$

Result: Marked improvement in P1NP response, but no improvement on CTx.

4. Apply a direct PTH effect on OB compartment, either via the trans compartment or OBfast.

$$\frac{\mathrm{d}}{\mathrm{dt}}trans = kin_{trans} \cdot \left(1 + \frac{EMAX_{\mathrm{SCLER}} \cdot \mathrm{SCLER}^{\gamma_{OB}}}{EC_{50,\mathrm{SCLER}}^{\gamma_{OB}} + \mathrm{SCLER}^{\gamma_{OB}}}\right) \cdot \left(\frac{PTH}{PTH_0}\right)^{\gamma_{PTH_{OB}}} - kout_{trans} \cdot trans, \tag{3.20}$$

$$\frac{\mathrm{d}}{\mathrm{dt}}OBfast = \frac{bigDb}{PicOB} \cdot D \cdot FracOBfast \cdot Frackb2 \cdot \left(\frac{PTH}{PTH_0}\right)^{\gamma_{PTH_{OB}}} - kbfast \cdot OBfast \tag{3.21}$$

Result: Again, there is a marked improvement in P1NP response, but this is artificially elevated and no feedback response is elicited to improve the CTx profile.

5. Apply a fractional contributions from OB and OCY to RANKL, so that when there is no sclerostin effect present, the OB effect on RANKL takes the value from the original model.

$$\mathrm{OSTEOEFFECT} = \left(\frac{OCY}{OCY_{\mathrm{baseline}}}\right)^{\delta} \cdot \mathrm{TOT}_{\mathrm{OsteoEffect}} \cdot \left(1 - \frac{1}{\mathrm{FRACTION}_{\mathrm{OBeffect}}}\right) \tag{3.22}$$

where $\mathrm{TOT}_{\mathrm{OsteoEffect}} = 0.173833$ and $\mathrm{FRACTION}_{\mathrm{OBeffect}} = 20$ (fixed values)

Result: Again there is a marked improvement in P1NP response, but this is artificially elevated and no feedback response is elicited to improve the CTx profile (see fig. 3.5).

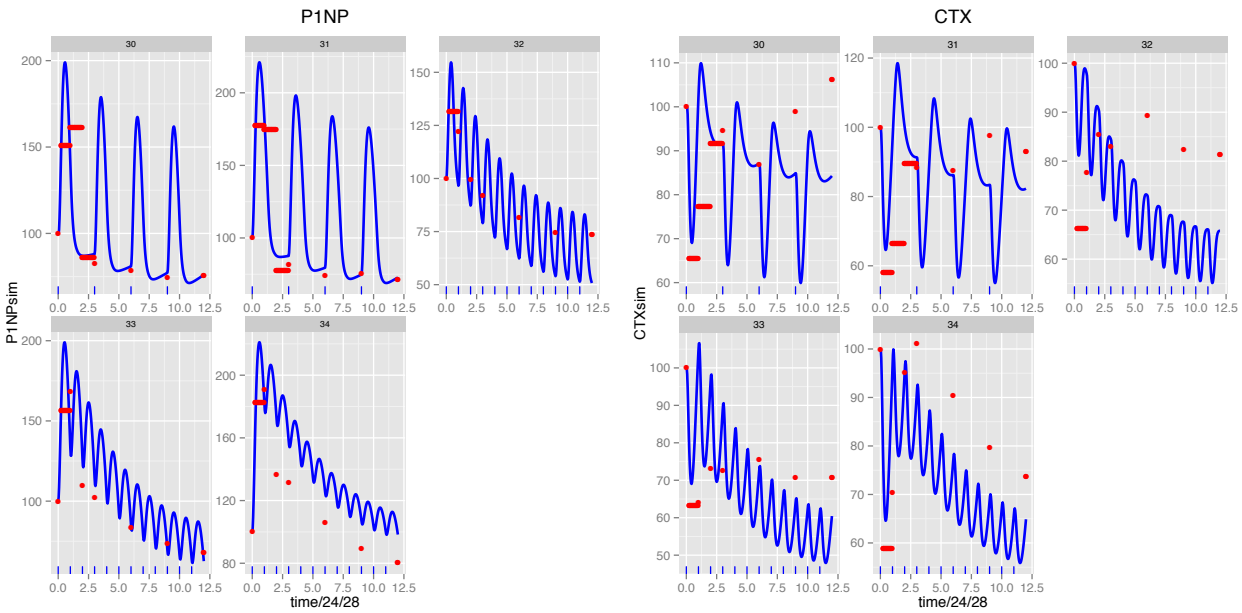

Figure 3.5: Results of fractionating RANKL signal between the OB and OCY: OB contribution is $\frac{1}{20}$th the OCY contribution. Magnitude of P1NP response (left) is slightly over-predicted, and initial decline in CTx (right) is still slightly under-predicted, for a subset of the clinical data (shown in red)

6. Apply an EMAX "tolerance" model, whereby the OCY contribution to RANKL pool phases out with the sclerostin effect.

$$\mathrm{TOL}_{\mathrm{SCLER}} = \left(1 + \frac{\mathrm{SMAX} \cdot \mathrm{SCLER}_{\mathrm{EFFECT}}}{\mathrm{SC50} + \mathrm{SCLER}_{\mathrm{EFFECT}}}\right) \tag{3.23}$$

$$kout_{OCY} = OB_{\mathrm{baseline}} \cdot \mathrm{FRACTION}_{OCY} \cdot \mathrm{TOL}_{\mathrm{SCLER}} \tag{3.24}$$

Result: P1NP drops too quickly after repeated doses; CTx drops abruptly after initial dose and rebounds after therapy is removed.

7. Structure tolerance as an independent compartment, as in an indirect response model; apply this TOL effect on OCY compartment, in addition to sclerostin effect.

$$\frac{\mathrm{d}}{\mathrm{dt}}\mathrm{TOL} = kin_{TOL} \cdot \exp(-5 \cdot \mathrm{TOL}) - kout_{TOL} \cdot \mathrm{TOL} \tag{3.25}$$

where $kin_{TOL} = kout_{TOL}$

$$kout_{OCY} = OB_{\text{baseline}} \cdot \mathrm{FRACTION}_{OCY} \cdot \mathrm{SCLER}^{\gamma_{OCY}} \cdot \mathrm{TOL} \tag{3.26}$$

Result: Tolerance effect a little too strong. P1NP / CTx responses look like the clinical data during initial dose phase, but then increase as sclerostin-driven tolerance effect declines.

8. Use sclerostin effect as a signal to decrease TOL; Implement tolerance compartment like a precursor pool, tied into the osteocyte compartment.

   Use the EMAX effect for $\mathrm{TOL}_{\mathrm{SCLER}}$:

$$\mathrm{TOL}_{\mathrm{SCLER}} = \left(1 - \frac{\mathrm{SMAX} \cdot \mathrm{SCLER}_{\mathrm{EFFECT}}}{\mathrm{SC50} + \mathrm{SCLER}_{\mathrm{EFFECT}}}\right) \tag{3.27}$$

$$k0_{\mathrm{TOL}} = OB \cdot \mathrm{FRACTION}_{OCY} \cdot \mathrm{baseline} \tag{3.28}$$

$$kin_{\mathrm{TOL}} = OB_{\text{baseline}} \cdot OCY_{\text{baseline}} \mathrm{FRACTION}_{OCY} \mathrm{TOL}_{\text{baseline}} \tag{3.29}$$

$$kout_{OCY} = OB_{\text{baseline}} \cdot \mathrm{FRACTION}_{OCY} \cdot \mathrm{TOL}_{\mathrm{SCLER}} \tag{3.30}$$

$$\frac{\mathrm{d}}{\mathrm{dt}}\mathrm{TOL} = k0_{TOL} - kin_{TOL} \cdot \mathrm{TOL}_{\mathrm{SCLER}} - kout_{TOL} \cdot \mathrm{TOL} \tag{3.31}$$

$$\frac{\mathrm{d}}{\mathrm{dt}} OCY = OB \cdot \mathrm{FRACTION}_{OCY} - kout_{OCY} \cdot OCY \tag{3.32}$$

Result: P1NP profiles resemble the clinical data but CTx responses do not decline during the initial dose phase.

9. Final model: combine tolerance effect with portioned osteoeffect from #5: at full tolerance (TOL=1), the OBeffect is 1/20 of the OCYeffect:

$$\mathrm{FRACTION}_{\mathrm{OBeffect}} = 20/\mathrm{TOL} \tag{3.33}$$

Use the same equation for $\mathrm{TOL}_{\mathrm{SCLER}}$

$$\mathrm{TOL}_{\mathrm{SCLER}} = \left(\frac{\mathrm{SMAX} \cdot \mathrm{SCLER}_{\mathrm{EFFECT}}}{\mathrm{SC50} + \mathrm{SCLER}_{\mathrm{EFFECT}}} \right) \tag{3.34}$$

where $kin_{\mathrm{TOL}} = kout_{\mathrm{TOL}}$ and the OCY compartment structure returned to what it was before:

$$\frac{\mathrm{d}}{\mathrm{dt}} OCY = OB \cdot \mathrm{FRACTION}_{OCY} - OB_{\mathrm{baseline}} \cdot \mathrm{FRACTION}_{OCY} \cdot \mathrm{SCLER}^{\gamma_{OCY}} \cdot OCY \tag{3.35}$$

Result: Both P1NP and CTxprofiles are better described with tolerance compartment and proportioned osteoeffect (see fig. 3.6).

Additional modifications were made to the model in efforts to stabilize the model and allow anabolic mechanisms of PTH stimulations to persist along with anabolic effects of sclerostin modulation. In the final model, the osteocyte effect on RANKL was modified.

Model Stability

In order to address the problem of model stability (ie. obtaining a complete simulation with the same results every time without premature termination by the ODE solver), the steady-state principle

from the original bone model [47] was applied to the sclerostin effect, and the EC50 was solved in terms of EMAX:

$$\mathrm{EC50}_{\mathrm{SCLER}} = \exp\left(\frac{log(\mathrm{EMAX}_{\mathrm{SCLER}} - 1)}{\gamma_{\mathrm{SCLER}_{\mathrm{OB}}}}\right) \tag{3.36}$$

The final, globally-optimized parameter values are shown in table 3.2. The final estimated BMD parameters for teriparatide, denosumab, sclerostin mAbs and the combination of teriparatide and denosumab is shown in table 3.3. The parameter estimates for the BMD compartments representing combination treatment were expressed as fractions of monotherapy-related parameters, in order to make inferences about temporal aspects of modulation of two pathways at work in the combination arm, ie. anti-resorptive activity and anabolic activity. Simulated teriparatide and denosumab studies are shown in fig. 3.9 and fig. 3.10. Simulations for changes in LS BMD with the study design from the DATA trial are shown in fig. 3.8.

3.2.2 *Optimization Routines*

A visual demonstration of the results of simulation using different algorithms to fit a subset of parameters to a sclerostin P1NP dataset is shown in fig. 3.7. In addition to the methods displayed, Rsolnp was also tried but was unsuccessful after only a couple of iterations. The parameters were not permitted to change very much and resulted in poor fits, but a hessian matrix was generated from the parameter estimates. Gradient-based methods proved to be unreliable because it was difficult for the solver to resolve at all possible values of the parameters, which the algorithm prompted it to explore. The derivative-free method, minqa::newua was used for local parameter estimates and for estimates of BMD parameters because the parameter sets were small and more manageable. The final parameter optimization step, in which all parameters describing the turnover makers were optimized simultaneously was performed using DEoptim, which terminated at a pre-specified number of maximum iterations (300), yielded a lower objective function than the initial estimates, which had been determined by tuning and prior optimization, and resulted in good predictions of P1NP and CTx by visual inspection.

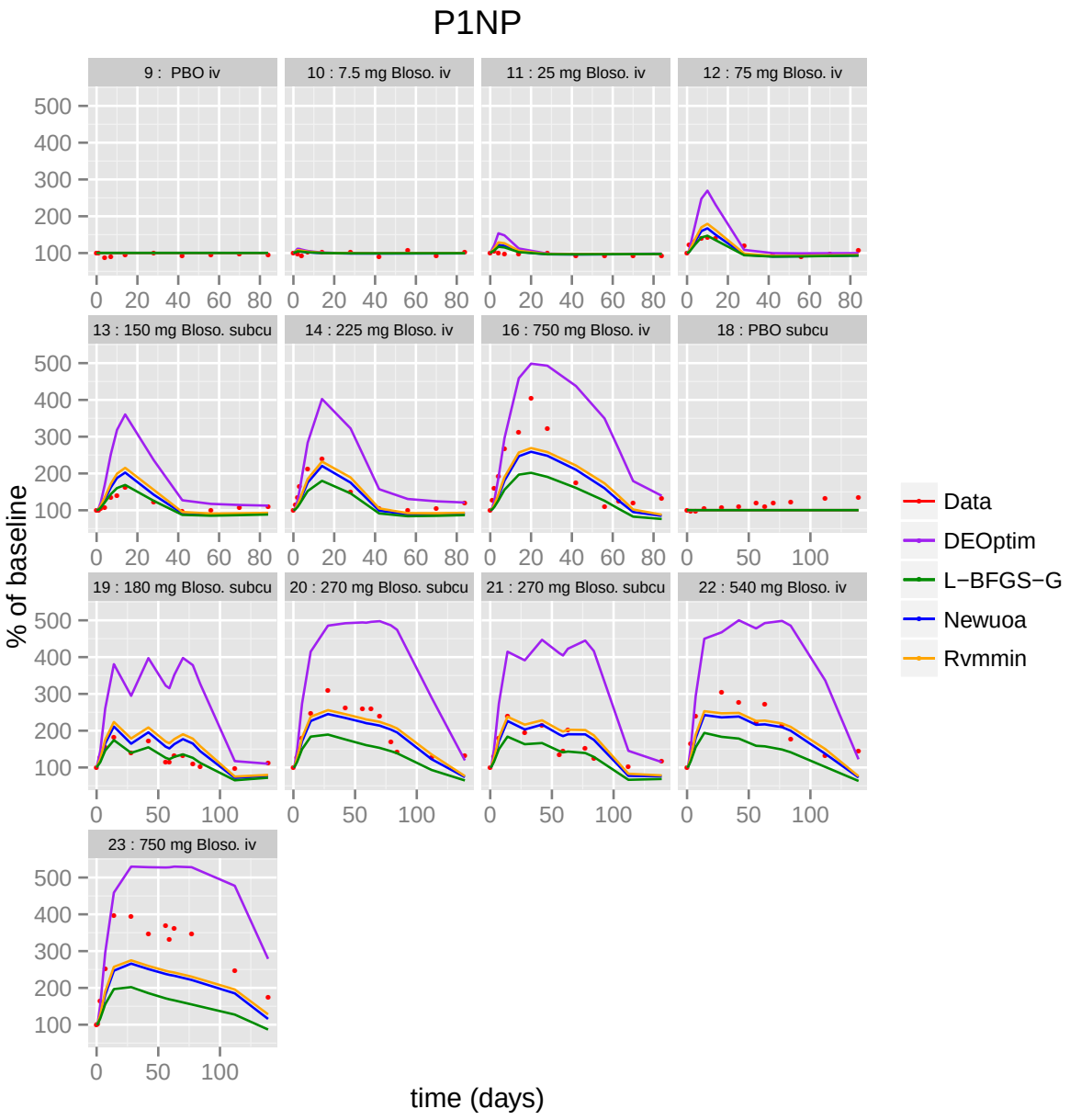

Figure 3.7: A comparison of optimization methods using the blosozumab P1NP dataset and optimizing $EC50_{SCLER}$, $EMAX_{SCLER}$ and γ_{SCLER}. Max interactions for DEoptim fits was 200

Table 3.2: Final Estimated Values for Parameters Involved in Estimation of Turnover Markers

Variable	**Value**	
$EMAX_{\text{SCLER}}$ (nM)	4.67	
$\text{FRACTION}_{\text{OBeffect}}$ (unitless)	20.0	fixed
FRACTION_{OCY} (1/hrs)	0.50	fixed
γ_{Dr} (unitless)	0.0446	
γ_{OCY} (unitless)	0.276	
γ_{OPG} (unitless)	1.60	
γ_{OB} (unitless)	0.163	
$kout_T$ (1/hrs)	0.00607	
$kout_{TOL}$ (1/hrs)	0.00190	
SMAX (unitless)	8.69	
$\text{TOT}_{\text{OsteoEffect}}$ (unitless)	0.174	fixed

Table 3.3: Estimated BMD Parameters

LUMBAR SPINE				
	kout (1/hrs)	*gamOC* (unitless)	*gamOB* (unitless)	*del* (1/hrs)
SCLER	0.000145	0.0653	0.758	0.00246
DENO	0.0000740	0.0791	0.0793	-
TERI	0.000554	0.0169	0.271	0.00100
COMBO	$1.86 \cdot DENO$	$1.28 \cdot DENO$	$1 \cdot DENO$	-
TOTAL HIP				
	kout (1/hrs)	*gamOC* (unitless)	*gamOB* (unitless)	*del* (1/hrs)
SCLER	0.000145	0.0653	0.225	0.00246
DENO	0.000108	0.0552	0.0793	-
TERI	0.000139	0.131	0.298	0.00100
COMBO	$0.971 \cdot DENO$	$1.28 \cdot DENO$	$1.00 \cdot DENO$	-
FEMORAL NECK				
	kout (1/hrs)	*gamOC* (unitless)	*gamOB* (unitless)	*del* (1/hrs)
SCLER	0.000145	0.0653	0.131	0.00246
DENO	0.000119	0.0515	0.0793	-
TERI	6.63E-05	0.212	0.496	0.00100
COMBO	$1.08 \cdot DENO$	$1.30 \cdot DENO$	$1.00 \cdot DENO$	-

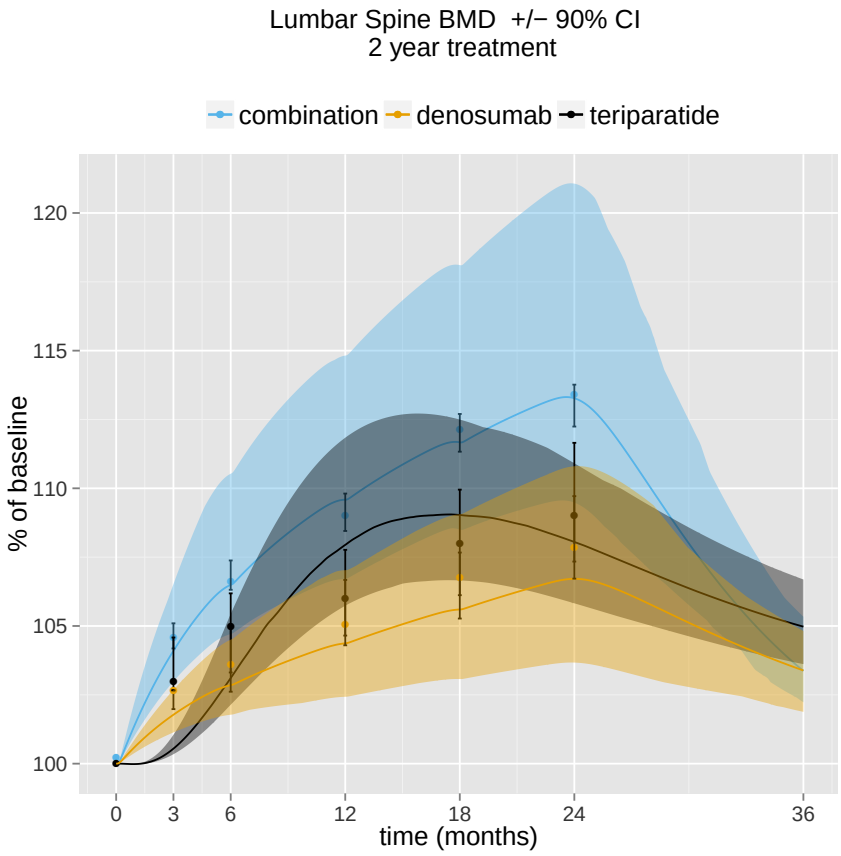

Figure 3.8: Simulated changes in LS BMD in DATA trial. Points and bars indicate mean and 95%CIs from the clinical trial [58]. Lines and ribbons are simulated means and 90%CI

3.3 AIM III. Development of a Hazard Model of Fracture (PAPER III, Chapter 9)

The results for the hazard model simulations are discussed in chapter 9. Section 3.3 shows the relative hazard ratio for the additional drug effect for each class of drug represented in the metadataset. DATA trial simulations for fracture rate are shown in fig. 3.12. This is the simulated survival (probability of no fracture) if the DATA trial had been extended for 10 years.

The STRUCTURE study is an ongoing Ph3 study comparing head-head treatment of romosozumab and teriparatide in women with osteoporosis with a high risk of fracture. The primary endpoint in this

study is longitudinal changes in TH BMD over one year. STRUCTURE trial simulations are shown in figs. 3.13 and 3.14. These are hypothetical three-year trial simulations, as the STRUCTURE trial is only one year in duration. 3-year probability of fracture is shown in fig. 3.15.

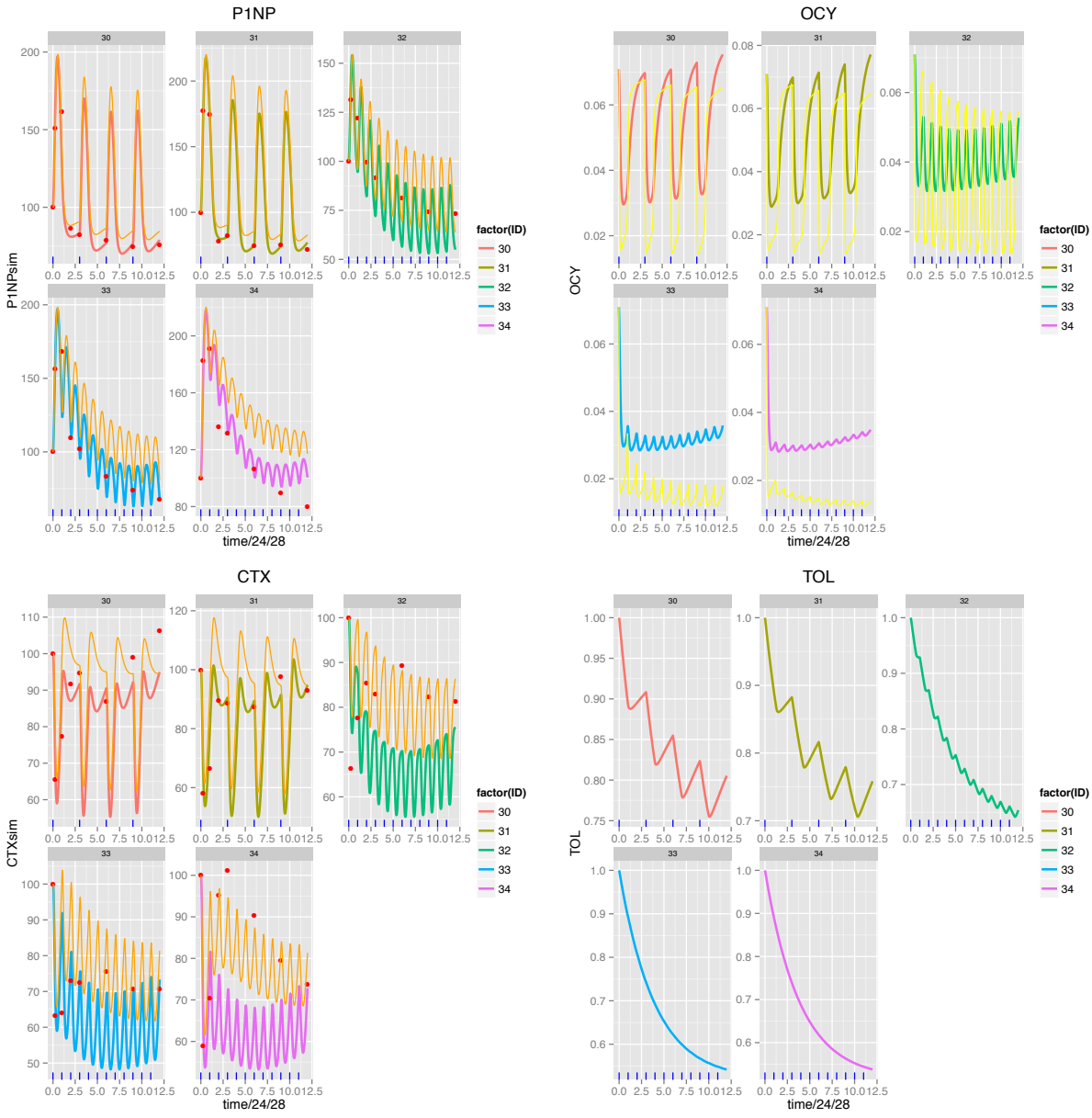

Figure 3.6: Results of using a tolerance model structure to describe OCY signaling on RANKL and effects on P1NP, OCY, CTx and TOL compartments. A subset of the sclerostin mAb dataset is simulated here; yellow and orange lines represent the simulations from the model without a tolerance compartment. Clinical data is shown in red

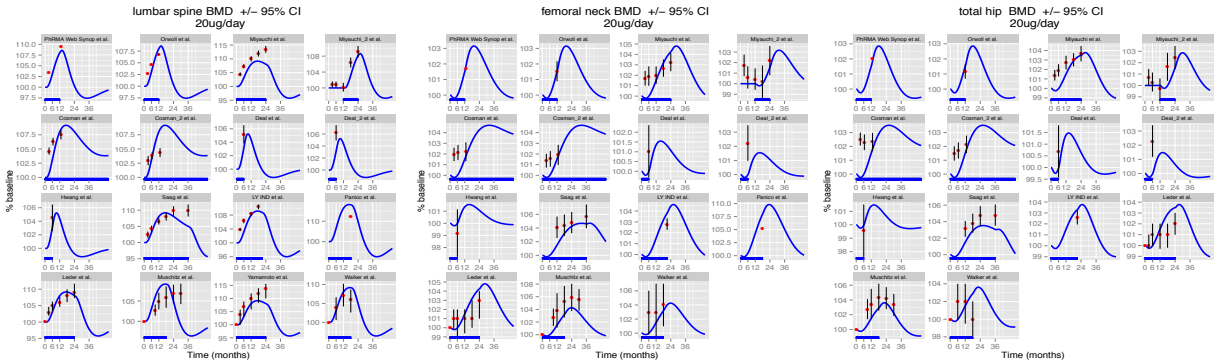

Figure 3.9: Trials with teriparatide. Graphs show simulated (blue) overlaying data (red) and 95%CIs

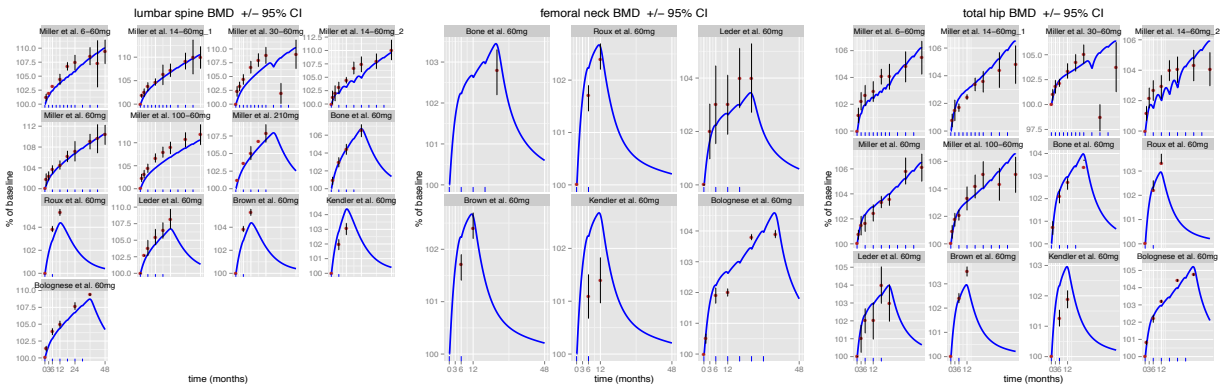

Figure 3.10: Trials with denosumab. Graphs show simulated (blue) overlaying data (red) and 95%CIs

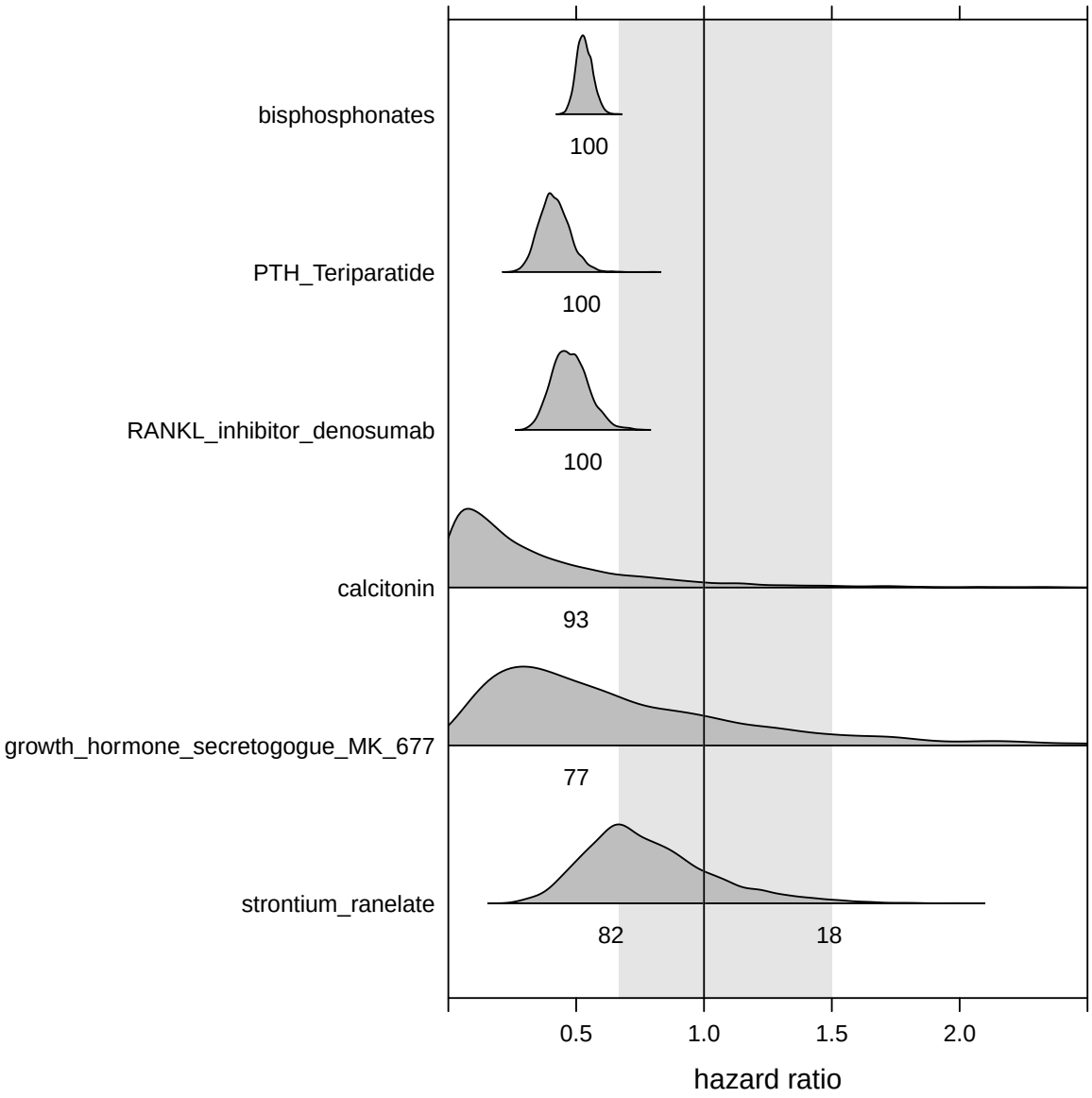

Figure 3.11: Hazard ratios and posterior distributions for the additional drug effect covariates. Hazard ratios were calculated relative to placebo

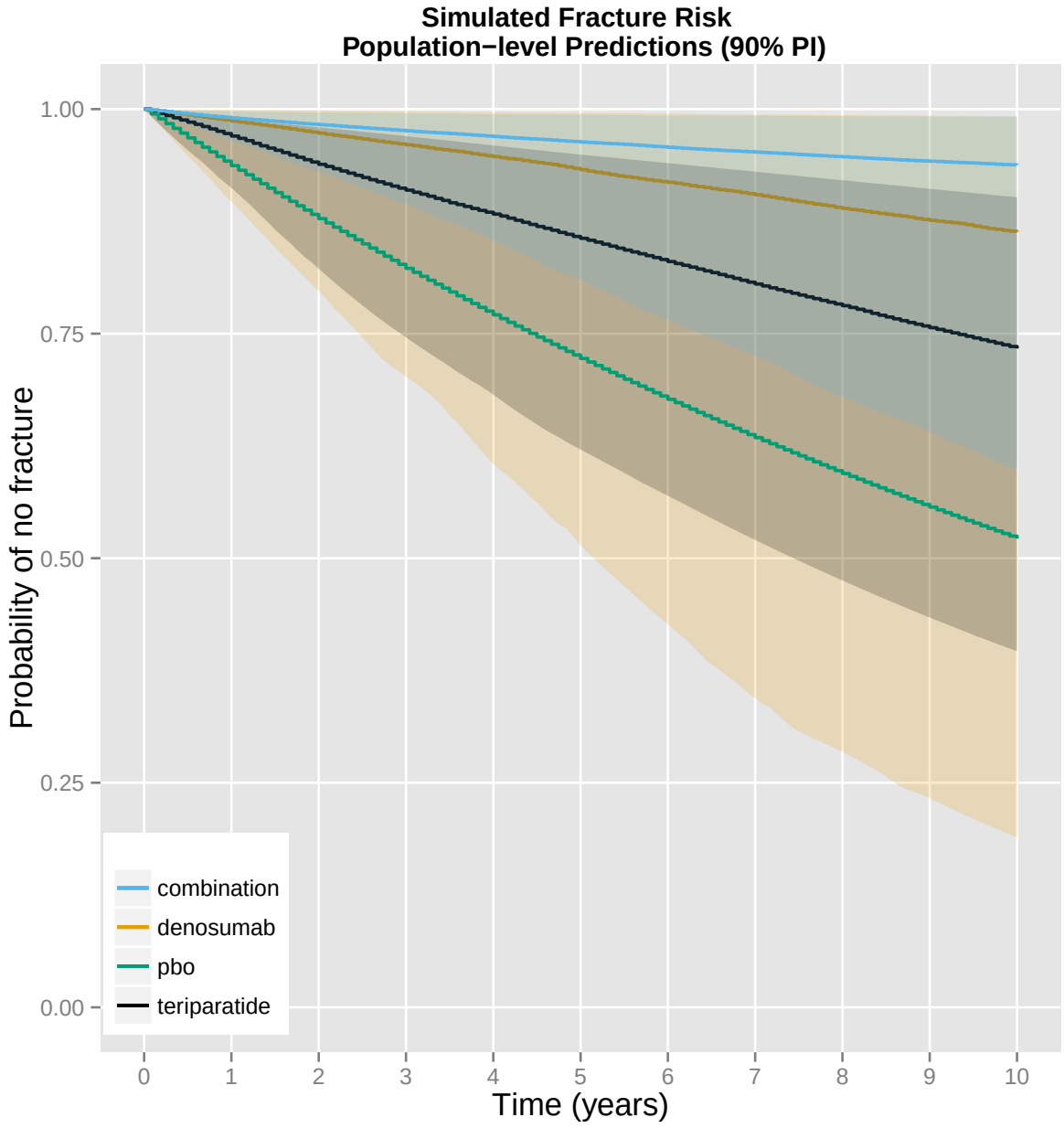

Figure 3.12: Survival curves simulated with the hazard model using predicted changes in BMD generated by the MSPM. Shading represents 90% prediction intervals

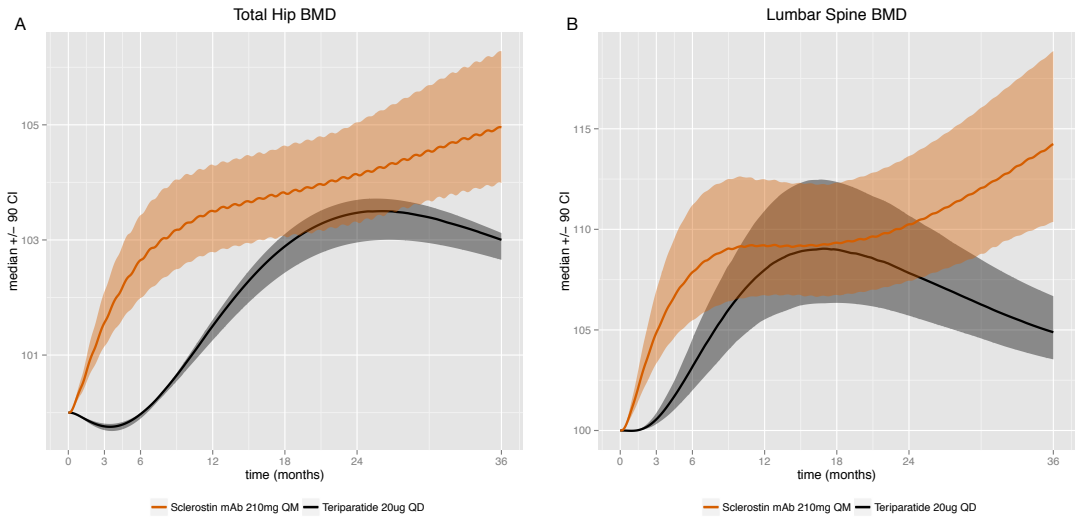

Figure 3.13: Simulated changes in TH BMD (A) and LS BMD (B) during 3 years of treatment

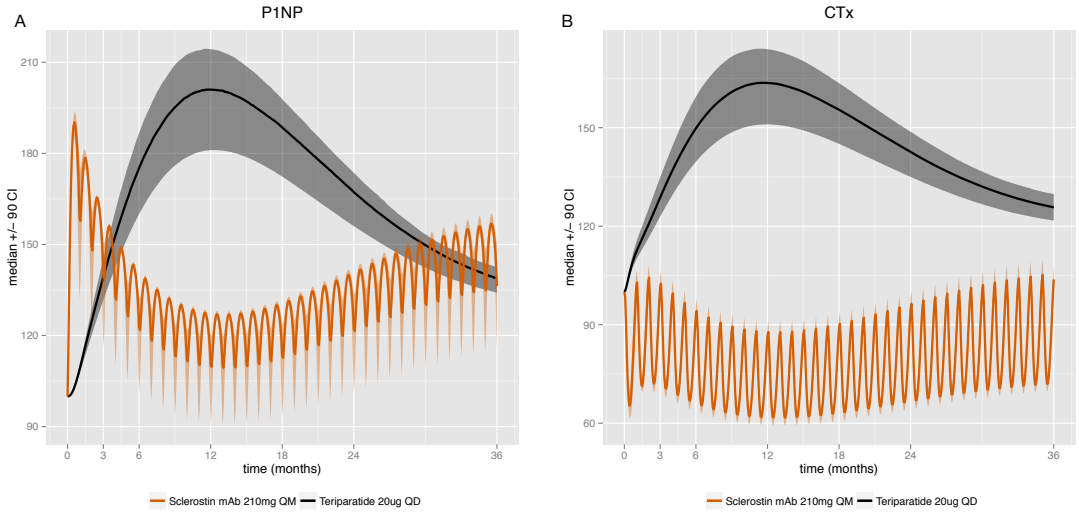

Figure 3.14: Simulated changes in P1NP (A) and CTx (B) during 3 years of treatment

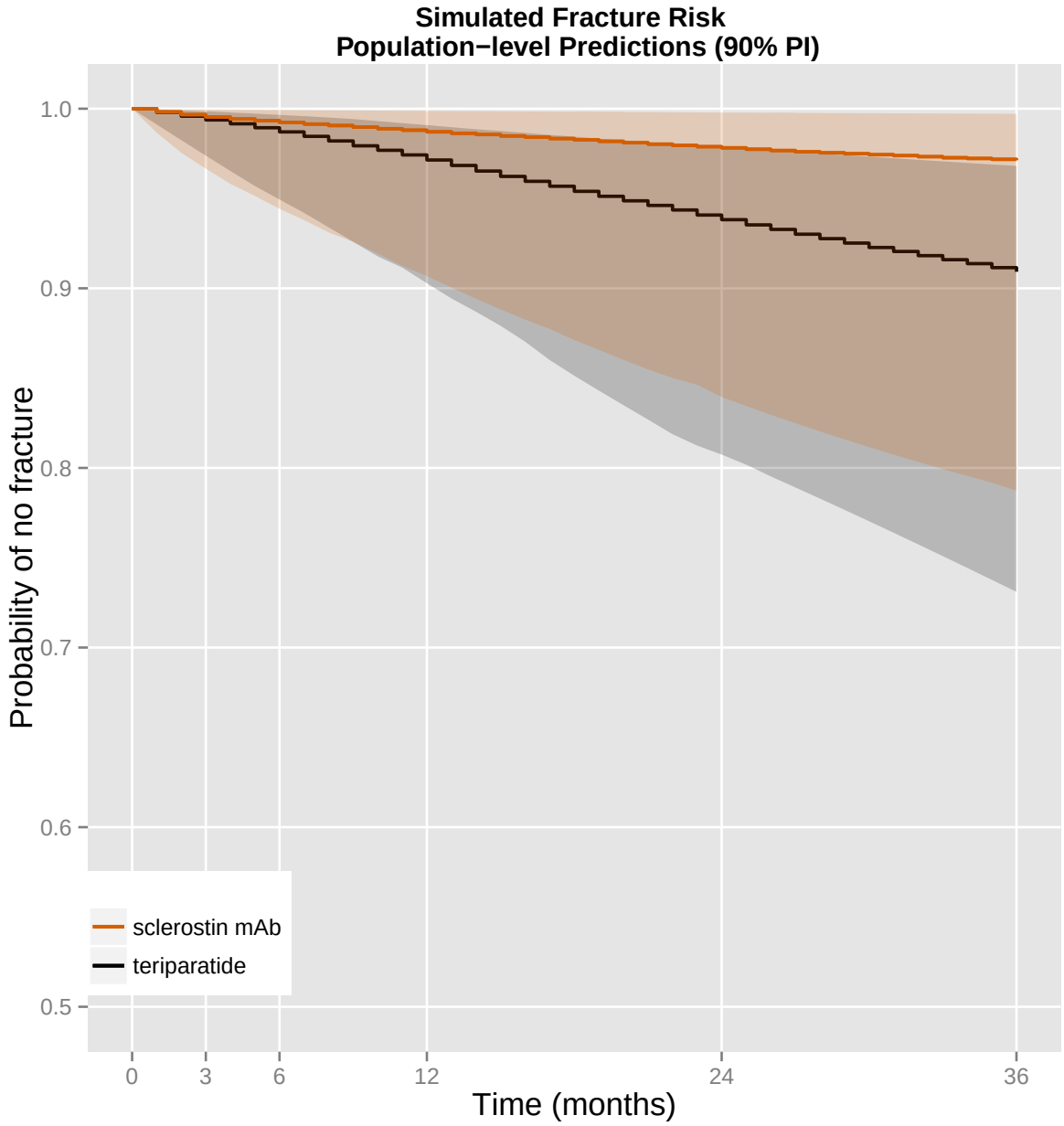

Figure 3.15: Simulated predicted 3-year fracture rate for teriparatide and sclerostin mAb. The shading represents the 90% prediction interval

Chapter 4

Discussion

4.1 AIM I. *A Priori* Analysis: A Comparison of Methods

In almost all cases, the results generated in DAISY and EAR were in agreement, except for instances when DAISY could not resolve the model structure, took an unreasonably long time to compile, or when the initial conditions influenced the EAR analysis. Software specific limitations were encountered in some cases that impacted identifiability results, specifically when DAISY was unable to generate a characteristic set from state variables represented by rational expressions. Differential algebra-based algorithms like DAISY are one of the few types of algorithms that can systematically distinguish global and local identifiability without a user-supplied domain of definition of the parameters or the initial conditions [88]. However, DAISY can accept only some polynomial forms of state variables and cannot analyze QE and QSS approximations which include quadratic expressions. Also in most cases the DAISY program is very fast, but when the model system had a limited number of outputs relative to the number of parameters, the program failed to converge within a reasonable timeframe.

In contrast, EAR can support large and complex systems and is easier to implement because it operates within the Mathematica software package. A limitation of EAR is that the algorithm relies on initial conditions. The inability to perform rank testing independent of initial conditions limits the abil-

ity to establish unique solutions for some TMDD systems with initial conditions equal to zero. DAISY was able to establish identifiability for these systems. Of the three approaches, the profile likelihood (PL) approach requires more in-depth knowledge of the required software and it took the most time to implement. It is also the only approach tested that is sensitive to both *a priori* and *a posteriori* identifiability of model parameters. The PL analysis performed on simulated TMDD data with low variability confirms that all parameters are both *a priori* and *a posteriori* identifiable (see fig. 3.1).

Cheung, et al. [89] illustrated how the issue of nonidentifiablity of PK/PD models can be formally solved by reparameterization or by analysis of parallel experiments [90]. A prerequisite of the reparameterization process is that all system parameters need to be at least locally identifiable, and globally identifiable parameters can be grouped in order to render the entire system globally identifiable. However the nonlinear similarity transformation approach used is highly complex if the system cannot be made into a polynomial form with a linear observation, which was also what prevented global identifiability of the QE system in DAISY. The parallel experiments analysis is a way of achieving global identifiability by formally constraining the system. Neither of these processes can be applied to the antibody-drug conjugate (ADC) system in such a way that the elimination rate of the toxin can be rendered identifiable without explicitly measuring free toxin in the experiment, or by making the assumption that kelT is somehow a function of the other parameters in the system (see table 3.1).

Often achieving TMDD model convergence and well-defined minima under real world experimental conditions is impossible without fixing some parameters or making assumptions to simplify the model [54]. Given the findings of this work, a likely explanation is that it is impractical to achieve an adequate experimental design at the time scales necessary for *a posteriori* identifiability of all parameters and appropriate model approximations should be used to estimate parameters. Following *a priori* identifiability analyses for other complex systems, deoptimization and simulation can be used to explore and explain sources of *a posteriori* nonidentifiability due to experimental noise or sampling conditions.

4.2 AIM II. Implementing PK/PD Model in Bone Model and Determining Model Structure and Parameter Values to Describe Changes in Turnover Markers and BMD

Discussion around the results of parameter estimation and the sclerostin-related changes made to the model is included in chapter 8. An interesting finding of this work is that the BMD compartmental structure describing anabolics and anti-resorbtives is similar, however, an additional compartment added to describe the delay for anabolic therapies to lay down new bone matrix and become mineralized. Within the compartmental structure for each mechanism, parameters were shared between regions. For romosozumab and blosozumab, only the power term on the OB effect was re-estimated for each region. This description supports a dose-dependent response of the mAb according to sclerostin expression in the region tied to the degree of loading in that region [91]. For denosumab and teriparatide, there were different time constants (*kin, kout*) estimated for each region. This supports site-specific remodeling/modeling activity characteristic of each mechanism. Denosumab has demonstrated differential effects of site-specific remodeling and modeling [92]. It has been suggested that teriparatide response is synergistic with loading and depends heavily on mechanical environment at each site [93].

To truly understand site-specific activity of each drug mechanism an understanding of the underlying factors involved in bone microarchitecture is required, but is very complex. It is also important to note not only the difficulties involved in acquisition and analysis of images of bone composition, but the high degree of variability in these process between studies [94]. Some examples of mis-guided interpretations can be 1.) interpreting cortical fragmentation measured as trabeculae [94], 2.) mis-interpretation of incomplete coalescence of adjacent trabeculae as higher cortical "porosity" in a transitional zone, or 3.) mis-interpreting increased cortical thickness as secondary mineralization [72]. These types of analyses should be interpreted with discretion.

However, these analyses are very important, as discussed in chapter 9, changes in turnover markers and aBMD do not automatically correlate with bone strength which is dictated by cortical and trabecular geometry [95, 96]. In fact, Burghardt, et al (2010) found that only volumetric BMD measures

and cortical porosity at the tibia correlated with changes in turnover marker BSAP (not areal BMD or trabecular microarchitecture) [95]. Findings like these have large implications on development of new therapies or combination treatment strategies, especially when only turnover markers and aBMD are measured in early clinical trials.

A few patterns emerge when examining the relationship between changes in microarchitecture, areal bone mineral density (aBMD), and turnover markers between therapies. Anabolic therapies with a strong renewing bone resorption mechanism, as indicated by a decline in CTx, tend to have no change or a decrease in distal 1/3 radius BMD, a site usually associated with changes in cortical bone. However, an analysis by Poole [97] found that teriparatide increased cortical thickness in the femoral neck, an area which sustains habitual mechanical loading. The authors suggest that PTH augments the mechanical load signal to osteocytes to reduce sclerostin secretion and increase formation in these regions, similar to the mechanism of sclerostin inhibition by sclerostin mAbs. Teriparatide is known to increase cortical porosity, which is correlated with bone-specific alkaline phosphatatse (BSAP) [95] and cancellous bone volume [5] owing again to its metabolically active mechanism of high turnover. In essence, teriparatide over-replaces areas of older mineralized bone with new bone with lower mineral content in some areas.

Anti-resorptives, alendronate and denosumab, also elicit greater trabecular and cortical responses in regions of loading, although denosumab has demonstrated improvement over alendronate in total and cortical volumetric bone mineral density (vBMD) and cortical thickness [96]. In the DIRECT study, 3 years of denosumab treatment also resulted in significant increases in BMD from placebo in the 1/3 distal radius, unlike anabolic therapies [98]. It is possible that anti-resorptives are somewhat less discriminating of regions of loading because they have no direct effects on osteocytes (only indirectly through RANKL) and this, combined with increased vBMD at cortical sites, is why the mechanism is able to elicit increased BMD at the distal radius, unlike teriparatide and romosozumab.

The combination of teriparatide and denosumab resulted in a decline in osteoclasts (OC) number, and OB but to a lesser degree [58]. In this arm, trabecular and cortical vBMD increased, cortical thickness increased, consistent with mechanism of denosumab, and cortical porosity was unchanged. It is difficult to say what is the source of the significant improvement of BMD in the regions of loading

in the combination arm. The combination therapy resulted in a slight further reduction in resorbtion activity over the monotherapies, but formation activity was also reduced in this arm. It could be that, in accordance to Poole, et al. theory that PTH, by the same mechanism which causes a reduction in sclerostin, that is, by signaling a remodeling event in the osteocytes, causes more RANKL to be secreted, which in turn amplifies the denosumab effect as more target ligand is sequestered. Sugiyama et al. [93] suggest the significant reduction in OC activity results from the combination of modeling-based formation at specific sites and a non-site specific decline in remodeling-based bone formation. This is consistent with findings of anti-resorptives increasing periosteal bone formation in the hip but not the lumbar spine.

It is known that sclerostin inhibition, unlike teriparatide is not subject to coupled bone formation and resorbtion, dictated by bone remodeling processes, but is instead governed by uncoupled model-based formation and resorption [91, 99], as markers of formation increases while resorbtion markers simultaneously decrease. Sclerostin ablation results in increased cortical bone volume [100], although increases in distal 1/3 radius BMD have not been seen at the doses of sclerostin mAb tested in clinical trials to date. Sugiyama, et al. suggest that perhaps sclerostin levels are reduced in non-weight bearing sites like this and may require much higher doses to see dose-dependent increases in these regions. The attenuation of the modeling response after a year of continuous dosing suggests that there are other mechanostat-related mechanisms at play that cannot be overcome only by blocking sclerostin. The increase in bone mass after mechanical loading in the absence of sclerostin has been demonstrated in mice [100], indicating mechanisms other than sclerostin signaling are implicated in load response. Dkk-1 could increase Wnt/b-catenin in response to loading, independent of sclerostin. Other factors involved in mechanotransduction may include estrogen-receptor alpha (ER-a), insulin-like grown factor 1(IGF-1), leptin, prostanoids, prostaglandin E2 (PGE2), connexin 43, interleukin-11, or BMPs. For this reason, administering sclerostin mAbs in sequence, or in combination with, a remodeling-modifying therapy may be the best approach for achieving sustained increases in BMD.

As microarchitecture analyses become more robust and streamlined this information can be harnessed to inform parameters in the model-based framework developed here. Currently, the model links

aBMD to underlying metabolic processes in the bone, as described by the markers routinely measured in clinical studies. As discussed previously, time constants and implementations for lag-time may indicate translation and signal transduction processes that inform drug mechanism and may help optimize therapeutic combination strategies.

4.3 AIM III. Hazard Model Development to Predict Probability of Fracture

The discussion around the developed hazard model of fracture is included in chapter 9. The hazard model was also used to simulate possible fracture outcomes after combination therapy, similar to the regimen in the Leder study [58]. Both denosumab and teriparatide independently to improve fracture rate, likewise the combination arm showed improved reduction in 10-year probability of fracture (see fig. 3.12). Denosumab also showed improved reduction of fracture rate over teriparatide. This is because the model also predicts that LS BMD continues to rise with repeated dosing while teriparatide rapidly increases LS BMD returns to steady state (fig. 4.1). It is not completely understood why this is the case, but likely the model predicts anabolic effects (increased P1NP) to return to the range of normal even after persistent treatment (see fig. 3.14). CTx activity with denosumab remains significantly below baseline levels, indicating resorption activity is significantly curtailed throughout the duration of treatment with this mechanism.

One of the significant findings of the hazard model development was the necessity of a model parameter representing an additional drug effect, beyond the effects elicited by therapy on BMD. Because this cannot be estimated specifically for sclerostin mAb or combination treatment arms because there are no fracture data available for this new therapy, it is difficult to determine with certainty if these treatments will have an improved effect on fracture beyond denosumab or teriparatide. Simulations with these arms were performed using the same version of the model but without the drug effect. Hazard ratios for the additional drug effect, relative to placebo, are shown in section 3.3. The additional drug effect elicited by bisphosphonates, teriparatide/PTH and denosumab have high probabilities of significantly reducing the hazard of fracture, as compared to placebo, beyond the BMD effects elicited by each therapy. The additional drug effect of calcitonin, the growth secretagogue MK-677 and stron-

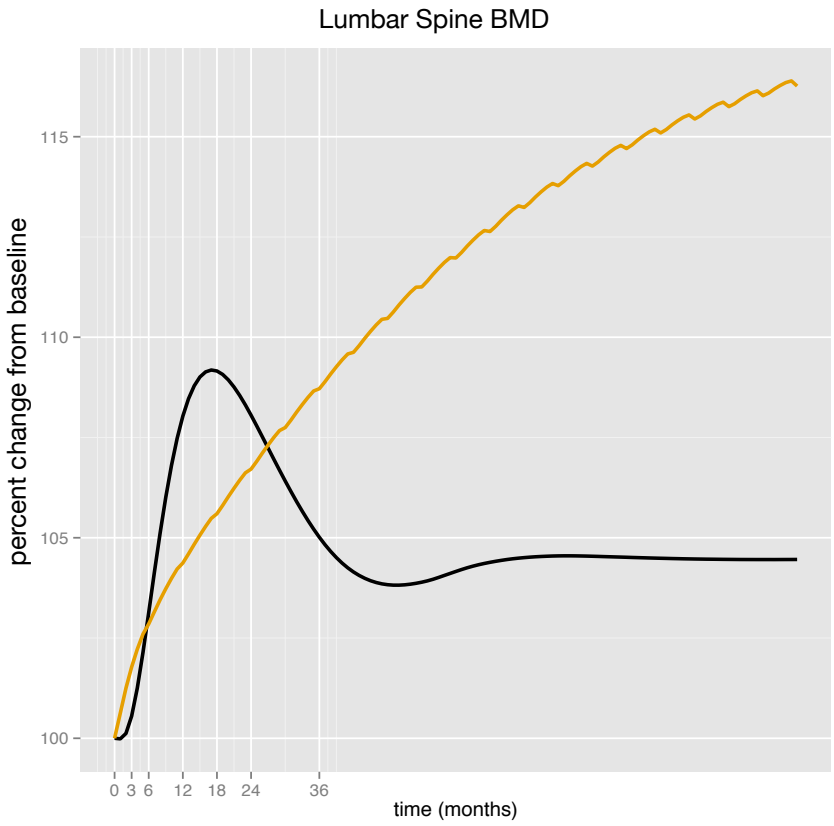

Figure 4.1: 10-year simulations of denosumab (yellow) and teriparatide (black), demonstrating denosumab causes continuous increase in BMD after repeated doses

tium ranelate are not statistically significantly different than the placebo but the sparse data for these treatments arms contribute to the long right tails of the respective posterior distributions.

Chapter 5

Limitations and Future Work

5.1 Limitations and Future Work

Many assumptions are made in the building of this systems model and are discussed at length in papers II and III (chapter 8, chapter 9). Acknowledging these assumptions, making full use of model diagnostic tools and fulfilling "good model criteria", as described in Agoram et al. [101], help to build an objective case for use of this systems model to generate hypotheses, explore optimal dosing regimens and combination therapies, and evaluate different classes of therapies for prevention of fracture.

A major contribution of this work is the ability to link clinical outcomes to underlying biology and microarchitecture in a more mechanistic way. More experimental data is needed to guide this effort. Specifically, there is also a lack of conclusive data linking Wnt-pathway intermediates to sclerostin. This makes it difficult to mechanistically describe the relationship between osteoblasts and osteocytes. β-catenin builds up in the presence of a Wnt signal, which is one of the mechanisms by which blocking sclerostin leads to increased osteoblast activity. Osteocytes also directly produce RANKL [102] but presentation of RANKL at the cell surface is also tightly regulated by OPG in osteocytes [103]. There is evidence to suggest membrane-bound RANKL on osteocytes plays a more significant physiological role on osteoclastogenesis, contributing to localized bone remodeling [104]. There is also a temporal element to Wnt signaling effects on osteoblast differentiation. For example, knocking out β-catenin in

osteoblasts did not change RunX2 levels, which suggests that early signals of osteoblast differentiation do not depend on β-catenin but β-catenin is essential for mature osteoblasts' performance through osteocalcin expression [33]. Because much is still unknown about the differentiation process of osteoblasts, osteocytes and osteoclasts and how the signaling pathways influence these processes, it is difficult to fully characterize the pathway intermediates in the model.

As discussed previously, there are also sclerostin-independent mechanisms which govern modeling [100]. BMP works upstream of sclerostin in osteoblasts to inhibit Wnt signaling [105]. However, sclerostin can, in turn, antagonize BMP [31]. Dkk-1, like sclerostin is also a Wnt-pathway inhibitor and is also regulated by BMP. In an *in vivo* study, sclerostin mAb administration resulted in an increase of dkk-1 [106]. The authors of this study suggest the osteocytes themselves may regulate modeling through the "mechanostat" mechanism by increasing expression of SOST and dkk-1. In a clinical study with denosumab circulating levels of sclerostin increased, while dkk-1 decreased [107], which may also indicate feedback signaling in response to treatment, at the level of the osteocyte. IL-6 has also been shown to increase during osteocyte apoptosis [31], but mRNA expression decreases during exercise in a rat model of osteoporosis [108], thereby reducing resorption during loading. These all represent additional layers of regulation by which osteocytes can direct modeling activity. These are mechanisms not currently represented in the bone model but should be implemented in future work.

In the fracture model, outlined in chapter 9, LS BMD is the major driver of changes in fracture rate contributed by most of the drug classes represented in the dataset. This assumes that the integrated effects on LS BMD resulting from the action of different drug mechanisms contribute to changes in fracture rate in the same way. This assumption does not account for differences in patient response to therapy and does not acknowledge that measures of LS BMD may not be fully representative of changes in bone quality attributed by each drug mechanism individually. In the latter case, including the additional drug effect covariate accounts for the contribution of each mechanism to the probability of fracture independent of LS BMD. The interpretation of this covariate is rather vague but is discussed at length in the discussion section of paper III (chapter 9). In future work the model maybe improved upon by including more data at the level of the individual patient and incorporate some measure of bone quality (volumetric BMD, trabecular or cortical thickness, ect) into the calculation of fracture

probability.

As described in Aim I (section 1.4), there are many mechanistic models in the literature which describe the effects of loading and shear stress on osteocyte activity and sclerostin production. Another future application of the model is leveraging finite element analysis data to describe localized remodeling in bone occurring during loading. This would allow model application to extend beyond osteoporosis with BMD outcomes to bone healing during traumatic events or implant placement [36]. Several efforts have been made to link the function of mechanoreceptors to biochemical signals in the loading process [41]. Still, all of the osteocytic signaling molecules involved in inhibition of bone resorption during loading and the extent of their involvement in this process have not been fully identified. Current models are limited to aspects of loading in narrower terms, such as osteon diameter in response to an osteocyte signal [41] or mechanical bone adaptation only at the bone surface [109]. Propagation of chemical signaling after mechanical stimuli to bone cell populations is an aspect of osteocyte function within the remodeling process that is still needed in the current model of calcium homeostasis.

Chapter 6

Conclusion

6.1 Conclusion

This work demonstrates:

- *A priori* identifiability of PK/PD models typically used to describe mAbs using differential algebra identifiability of systems (DAISY), exact arithmetic rank (EAR) and likelihood profiling (LP) and drawing a comparison of these methods.
- PK/PD model development of sclerostin mAb and circulating serum sclerostin using a TMDD approximation of Michaelis-Menten (MM) kinetics.
- Implementation of this PK/PD model into the MSPM in order to investigate the role of osteocytes in the remodeling process and link OCY activity to changes in OB and OC.
- Development of model structure and estimation of parameters for regional changes in BMD after sclerostin, teriparatide, denosumab, or combination therapy.
- Development of a hazard model for fracture using a systematically-derived metadata set
- Linking MSPM-simulated LS BMD to the fracture model in order to compare effects of therapy on fracture risk.

Quantitative model building can inform both experimental research and drug development. In the context of bone remodeling, models are used to understand signaling pathways and feedback processes that are highly regulated and often misunderstood. Models can also be used as powerful simulation tools to investigate dosing regimens or combinations of therapies in patients, when perhaps little information about a new therapy is available. As computational models increasingly become an integral part of experimental research, both bodies of work inform one another to quickly bring new therapies to market as well as promote a greater understanding of the underlying physiology. This original work is only a small representative piece of continuing advancements in mathematical modeling and points towards a future of stronger collaborative efforts between experimental and theoretical groups to advance bone biology research.

Chapter 7

PAPER I

The AAPS Journal, Vol. 17, No. 5, September 2015 (© 2015)
DOI: 10.1208/s12248-015-9795-8

Brief/Technical Note

A Priori Identifiability of Target-Mediated Drug Disposition Models and Approximations

Rena J. Eudy,[1,2,4] Matthew M. Riggs,[3] and Marc R. Gastonguay[1,2,3]

Received 23 March 2015; accepted 29 May 2015; published online 16 June 2015

Abstract. *A priori* identifiability of mathematical models assures that for a given input/output experiment, the parameter set has one unique solution within a defined space, independent of the experimental design. Many biologic therapeutics exhibit target-mediated drug disposition (TMDD), and use of the full compartmental model describing this system is well documented. In practice, estimation of the full parameter set for TMDD models, given real-world clinical data, is characterized by convergence difficulties and unstable solutions. Still, the formal assessment of the *a priori* identifiability of these systems has yet to be reported. The exact arithmetic rank (EAR) approach was used to test the *a priori* identifiability of a TMDD model as well as model approximations. The full TMDD and quasi-equilibrium/rapid binding (QE/RB), quasi-steady state (QSS), and Michaelis-Menten (MM) approximations were fully identifiable, *a priori*, regardless of whether observations were taken from a single or multiple compartments. The results of these identifiability analyses indicated that the difficulty with TMDD model convergence, *a posteriori*, lies in the experimental design, not in the mathematical identifiability in the lack of samples from several compartments. Experiments can be tailored to resolve these structurally non-identifiable parameters, notwithstanding practical implementation challenges. This work highlights the importance of identifiability analyses, specifically how they can influence experimental design and selection of the appropriate model structure to describe a dynamic biological system.

KEY WORDS: approximation; *a posteriori*; *a priori*; identifiability; target-mediated.

INTRODUCTION

A priori global identifiability analysis is the process of determining if different combinations of parameter values lead to indistinguishable model output in terms of inherent model structure (1). A system is *a priori* globally identifiable (also known as structurally or mathematically identifiable) if all parameters have a unique solution within the full domain of the parameter space, given specific observation points within the system. A system is locally identifiable if a unique solution to a parameter is found within some neighborhood of that parameter (2). In contrast, *a posteriori*, also known as practical identifiability, is the quality of a system that determines whether or not parameters can be estimated based on informativeness of an experimental design and resulting data. *A priori* identifiability is a requirement for a well-posed mathematical system and a prerequisite for parameter estimation because if identifiability is not achieved independent of experimental design conditions, the system will not be identifiable in practice. Determining which parameters in the system are not identifiable before running an experiment may save resources by informing experimental design. Unfortunately, this practice is underutilized because of the computational complexity involved in these analyses.

Establishing *a priori*, identifiability for the highly nonlinear models common in systems biology is especially nontrivial in cases when there are many more parameters than observables. A comparison of three approaches for evaluating identifiability for complex systems (two of these were focused on *a priori*) was recently published by Raue and colleagues (3) and forms the basis for the approaches considered in this analysis. Of these methods, the exact arithmetic rank (EAR) approach was the most robust and most easily implemented. The *a priori* identifiability of the widely used target-mediated drug disposition (TMDD) model, describing the dynamic system of antibodies binding to the target molecule (4), and approximations to this model has never been established. Gibiansky and Gibiansky also formulated extension of this model to include two-target TMDD (5). The model equations for the TMDD model represent amounts of free drug, target, the drug-target

Electronic supplementary material The online version of this article (doi:10.1208/s12248-015-9795-8) contains supplementary material, which is available to authorized users.

[1] Metrum Institute, 2 Tunxis Road, Suite 112, Tariffville, Connecticut 06081, USA.
[2] Department of Biomedical Engineering, University of Connecticut, A.B.. Bronwell Building, Room 217, 260 Glenbrook Road, Unit 3247, Storrs, Connecticut 06269-3247, USA.
[3] Metrum Research Group, LLC, 2 Tunxis Road, Suite 112, Tariffville, Connecticut 06081, USA.
[4] To whom correspondence should be addressed. (e-mail: renae@metrumrg.com)

complex, and the transfer rates between these states (Fig. 1), and the extension includes dual targets and complexes (Fig. 2). Model approximations include quasi-equilibrium or rapid binding (QE/RB), quasi-steady state (QSS), and Michaelis-Menten (MM) (6). While approximations to the model make it possible for one to mathematically describe experimental data, the interpretation of these model parameter values can be vague or even inaccurate (6). Identifying system parameters that are not unique, *a priori*, indicates the need for re-parameterization or model simplification in advance of the parameter estimation step. *A priori* analyses may also assist in understanding which modifications of the experimental design are necessary to achieve meaningful parameter estimates.

METHODS

Of the three different approaches discussed by Raue and colleagues (3), the exact arithmetic rank (EAR) approach was chosen to evaluate parameter identifiability for TMDD models and their approximations. The EAR approach was developed by Karlsson and colleagues (7) and is designed to handle larger systems with more generally parameterized initial conditions. This algorithm constructs a symbolic form of the Jacobian matrix by way of generating a truncated power series expansion of partial derivatives of the output with respect to state variable $x(0)$ (the value of each compartment at its initial condition) and parameter θ and performs rank testing, the process of relating higher order derivatives to lower order derivatives and using the inverse function theorem, to determine local identifiability.

Single-target TMDD (Fig. 1) and QE/RB, QSS, and MM approximation models were tested first, followed by a TMDD model with two targets (Fig. 2). The input of each model was an intravenous (i.v.) infusion or subcutaneous (s.c.) dose. Whether or not the output scenario was plausible, all were included in the analysis for completeness and for use as a reference. To use EAR, the package "IdentifiabilityAnalysis" was loaded in Mathematica (v9.0). The differential equation set and initial conditions were assigned to variable *deq*. In this approach, the initial conditions must be supplied by the user, even if they are unknown and set to zero, as they are required to construct the Jacobian. The arguments to the IdentifiabilityAnalysis function are simply *deq*, the system outputs, a vector of variables, the independent variable (*t*), and the input variable (*u*). The vector of variables represents the parameters in the model but are supplied symbolically and assigned no values or bounds. If the results of the analysis are "false," the system is unidentifiable and the parameters without unique solutions can be identified with the call "NonIdentifiableParameters." Example code for a full TMDD model analysis is included in the Supplementary Materials.

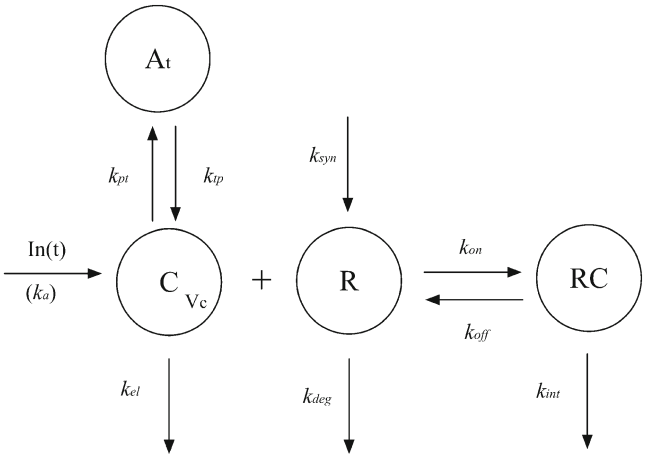

Fig. 1. TMDD model schematic. *C*, *R*, *RC*, and A_t represent the drug concentration, target, drug-target complex, and peripheral compartments, respectively. *Ks* indicate time constants

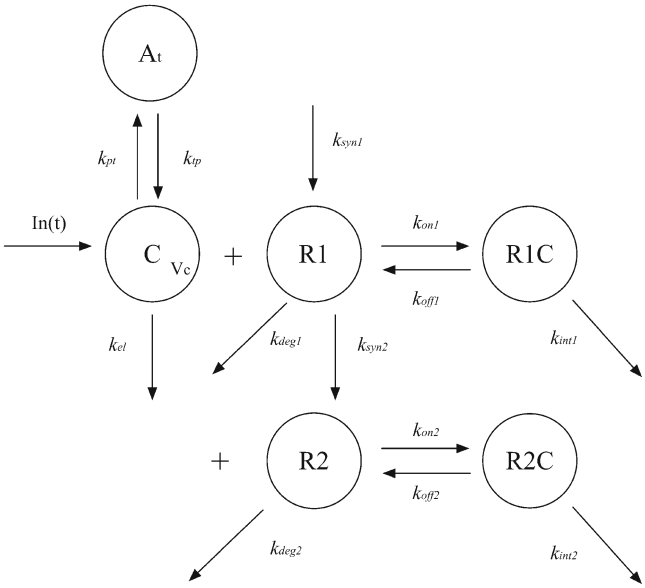

Fig. 2. Extension of the TMDD model to the two-target case. *C*, *R1*, *R2*, *R1C*, *R2C* and A_t represent the drug concentration, targets 1 and 2, drug-target complexes 1 and 2, and peripheral compartments, respectively. *Kss* indicate time constants

RESULTS

Results for all model structures and output scenarios are shown in Tables I and II. The full single-target TMDD model was identifiable with any system output. It follows that the QE/RB, QSS, and MM are also identifiable with any output. Like the single-target TMDD, the 2-target TMDD model structure was found to be identifiable under any output scenario.

DISCUSSION

The EAR application has been used to demonstrate *a priori* identifiability of TMDD models and model approximations within scenarios when different outputs are available. The full TMDD model is *a priori* identifiable, even when only information about the drug (free or total) is available. This was not an obvious finding because *a posteriori* parameter estimates are often imprecise at best, and usually at least one parameter must be fixed in order for the model to converge. Gibiansky et al. show many examples of this in their 2009 publication (8). Often, it is the time scale of the drug measurements being much greater than that of the

Table I. Identifiability Results for Full TMDD and Approximations (Supplemental 1 Eqs 1–20)

Model	Full TMDD, iv inf						
System parameters	k_{on}, k_{off}, k_{el}, k_{pt}, k_{tp}, Vc, k_{syn}, k_{deg}, k_{int}						
Possible outputs	Free drug	Target	Complex	Free drug and target	Free drug and complex	Target and complex	Free drug, target, and complex
Result	Model is locally identifiable with any output						
Model	Full TMDD, sc dose						
System parameters	k_a, k_{off}, k_{el}, k_{pt}, k_{tp}, Vc, k_{syn}, k_{deg}, k_{int}						
Possible outputs	Free drug	Target	Complex	Free drug and target	Free drug and complex	Target and complex	Free drug, target, and complex
Result	Model is locally identifiable with any output						
Model	Quasi-equilibrium (QE) approximation, iv inf						
System parameters	k_d, k_{el}, k_{pt}, k_{tp}, Vc, k_{syn}, k_{deg}						
Possible outputs	Free drug	Target	Total target	Free drug andtotal drug	Free drug and total target	Total drugand total target	Free drug, total drug, and total target
Result	Model is locally identifiable with any output						
Model	Quasi-steady-state (QSS) approximation, iv inf						
System parameters	K_{ss}, k_{el}, k_{pt}, k_{tp}, Vc, k_{syn}, k_{deg}						
Possible outputs	Free drug	Target	Total target	Free drug and total drug	Free drug and total target	Total drug and total target	Free drug, total drug, and total target
Result	Model is locally identifiable with any output						
Model	Michaelis-Menton (MM), iv inf						
System parameters	K_m, k_{int}, k_{el}, k_{pt}, k_{tp}, Vc, k_{syn}, k_{deg}						
Possible outputs	Free drug	Total target	Free drug and total target				
Result	Model is locally identifiable with any output						

TMDD target-mediated drug disposition, *QSS* quasi-steady-state, *QE* quasi-equilibrium, *MM* Michaelis-Menten, *iv inf* intravenous infusion, *sc* subcutaneous

Table II. Identifiability Results for TMDD Model Extension (Supplemental 1 Eqs 21–27)

Model	TMDD 2-target, iv inf			
System parameters	k_{deg1}, k_{deg2}, k_{on1}, k_{on2}, k_{off1}, k_{off2}, k_{el}, k_{pt}, k_{tp}, Vc, k_{syn1}, k_{syn2}, k_{int1}, k_{int2}			
Possible outputs	Free drug	Targets	Complexes	Free drug and a single target	Free drug and a single complex
	Free drug and both targets	Free drug and both complexes	Targets and complexes	Free drug, target, and complex for a single target	Free drug, target, and complex for both targets
Results	Model is locally identifiable with any output				

TMDD target-mediated drug disposition, *QSS* quasi-steady-state, *QE* quasi-equilibrium, *MM* Michaelis-Menten, *iv inf* intravenous infusion

binding process that limits practical identifiability of kon and koff. The QE or QSS approximations are often used to avoid overparameterization. Selection between these approximations involves availability of target dynamics or pharmacodynamic data (9). Peletier and Gabrielson determined that specific regions of the drug concentration curve inform specific model parameters and parameter identifiability largely depends on the richness of data in each of these regions (10). These identifiability results confirm that all parameters in a full TMDD model can be uniquely estimated using a dataset with ideal sampling and no experimental noise. The full two-target TMDD system is also structurally identifiable under the same conditions.

Of the available approaches used for establishing structural identifiability of a system, the EAR algorithm was relied upon as the more robust of the approaches, specifically for approximations to the TMDD model when the model contains rational expressions that cannot easily be converted to polynomial. A limitation of EAR is that the algorithm cannot perform rank testing independent of initial conditions, and this limits the ability to establish unique solutions for some systems with initial conditions equal to zero. The differential identifiability of systems (DAISY) approach (11) was used as a first-pass attempt at establishing global *a priori* identifiability. Unfortunately, DAISY can only deal directly with pure polynomial forms for the differential equations, and the program did not accept the quadratic solution form for free drug concentration, *C*, that is used in the QE and QSS approximations. This shortcoming of DAISY is well documented (3, 12). Finally, the profile likelihood (PL) approach was also considered, but it is a data-based approach and not a specific analysis of *a priori* identifiability.

CONCLUSION

In the case of single-target TMDD models and approximations, all parameters are *a priori* identifiable, as is the full two-target TMDD model. These findings indicate that sampling times relative to the widely varying time scale of binding kinetics *vs*. distribution and elimination kinetics are the most likely culprit limiting *a posteriori* identifiability of TMDD model parameters. The principle of *a priori* identifiability is that a unique solution can be found under ideal sampling times and error-free experimental conditions. While noise-free systems do not exist, identifiability analyses are an important first step in model design. If parameters are found not to be structurally identifiable, they will never be *a posteriori* identifiable when experimental noise and design limitations abound. As shown in Gibiansky and Gibiansky (13), it is possible to achieve good model fits without establishing identifiability of model parameters. In this same work, however, it was noted that resulting parameter estimates were not always accurate or reliable reflections of the proposed drug disposition mechanisms. Identifiability analyses, on the other hand, allow for meaningful interpretation of parameters under "real-world" conditions if model assumptions hold. Non-identifiability in these types of analyses can indicate the necessity for model simplification and show when more information is needed within a given experimental design to achieve *a posteriori* identifiability of

all parameters. Recent advances of computational algorithms allow for easy and fast determination of structural identifiability of a biological system.

REFERENCES

1. Lamberton TO, Condon ND, Stow JL, Hamilton NA. On linear models and parameter identifiability in experimental biological systems. J Theor Biol. 2014;358:102–21. doi:10.1016/j.jtbi.2014.05.028.
2. Jacqueiz JA, Greif P. Numerical parameter identifiability and estimability: integrating identifiability, estimability, and optimal sampling design. Math Biosci. 1985;(77):201–27. doi:10.1016/0025-5564(85)90098-7.
3. Raue A, Karlsson J, Saccomani MP, Jirstrand M, Timmer J. Comparison of approaches for parameter identifiability analysis of biological systems. Bioinformatics. 25(15):1923–9. doi:10.1063/1.3528102.
4. Mager DE, Jusko WJ. General pharmacokinetic model for drugs exhibiting target-mediated drug disposition. J Pharmacokinet Pharmacodyn. 2001;28(6):507–32.
5. Gibiansky L, Gibiansky E. Target-mediated drug disposition model for drugs that bind to more than one target. J Pharmacokinet Pharmacodyn. 2010;37(4):323–46. doi:10.1007/s10928-010-9163-3.
6. Gibiansky L, Gibiansky E, Kakkar T, Ma P. Approximations of the target-mediated drug disposition model and identifiability of model parameters. J Pharmacokinet Pharmacodyn. 2008;35(5):573–91. doi:10.1007/s10928-008-9102-8.
7. Karlsson, J, Anguelova M, Jirstrand, M. An Efficient Method for Structural Identiability Analysis of Large Dynamic Systems. SYSID 2012: Proceedings of the 16th IFAC Symposium on System Identification; 2012 Jul 11-13; Brussels, Belgium. p. 941–946.
8. Gibiansky L, Gibiansky E. Target-mediated drug disposition model: approximations, identifiability of model parameters and applications to the population pharmacokinetic-pharmacodynamic modeling of biologics. Expert Opin Drug Metab Toxicol. 2009;5(7):803–12. doi:10.1517/17425250902992901.
9. Yan X, Mager DE, Krzyzanski W. Selection between Michaelis-Menten and target-mediated drug disposition pharmacokinetic models. J Pharmacokinet Pharmacodyn. 2010;37(1):25–47. doi:10.1007/s10928-009-9142-8.
10. Peletier LA, Gabrielsson J. Dynamics of target-mediated drug disposition: characteristic profiles and parameter identification. J Pharmacokinet Pharmacodyn. 2012;39(5):429–51. doi:10.1007/s10928-012-9260-6.
11. Saccomani MP, Bellu G. DAISY: an efficient tool to test global identifiability. Some case studies. Proceedings of the16th Mediterr Conf Control Autom. 2008 Jun 25-27; Ajaccio, France. p. 1723–8. doi:10.1109/MED.2008.4602152.
12. Chis O-T, Banga JR, Balsa-Canto E. Structural identifiability of systems biology models: a critical comparison of methods. PLoS ONE. 2011;6(11):e27755. doi:10.1371/journal.pone.0027755.
13. Gibiansky, L, Gibiansky E. Numerical Testing of Assumptions for Target-Mediated Drug Disposition (TMDD) Equations: Why Inexact Model Provides Satisfactory Description? PAGE 2014; Proceedings of Population Approach Group Europe Conference; 2014 Jun 11-14; Alicante, Spain.

Supplemental 1: Model Equations

Full Target-Mediated Drug Disposition (TMDD) Model

In(t) refers to a continuous i.v. infusion

$$\frac{dA_d}{dt} = -k_a A_d \tag{1}$$

$$\frac{dC}{dt} = \frac{ln(t) + k_a A_d}{Vc} - (k_{el} + k_{pt})C - k_{on} C \cdot R + k_{off} RC + k_{tp} \frac{A_T}{Vc} \tag{2}$$

$$\frac{dA_T}{dt} = k_{pt} C \cdot Vc - k_{tp} A_T \tag{3}$$

$$\frac{dR}{dt} = k_{syn} - k_{deg} R - k_{on} C \cdot R + k_{off} RC \tag{4}$$

$$\frac{dRC}{dt} = k_{on} C \cdot R - (k_{int} + k_{off})RC \tag{5}$$

$$A_d = Dose; \quad C(0) = 0; \quad A_T(0) = 0; \quad RC(0) = 0; \quad R(0) = \frac{k_{syn}}{k_{deg}} \tag{6}$$

Equations from: D. E. Mager and W. J. Jusko. General pharmacokinetic model for drugs exhibiting target-mediated drug disposition. *J Pharmacokinet Pharmacodyn*, 28(6):507-532, Dec 2001.

Quasi-Equilibrum/Rapid Binding (QE/RB) Approximation

In(t) refers to a continuous i.v. infusion

$$C = \frac{1}{2}\left[(C_{tot} - R_{tot} - K_D) + \sqrt{(C_{tot} - R_{tot} - K_D)^2 + 4K_D C_{tot}}\right] \tag{7}$$

$$\frac{dC_{tot}}{dt} = \frac{ln(t)}{Vc} - k_{int}C_{tot} - (k_{el} + k_{pt} - k_{int})C + \frac{k_{tp}A_T}{Vc} \tag{8}$$

$$\frac{dA_T}{dt} = k_{pt}C \cdot Vc - k_{tp}A_T \tag{9}$$

$$\frac{dR_{tot}}{dt} = k_{syn} - k_{deg}R_{tot} - (k_{int} - k_{deg})(C_{tot} - C) \tag{10}$$

$$C_{tot}(0) = 0; \quad A_T(0) = 0; \quad R_{tot}(0) = \frac{k_{syn}}{k_{deg}} \tag{11}$$

Equations from: L. Gibiansky, E. Gibiansky, T. Kakkar, and P. Ma. Approximations of the target-mediated drug disposition model and identifiability of model parameters. *J Pharmacokinet Pharmacodyn*, 35(5):573-591, Oct 2008.

Quasi-Steady-State (QSS) Approximation

In(t) refers to a continuous i.v. infusion

$$C = \frac{1}{2}\left[(C_{tot} - R_{tot} - K_{SS}) + \sqrt{(C_{tot} - R_{tot} - K_{SS})^2 + 4K_{SS}C_{tot}}\right] \tag{12}$$

$$\frac{dC_{tot}}{dt} = \frac{ln(t)}{Vc} - (k_{el} + k_{pt})C - \frac{R_{tot}k_{int}C}{K_{SS} + C} + \frac{K_{tp}A_T}{Vc} \tag{13}$$

$$\frac{dA_T}{dt} = k_{pt}C \cdot Vc - k_{tp}A_T \tag{14}$$

$$\frac{dR_{tot}}{dt} = k_{syn} - k_{deg}R_{tot} - (k_{int} - k_{deg})\frac{R_{tot}C}{K_{SS} + C} \tag{15}$$

$$C_{tot}(0) = 0; \quad A_T(0) = 0; \quad R_{tot}(0) = \frac{k_{syn}}{k_{deg}} \tag{16}$$

Equations from: L. Gibiansky, E. Gibiansky, T. Kakkar, and P. Ma. Approximations of the target-mediated drug disposition model and identifiability of model parameters. *J Pharmacokinet Pharmacodyn*, 35(5):573-591, Oct 2008.

Michaelis Menten (MM) Approximation

In(t) refers to a continuous i.v. infusion

$$\frac{dC}{dt} = \frac{ln(t)}{Vc} - (k_{el} + k_{pt})C - \frac{R_{tot}k_{int}}{K_m + C} + \frac{k_{tp}A_T}{Vc} \tag{17}$$

$$\frac{dA_T}{dt} = k_{pt}C \cdot Vc - k_{tp}A_T \tag{18}$$

$$\frac{dR_{tot}}{dt} = R_{syn} - k_{deg}R_{tot} - (k_{int} - k_{deg})\frac{R_{tot}C}{K_m + C} \tag{19}$$

$$C(0) = 0; \quad A_T(0) = 0; \quad R_{tot}(0) = \frac{k_{syn}}{k_{deg}} \tag{20}$$

Equations from: L. Gibiansky, E. Gibiansky, T. Kakkar, and P. Ma. Approximations of the target-mediated drug disposition model and identifiability of model parameters. *J Pharmacokinet Pharmacodyn*, 35(5):573-591, Oct 2008.

TMDD Extended to Two Targets

In(t) refers to a continuous i.v. infusion

$$\frac{dC}{dt} = \frac{k_{tp}A_T + In(t)}{Vc} - (k_{el} + k_{pt})C - (k_{on1}C \cdot R_1 + k_{on2}C \cdot R_2) + (k_{off1}R_1C + k_{off2}R_2C) \quad (21)$$

$$\frac{dA_T}{dt} = k_{pt}CVc - k_{tp}A_T \quad (22)$$

$$\frac{dR_1}{dt} = k_{syn1} - k_{deg1}R_1 - k_{on1}C \cdot R_1 + k_{off1}R_1C \quad (23)$$

$$\frac{dR_2}{dt} = k_{syn2} - k_{deg2}R_2 - k_{on2}C \cdot R_2 + k_{off2}R_2C \quad (24)$$

$$\frac{dR_1C}{dt} = k_{on1}C \cdot R_1 - (k_{int1} + k_{off1})R_1C \quad (25)$$

$$\frac{dR_2C}{dt} = k_{on2}C \cdot R_2 - (k_{int2} + k_{off2})R_2C \quad (26)$$

$$C(0) = 0;\ \ A_T(0) = 0;\ \ R_1(0) = \frac{k_{syn1}}{k_{deg1}};\ \ R_2(0) = \frac{k_{syn2}}{k_{deg2}};\ \ R_1C(0) = 0;\ \ R_2C(0) = 0 \quad (27)$$

Equations from: L. Gibiansky and E. Gibiansky. Target-mediated drug disposition model for drugs that bind to more than one target. *J Pharmacokinet Pharmacodyn*, 37(4):323-46, Aug 2010.

Chapter 8

PAPER II

Citation: CPT Pharmacometrics Syst. Pharmacol. (2015) 00, 00; doi:10.1002/psp4.12013

ORIGINAL ARTICLE

Connecting the Dots: Linking Osteocyte Activity and Therapeutic Modulation of Sclerostin by Extending a Multiscale Systems Model

RJ Eudy[1,2], MR Gastonguay[1,2,3], KT Baron[3] and MM Riggs[3]

The goal of this work was to extend a mathematical, multiscale systems model of bone function, remodeling, and health in order to explore hypotheses related to therapeutic modulation of sclerostin and quantitatively describe purported osteocyte activity within bone remodeling events. A pharmacokinetic model with first-order absorption and dual elimination pathways was used to describe the kinetics of romosozumab, a monoclonal antibody (mAb) against sclerostin. To describe total circulating sclerostin, an extended indirect response model of inhibition of offset was developed. These models were subsequently linked to the systems model, with sclerostin signaling changes in resorption and formation through established osteocyte-mediated mechanisms. The model proposes relative contributions of the osteocyte to the RANKL pool, a major player in feedback signaling, and is used to explore hypotheses surrounding attenuation of anabolic activity after multiple doses of sclerostin mAbs, a phenomenon whose mechanism is poorly understood.
CPT Pharmacometrics Syst. Pharmacol. (2015) **00**, 00; doi:10.1002/psp4.12013; published online on 0 Month 2015.

Study Highlights

WHAT IS THE CURRENT KNOWLEDGE ON THE TOPIC? ☑ The current systems pharmacology models that include osteocyte activity or sclerostin mAb intervention are not designed to predict quantitative clinical outcomes. • WHAT QUESTIONS DID THIS STUDY ADDRESS? ☑ Is it possible to leverage the clinical study data available with sclerostin mAbs to extend a systems model to predict responses to therapeutic modulation of sclerostin and describe osteocyte activity within bone remodeling events? • WHAT THIS STUDY ADDS TO OUR KNOWLEDGE ☑ The extended systems model can be used to examine hypotheses surrounding the mechanism for attenuation of anabolic activity after multiple doses of sclerostin mAbs. This has not been fully explored by laboratory experimentation. It is also used to investigate the relative contribution of osteocytes to feedback regulation within the bone. • HOW THIS MIGHT CHANGE CLINICAL PHARMACOLOGY AND THERAPEUTICS ☑ The extended model can be used to explore therapeutic target modulation in order to maximize and maintain increased BMD in osteoporosis patients.

Sclerostin has been identified as a target for osteoporosis treatment because preventing sclerostin inhibition of Wnt has been shown to both increase markers of bone formation and decrease markers of resorption, expanding net gain of bone calcification and increasing bone mineral density (BMD).[1] This mechanism, which "decouples" bone formation and resorption, is differentiated from other osteoporosis treatment mechanisms that are either purely anabolic (both formation and resorption increase, e.g., intermittent parathyroid hormone (PTH)) or catabolic (both formation and resorption decrease, e.g., bisphosphonates, RANKL-inhibition). Furthermore, sclerostin is mainly expressed in the osteocyte, limiting off-target effects of inhibition in other tissues.

Questions remain about the mechanism of sclerostin inhibition and how this is linked to osteocyte activity and feedback regulation in bone remodeling.[2] One clinical question is whether or not efficacy can be maintained after multiple doses of an anti-sclerostin monoclonal antibody (mAb). Identification of appropriate dosing regimens of sclerostin mAb and/or its combination with an antiresorptive to promote greater formation and prolonged maintenance of strong bone is a critical step in the advancement of this therapy. Potential for a model that is aimed at elucidating the mechanisms of sclerostin modulation includes exploration of dosing regimen and trial design considerations. Such inputs, although not meant at this stage to generate statistical probabilities, could generate hypotheses (learnings) for further experimental confirmation, e.g., through clinical investigation.

A multiscale bone model has been published[3] that combines important aspects of three previous models of bone in order to combine quantitative aspects of bone physiology: all major organ systems involved in calcium handling,[4] feedback control between osteoblasts (OB) and osteoclasts (OC) through the Receptor Activator of Nuclear Factor κ#/RANK-ligand/Osteoprogerin (RANK/RANKL/OPG) axis,[5] and dynamics of intermittent PTH administration.[6] In its current construct, the model lacks the osteocyte and sclerostin-related components necessary to predict effects of sclerostin mAb treatment on clinical outcomes like BMD. Other published models of sclerostin, osteocytes (OCY),

[1]Department of Biomedical Engineering, University of Connecticut, Storrs, Connecticut, USA; [2]Metrum Institute, Tariffville, Connecticut, USA; [3]Metrum Research Group, Tariffville, Connecticut, USA. Correspondence: RJ Eudy (renae@metrumrg.com)
Received 1 May 2015; accepted 12 July 2015; published online on 0 Month 2015. doi:10.1002/psp4.12013

and Wnt signaling are either qualitative in nature, with model variables lacking physiological meaning,[7] or they are focused on mechanical strain analysis.[8,9] The "strain" models depict quantitative changes in a single bone unit during loading, but they do not account for feedback signaling between bone cells, which largely contribute to signal transduction and remodeling. In contrast with other models, the multiscale bone model provides an evaluated platform to predict changes in BMD based on clinical markers of formation and resorption. It has already been used to predict changes in BMD after treatment with denosumab.[10] The new model components were developed by incorporating knowledge of the Wnt/β-catenin signaling and its role in bone formation by leveraging data from recent clinical studies.[1,11,12] The updated model promotes understanding of how OCY signals contribute to remodeling within the bone and how sclerostin mAbs can be used to harness these signals to maximize bone formation in patients with osteoporosis.

MATERIALS AND METHODS

Data

A phase I study reporting time–concentration profiles of romosozumab after a single dose[1] was used to build the pharmacokinetic (PK) model. Total sclerostin concentrations measured in two phase I studies over a range of single and multiple doses of blosozumab[12] were used to estimate parameters in the pharmacodynamics (PD) model. C-terminal telopeptide (CTx) and procollagen type 1 N propeptide (P1NP) data from these three studies and two additional studies[11,13] were used to build the sclerostin-related components and BMD changes into the model. A sixth was used as a qualification dataset.[14]

The bone formation marker, serum P1NP, as a marker of bone formation, has replaced serum bone-specific-alkaline-phosphatase (BSAP) in newer clinical trials. Since the existing model only described changes in BSAP, a regression model was developed to calculate P1NP as a function of BSAP. Data collected from 21 different studies (Supporting Information refs. 4-22) identified by a PubMed search conducted on or around March 6, 2014, using keywords "osteoporosis" or "postmenopausal," and "alkaline phosphatase," or "ALP," "amino-terminal propeptide," or "P1NP," and "clinical trials," and "humans." Graphical presented data from these publications were digitized using GraphClick (v. 3.0 Arizona Software).

PK/PD model

A PK model was used to describe nonlinear kinetics of sclerostin mAbs and this was linked to a PD model describing changes in levels of circulating sclerostin. Typical values for PK parameters were estimated using a maximum likelihood (MLE) approach, based on the reported treatment arm-level data. Unexplained residual variation was described with a proportional residual variance model, with residual random effect assumed to be normally distributed with mean zero and variance, σ.[2] Four subcutaneous dose levels of 1, 3, 5, and 10 mg/kg and two intravenous (i.v.) dose levels of 1 mg/kg and 5 mg/kg were used to fit a two-compartment model with first-order absorption and parallel linear and nonlinear clearance pathways. An indirect response PD model was used to describe changes in total circulating sclerostin. The PK/PD parameters were estimated using nonlinear-mixed effects models (NONMEM software, v. 7.2, ICON Development Solutions, Hanover, MD).

Translational relationship between formation markers

Regression models were used to explore the relationship between time-matched BSAP and P1NP, both normalized to baseline. Model development considered linear and nonlinear relationships between P1NP and BSAP. Inter-arm variance for BSAP was weighted by the inverse of the sample size for each arm[15]:

$$BSAP_{TV} = BSAP_i * e^{(\epsilon/\sqrt{n_i})}, \quad (1)$$

where ε represents the random effect and n = the number of subjects contributing to the data point for the ith arm.

A random effect was applied to the slope term in linear and nonlinear models to account for longitudinal differences between arms. Model selection was based on successful model minimization and the Akaike Information Criteria (AIC).[16]

Multiscale model expansion to include osteocyte function and sclerostin modulation

Code to represent the multiscale bone model has been developed in R.[17] Simulations were performed using the DLSODA differential equation solver provided through ODEPACK within C++ interfaced to R ("Rcpp" package[18]). Parameters were coarsely estimated by tuning individual parameters involved in indirect changes in OB and OC over physiological ranges, solvable by the ODEsolver. Model performance was evaluated by visual inspection, compared to the clinical data. After model structure and initial parameter estimates were in place, the parameters were optimized, individually or in groups, using the R package "minqa."[19] This is a derivative-free optimization algorithm by quadratic approximation, used to minimize an ordinary least-squares objective function. BMD-related parameters were tuned and optimized last. The order in which parameters were optimized and the data used to optimize each parameter is summarized in **Table 3**.

Qualification of expanded multiscale model

To evaluate model structure, simulated data were plotted against the model-building dataset.[1,11–13] After the final model structure was in place and the univariate parameter optimization step was performed, a local sensitivity analysis was conducted on all of the 23 estimated sclerostin-related parameters (**Tables 2**, **3; Supplementary Figure 1**). This analysis determined the influence of each parameter estimate on clinical endpoints, since simultaneous optimization in this context was not possible. Monte Carlo simulations over a range of parameter estimates spanning ± 0.8 * the value of the final parameter estimate were plotted against time-matched changes in P1NP and CTX from a new clinical study,[14] which had not been used for the initial parameter estimation. This same analysis was also performed for

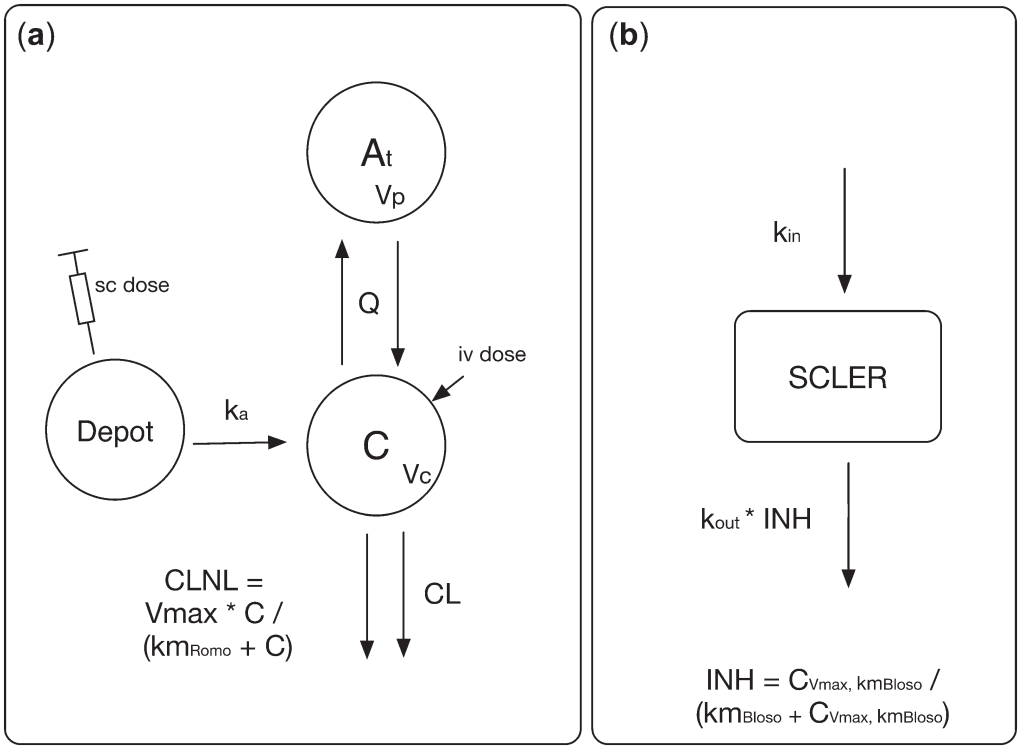

Figure 1 (**a**) The PK model describes circulating sclerostin mAb concentrations that drive changes in circulating total sclerostin protein (SCLER) in the PD model. C represents drug concentration; At is the peripheral compartment; sc = subcutaneous; iv = intravenous; Vc, Vp, CL, Kin, Kout, Vmax, Km are model parameters defined in **Table 1**. (**b**) Parameter estimates for the PK model were generated by fitting the model to romosozumab data, and parameter estimates for the PD model were generated by fitting the model to blosozumab data.

each of the lumbar spine (LS) and total hip (TH) BMD parameters (femoral neck (FN) BMD was not reported in the new study).

Simulations were performed to verify that changes made in the model did not negatively impact the denosumab therapy simulations from previous works.[10] The simulated denosumab dataset contained nine treatment arms with doses taken from several clinical trials of denosumab: placebo, 6, 60, 140, 100, and 210 mg at dosing intervals of 3 and 6 months.[20–24] Simulated P1NP and CTx concentrations for each of these arms were overlaid with time-matched observations and validated by visual inspection (**Supplementary Figure 2**). Dose-matched simulations were performed to explore the impact of dosing interval on clinical outcomes. The final model was evaluated according to the criteria outlined by Agoram[25] for large systems pharmacology models.

RESULTS

PK/PD model

The PK of rosozumab and blosozumab were used to drive the PD response in sclerostin (**Figure 1**). Identifiability of PK and PD parameter estimates for each drug was dictated by data availability. Currently, public-source data included only PK data for romosozumab, but not blosozumab, and only sclerostin data for blosozumab, but not romosozumab. Therefore, the PK parameters were estimated from the antibody concentration–time profiles of romosozumab[1] and the PD parameters were estimated from blosozumab[12] (**Table 1**).

For the PD estimates, the PK parameters, including the V_{max} parameter describing binding kinetics, were assumed to be the same for both mAbs and the PD parameters were subsequently estimated. In this sequence, the K_m

Table 1 Estimated PK/PD parameters for antibodies against sclerostin

Parameter	Value (95% CI)
Absorption rate constant k_a	0.187 (0.142, 0.233) day^{-1}
Linear clearance, CL	0.254 (0.228, 0.281) L/day
Maximum elimination rate constant, V_{max}	5.87 (2.49, 9.26) L/day^{-1}
Michaelis-Menten constant, k_m	0.423 (0−1.64) nM for blosozumab and 9.93 (0.777−1.03) nM for romosozumab
Volume of the central compartment, Vc	2.9 (2.31, 3.48) L
Volume of peripheral compartment, Vp	3.29 (2.43, 4.16) L
Intercompartmental clearance, Q	0.467 (0.326, 0.609) L/day
Bioavailability, F	0.904 unitless
Synthesis rate constant, k_{in}	3.68 (0−15.3) nM/day
Degradation rate constant, k_{out}	26.0 (0–95.9) day^{-1}
Internalization rate constant, k_0	0.195 (0.0349–0.356) day^{-1}

CIs were calculated as the estimate ± 1.96* asymptotic standard error of the estimate; symmetric CIs were truncated at 0 for rate constants k_m, k_{in}, and k_{out}.

Table 2 Six candidate models describing the relationship between time-matched BSAP and P1NP

Model	Model equation	Random effects	AIC
Linear	$y = Ax + b$	On A	5,035.57
Exponential	$y = Ae^{x} + b$	On A	4,904.99
E_{max}	$y = \frac{Emax * x}{EC_{50} + x}$	On EC_{50}	5,036.15
Sigmoid E_{max}	$y = \frac{Emax * x^{\gamma}}{EC_{50}^{\gamma} + x^{\gamma}}$	On EC_{50}	4,707.93
Sigmoid E_{max} + Intercept	$y = \frac{Emax * x^{\gamma}}{EC_{50}^{\gamma} + x^{\gamma}} + int$	On EC_{50}	4,710.38
Quadratic	$y = Ax^{b} + Cx$	On A	4,721.53

Data from 21 clinical trials were evaluated. Random effects were added on the "slope" parameters in each model to account for variability between arms.

parameter in the nonlinear clearance component of the PK model was estimated based on romosozumab concentration and was estimated separately for blosozumab using the sclerostin response. Therefore, all the PK parameters derived for romosozumab were fixed and used to simulate mAb concentration in the PD model, with the exception of k_m, which was reestimated for blosozumab. The rationale for this is discussed further in the Supporting Information.

Translational relationship between formation markers

Various linear and nonlinear relationships were explored to describe the BSAP-P1NP translation (**Table 2**). The lowest calculated AIC value resulted from the sigmoid E_{max} model (AIC = 4707.93), and this model structure was carried forward. An intercept parameter of int = 20.4181 was also added to this model within the multiscale bone model, so that at the initial conditions, percentage of baseline BSAP = P1NP = 100%.

The estimated parameters for this model were E_{max} = 2,050, 95% CI: (295, 3,800), $\gamma = 1.8$, 95% CI: (1.52, 2.08), and $EC_{50} = 467$, 95% CI: (128,805). $\Omega_A = 2.27$, 95% CI: (0.376–4.16), %CV = 38.2, $\sigma = 0.515$, 95% CI: (0.0756–0.955), %CV = 18.0, for $n = 50$ subjects.

Developing model structure to describe changes in turnover markers and BMD

Based on supporting literature, six points of intersection were identified within the multiscale bone model where changes in sclerostin have a known effect. These are (i) the depletion rate of pre-osteoblasts (ROB); (ii) the formation rate of OB; (iii) the rate of OCY apoptosis; (iv) the level of OCY effect applied to RANKL; (v) the accumulation of OPG; and (vi) the differential effects of sclerostin on regional changes in BMD. See **Figure 2** to see schematically how these pieces fit into the model structure. Because identifiability of new model parameters is problematic if all are estimated simultaneously, P1NP-associated parameters were estimated first, followed by those parameters affecting CTx. This follows our understanding of the mechanism of Wnt pathway upregulation; β-catenin accumulates and causes changes in transcription factors regulating differentiation of pre-OB to OB. This effect is upstream, or takes place ahead, of modification of bone resorption through this pathway, which is largely controlled by signaling through RANK/RANKL/OPG in OB[26] and OCY.[27]

To apply a sclerostin signal to the OB, two methods were tried. First, a "precursor pool" compartment was applied upstream of the ROB. This physiologically represents cells earlier in the OB lineage being recruited for differentiation which cause an increase in formation activity, as the flux of substrate moving through the OB differentiation pathway increases.[28] The precursor-pool approach resulted in a very rapid depletion of the ROB pool and a peak P1NP concentration–time profile that was right-shifted relative to the true response. An alternative way to signal the flux of substrate through the OB pathway was to use a direct approach whereby a sclerostin effect was applied to the depletion rate of ROB and a separate effect was applied directly to the OB accumulation rate. Together, these increased OB activity, but caused an attenuation of OB activity over time as the ROB became depleted, which is consistent with the pattern of anabolic turnover markers seen after multiple doses of sclerostin mAb.[12] A "translation" compartment was also added in the direct approach to delay the effect of sclerostin on the increase in OB activity only slightly, relative to the delay that was elicited by the precursor-pool approach. Together, these additions represent the first two points of interaction in the modified model.

OCY are the major source of sclerostin,[2] and the cell type responsible for sclerostin modulation in response to mechanical stimulation.[29] Studies have also shown that OCY are a major contributor to RANKL trafficking and regulation of osteoblast- and osteoclast-ogenesis at the level of the RANK/RANKL/OPG axis.[30] Membrane-bound RANKL is provided by dendritic processes on the osteocyte to signal to osteoclast precursors and upregulate osteoclastogenesis. Conversely, upregulating the Wnt pathway can suppress osteoclast-mediated bone resorption through reduced expression of RANKL.[26,31] For the third and fourth points of intersection, a sclerostin effect was applied to the depletion rate (or rate of apoptosis) of OCY and an osteocyte effect was applied to the RANKL production rate. The combined result is that when sclerostin mAb is dosed, OCY activity is purportedly decreased, concurrent with diminished SOST expression[29] and RANKL production falls as well, gradually inhibiting osteoclastogenesis.

For the fifth point of intersection, a direct sclerostin effect, was applied to the production rate of OPG to simulate the effect of Wnt-pathway regulation of OPG secretion. In the literature, this level of regulation was demonstrated by knocking out osteocytic β-catenin in mice. These mice became osteoporotic due to increased numbers of OC and increased bone resorption[27] and had diminished expression of osteocytic OPG, demonstrating that signaling through β-catenin in the osteocytes is required for regulation of resorption activity. Modeling a direct sclerostin signal on OPG production rate had the desired effect of rapidly decreasing the simulated CTx levels, immediately following a dose of sclerostin mAb.

To model sclerostin antibody effects on FN, TH, and LS BMD, the same model structure as was used to describe denosumab effects on BMD[10] was adapted, by reestimating the power term reflecting the impact of OB activity on BMD.

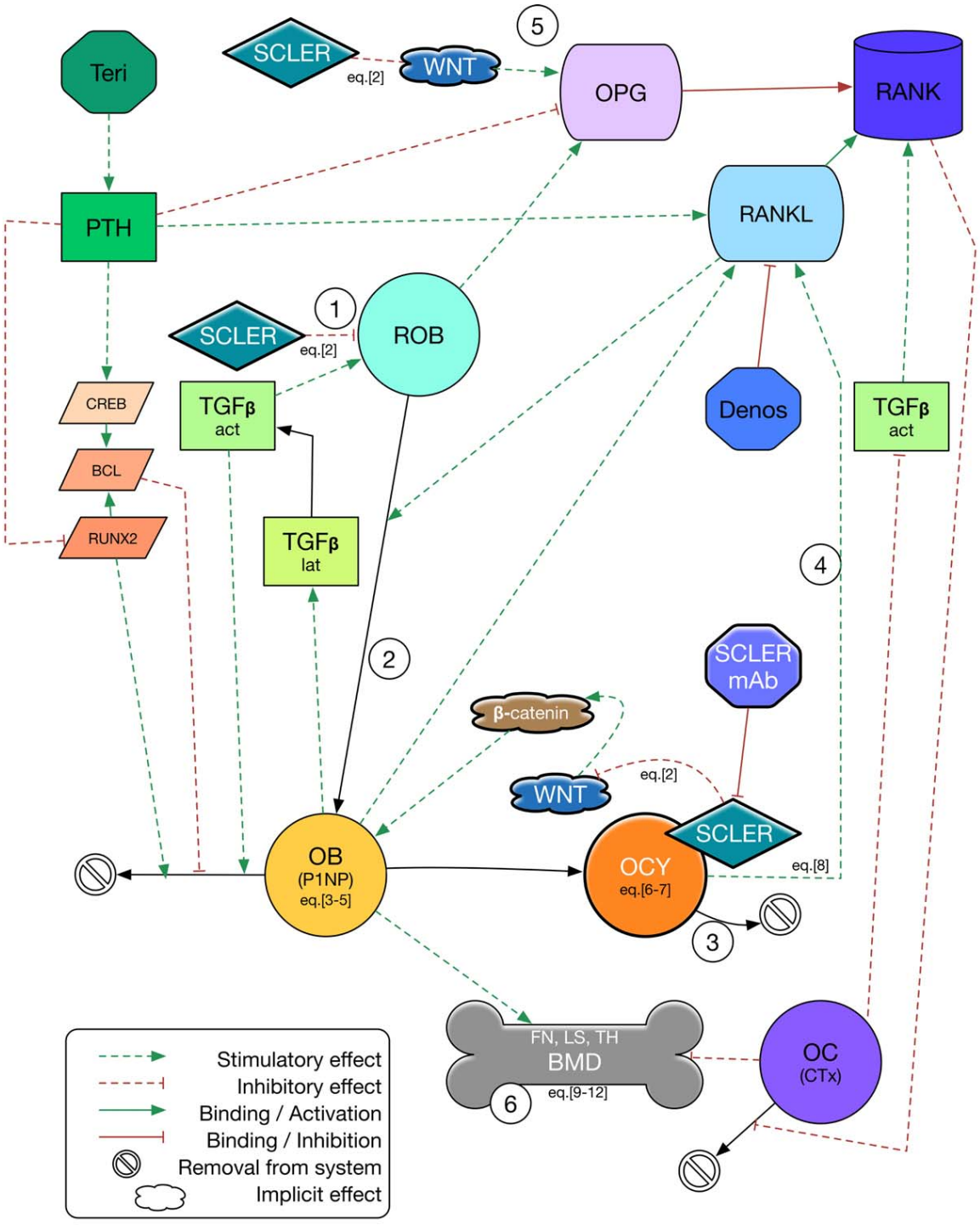

Teri = teriparatide, SCLER = sclerostin, WNT = Wnt gene, OPG = osteoprogerin, RANK/L = Receptor activator of nuclear factor κ B / - ligand, PTH = parathyroid hormone, CREB = cAMP response element binding protein, BCL = B-cell lymphoma 2, RUNX2 = Runt-related transcription factor 2, TGF-β = transforming growth factor beta (active and latent forms), ROB = responding osteoblasts, Denos = denosumab, OB = osteoblasts, P1NP = procollagen type 1 amino-terminal propeptide, OCY = osteocytes, SCLER mAb = monoclonal antibody against sclerostin, OC = osteoclasts, CTX = cross-linked C-telopeptide, FN, LS, TH BMD = femoral neck, lumbar spine, and total hip bone mineral density

Figure 2 Schematic of the bone-remodeling systems model. Intersection points of sclerostin signaling effects within the model are identified with numbers corresponding to description in the text. New model compartments are indicated with white text and shading and corresponding equation numbers.

The predictions resulting from this model yielded a peak increase in BMD that occurred earlier than it did in clinical reports. In order to correct for this, a delay compartment was used to adjust the rate of anabolic bone formation under the premise that it takes more time for OB to become embedded in the bone matrix, calcify, and contribute to an increase in overall BMD than it does for catabolic (OC-driven) impact on BMD.

Model equations and parameter estimates describing turnover markers and BMD

For all of the intersection points added to the model, the sclerostin effect was applied as a power model in the form of:

$$SCLEREFF = \left(\frac{\text{SCLER}}{SCLER_{BASELINE}}\right)^{\gamma} \quad (2)$$

where γ = a parameter modulating the sclerostin effect.

In general, the steady state assumption used in the original publication[3] was used and compartmental equations were solved at initial conditions to minimize identifiability problems for estimated rate constants. The OB effect took the form:

$$\frac{d\ trans}{dx} = kin_T * \left(1 + \frac{EMAXSCLER * SCLEREFF^{\gamma SCLEROB}}{EC50SCLER^{\gamma SCLEROB} + SCLEREFF^{\gamma SCLEROB}}\right) - kout_T \quad (3)$$

$$kin_T = kout_T \quad (4)$$

$$OB = (OBfast * trans + OBslow) \quad (5)$$

OBfast and OBslow represent the two pathways of active OB elimination described in the original model publication.[3]

The osteocyte compartment was represented as:

$$\frac{d\ OCY}{dx} = OB * Frac_{OCY} - kout_{OCY} * OCY \quad (6)$$

where $Frac_{OCY}$ represents the rate of conversion of OB to OCY and

$$kout_{OCY} = OB0 * Frac_{OCY} * SCLEREFF^{\gamma OCY} \quad (7)$$

The osteocyte effect took the same form as the sclerostin effect:

$$OSTEOCYEFFECT = \left(\frac{\text{OCY}}{\text{OCY}_{BASELINE}}\right)^{\delta} \quad (8)$$

where δ = a parameter modulating the osteocyte effect.

The final BMD model for sclerostin has separate compartments for TH, FN, and LS BMD, where the $kout_{DELAY}$ and γ_{OB} were estimated separately for each region and each region's set of compartmental equations took the form:

$$kin = kout * BMD_{baseline} \quad (9)$$

$$kin_{DELAY} = kout_{DELAY} \quad (10)$$

$$\frac{d\ DELAY}{dx} = kin_{DELAY} * \frac{OB}{OB_{BASELINE}}^{\gamma_{OB}} - kout_{DELAY} * DELAY \quad (11)$$

$$\frac{d\ BMD}{dx} = kin * DELAY - \frac{OC}{OC_{BASELINE}}^{\gamma_{OC}} * kout * BMD \quad (12)$$

Because simultaneous parameter optimization was not possible, considerations with regards to the parameters describing the turnover markers and BMD included the order in which they were implemented and optimized, and the data used to fit each parameter (**Table 3**).

Qualification

In the model qualification step, simulated P1NP and CTX were consistent with changes in the turnover markers from three clinical trials with romosozumab and two clinical trials with blosozumab (**Supplementary Figure 3**). TH, FN, and LS BMD profiles from these same studies were also well described by the model **(Supplementary Figure 4**). A qualification dataset from a phase II clinical trial with blosozumab in postmenopausal women was simulated using the final model and changes in turnover markers and LS and TH BMD were plotted (**Figure 3**). The predicted mean change from baseline for the 180 mg dosed Q2W arm at 4 and 52 weeks were 229% (observed median; 95% CI: 231; 199–262%); for P1NP and 73.5% (83.9; 73.7; 94.2); for CTX and 152% (90.2; 81.4–99.0%); for P1NP, and 79.2 (84.6; 69.7–99.6%); for CTX, respectively. The predicted mean change from baseline at 52 weeks (180 mg dosed Q2W) for LS BMD was 16.5% (observed; 95% CI: 14.9; 12.6–17.1%) and 6.8% (4.5; 3.2–5.8%) for TH BMD. Despite the small dataset, for most data points the model predicted the change in the clinical endpoint that fell within the 95% CI reported in the literature.

In order to demonstrate how the model can be used to investigate the role of dosing protocol on clinical outcomes, dose-matched administrations of sclerostin mAb were simulated at several dosing intervals (**Figure 4**). Simulations of larger dosing intervals promote greater increases in P1NP (**Figure 4a**), due to precursors also achieving higher levels (**Figure 4b**). Maximum simulated resorption activity, however, is also increased with a larger dosing interval (**Figure 4c**), resulting in lower increases in total hip BMD when compared to smaller dosing intervals (**Figure 4d**).

DISCUSSION

Despite having a limited availability of clinical data, the updated model was able to capture the central tendency of the changes in turnover markers and BMD after single and multiple doses of sclerostin mAb, over a large dose range. The model, however, greatly underpredicted the peak percentage change of P1NP in the highest dosing groups with blosozumab (**Supplementary Figure 1**, arms 16 and 23). This was a consequence of the blosozumab data showing that a single 750 mg dose did not greatly increase sclerostin change from baseline over a single dose of 225 mg. The 270 mg dose elicited much greater changes than the

Table 3 Parameters describing changes in turnover makers and BMD associated with sclerostin mAbs

Order	Parameter	Definition	Value (units)	Data used to estimate
1	γROB	Exponent on sclerostin effect on differentiation rate of OB	0.0703 (unitless)	P1NP
2	EMAXSCLER	Max sclerostin effect on OB	5.22 (hours)	P1NP
2	γSCLEROB	Hill coefficient for sclerostin effect on OB	1.15 (unitless)	P1NP
2	EC50SCLER	Half-max effect of sclerostin on OB	667 (hr^{-1})	P1NP
3	kout_T	Depletion rate on translation compartment	0.00692 (hr^{-1})	P1NP
Fixed*	FracOCY	Fraction of OB becoming OCY	0.50 (unitless)	–
Fixed*	ρ	Exponent on osteoblast effect on RANKL	0.0100 (unitless)	–
4	δ	Exponent on osteocyte effect on RANKL; scales PTH effect on RANKL	0.0592 (unitless)	P1NP, CTx
4	γOCY	Exponent on sclerostin effect on OCY apoptosis rate	0.405 (unitless)	P1NP, CTx
5	γOPG	Exponent on sclerostin effect on OPG	1.61 (unitless)	CTx
Fixed*	kout_BMDdel	Delay parameter on anabolic effects on BMD	0.001 (unitless)	Lumbar spine BMD
6	γOB_{LS}	Exponent on anabolic contribution to overall lumbar spine BMD	0.711 (unitless)	Lumbar spine BMD
6	γOB_{FN}	Exponent on anabolic contribution to overall femoral neck BMD	0.0934 (unitless)	Femoral neck BMD
6	γOB_{TH}	Exponent on anabolic contribution to overall total hip BMD	0.686 (unitless)	Total hip BMD

*These parameters were shown to be relatively insensitive within the tested range so these values were fixed prior to optimization.

750 mg dose with the same dosing interval (see ref. 12, fig 4). Because the model relies on the change in sclerostin as the signal for increase in P1NP, this apparent discrepancy can be seen in the model predictions at the 750 mg dose level, and to some degree in the 540 mg dosing arms.

There are many regulating elements of cellular feedback that are not explicitly defined in the model. This may explain why the model failed to recapitulate some of the dynamics of the CTX-time profile, which was also highly variable between arms. Recent data has shown that OCY and OB can also control bone remodeling directly through bone morphogenetic protein (BMP), which can affect endogenous sclerostin, independent of Wnt signaling,[32] but sclerostin is also a potent antagonist of some BMPs.[33] This feedback mechanism needs to be fully elucidated by experimental data before implementation into the model. OCY undergoing apoptosis also secrete interleukin (IL)−1 and IL-6, which promote osteoclastogenesis[34] and provide another layer of feedback control that is not yet represented in the model. OB are also a source of IL-6, as well as macrophage-colony-stimulating factor (M-CSF), which also contributes to osteoclastogenesis.[34] Supporting data are needed to fully characterize effects of sclerostin mAb on changes in CTx, as even the PBO arms show relatively large fluctuations in CTx over several months.[1,11,12]

It was hypothesized that diminishing the pre-OB pool with sclerostin inhibition contributes to attenuation in bone-formation activity after multiple doses. A consequence of this from a treatment perspective is that if a sclerostin mAb is dosed with a small dosing interval, and the mesenchymal-derived pre-OB do not have sufficient time to be replenished, the anabolic effect of the mAb will be diminished with repeated doses. Indeed, simulations of sclerostin mAb administration at equivalent dose levels, but at different dosing intervals, demonstrate that higher P1NP levels can be achieved by dosing in longer intervals (**Figure 4a**), because levels of pre-osteoblasts have time to recover between doses (**Figure 4b**). However, achieving the greatest magnitude of anabolic activity does not necessarily translate into larger gains in BMD, due to feedback signaling to OC. Simulations also show that at longer dosing intervals peak levels of resorption activity are also higher than at smaller dosing intervals, blunting the net gain in total BMD that can be achieved within the dosing interval (**Figure 4c,d**). This finding suggests that osteocyte-controlled feedback involved in sclerostin modulation has a considerable impact on turnover markers and that dosing protocol of sclerostin mAbs impacts these markers as well as changes in BMD. This model therefore offers a potential platform for simulating different regimens in order to explore the effect of dose strength, interval, and/or combination with other treatment combinations. The multiscale functionality enables consideration of feedback effects, for example, and how these mechanisms relate to BMD changes over a prolonged treatment period.

The model underpredicts BMD changes at the lumbar spine and total hip after multiple doses in the low dosing arm (**Supplementary Figure 2A,B**, arms 32, 33). This is likely due to the simulated peak P1NP responses, which reflect OB activity, at these later timepoints falling below baseline values (see **Supplementary Figure 1A**). Although it is difficult to assess what the true peak P1NP values are under this dosing regimen, it appears that P1NP response is attenuated after multiple doses in this arm, for reasons discussed previously. It is unclear what is responsible for maintaining the increase in BMD seen in the clinic at these later timepoints. It is possible that the decreased rates of resorption play more of a role at these later timepoints and account for a greater amount of the increase in BMD than the model currently predicts.

Another interesting finding of this work is the interaction of sclerostin modification with the RANK/RANKL/OPG axis and resulting dynamic changes in resorption/OC activity. The model suggests the immediate and significant decrease in CTx results from osteocytic Wnt signaling, which is known to increase OPG directly.[33] This effect is coupled with a more gradual decline in CTx due to a drop in osteocytic contribution to RANKL. Finally, a mechanism in the model was needed to delay the anabolic effects of

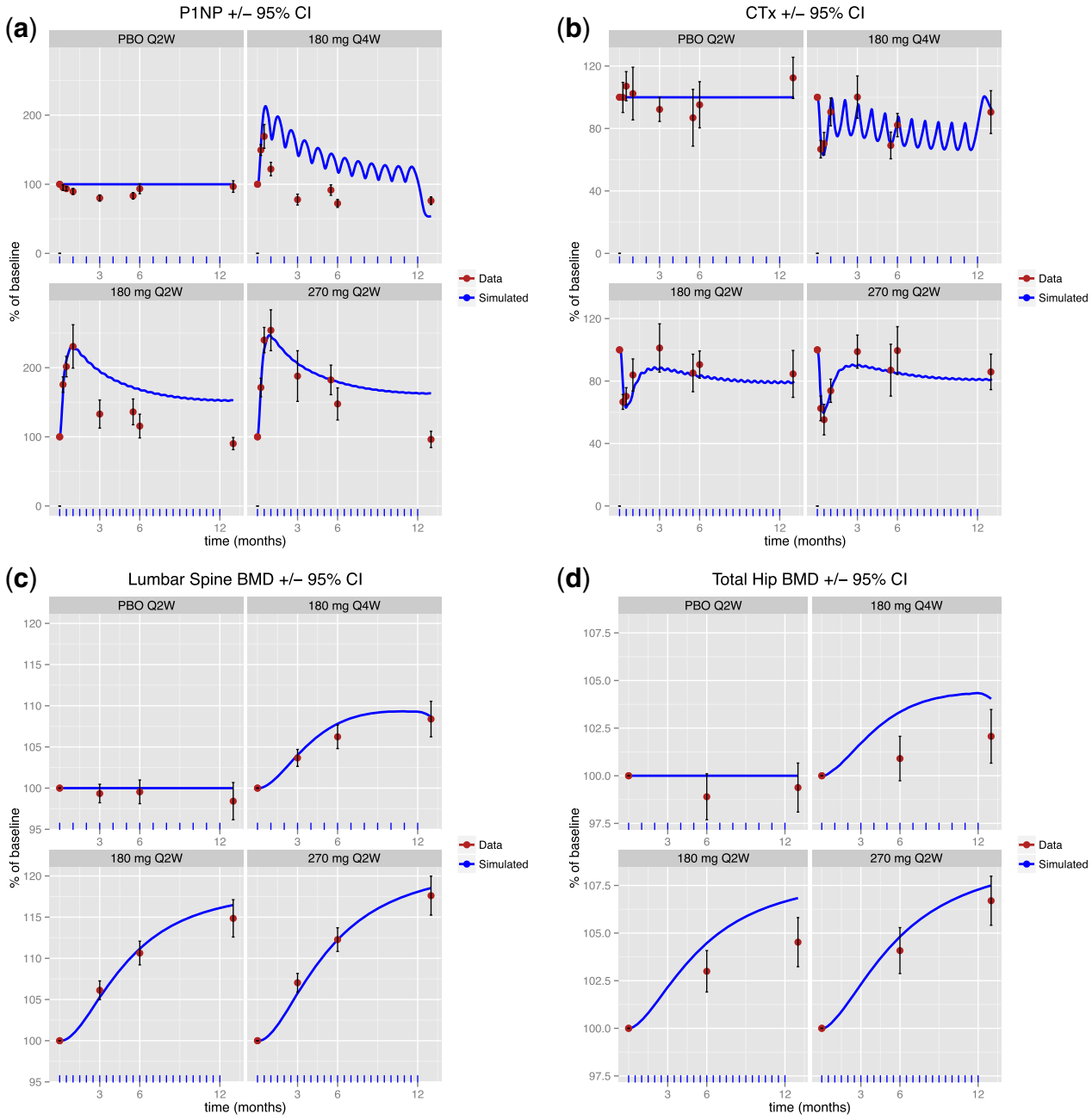

Figure 3 Simulated P1NP (**a**), CTx (**b**), lumbar spine BMD (**c**), and total hip BMD (**d**) (blue line) overlaying data from a clinical trial with blosozumab (red points). This qualification dataset was not used in constructing the model ($n = 29$, 31, 30, 30 for arms PBO, 180 mg Q2W, 180 mg Q4W, and 270 mg Q2W, respectively).

sclerostin inhibition on overall BMD. We conjecture that it takes more time for OB to embed themselves in the matrix and form new bone than it does for a decrease in resorption to produce an increase in BMD. This finding may help efforts to characterize the effects of other anabolic therapies like PTH and teriparatide on regional changes in BMD within the modeling framework.

Although simultaneous parameter fitting and full parameter identifiability could not be accomplished in this context, the updated model fulfilled the Agoram[25] criteria: (i) Fit for purpose: only compartments and parameters that were necessary to improve predictions of specific measurable clinical endpoints were added to the model. (ii) Justification of model structure: every point of intersection for a sclerostin effect has an experimental or clinical basis in the published literature. (iii) Evaluation of component submodels: models were evaluated by goodness-of-fit and individual parameter sensitivity analyses were conducted. (iv) Qualification of the emergent properties of the system: the final model was cross-validated with denosumab therapy simulations to ensure the changes in turnover

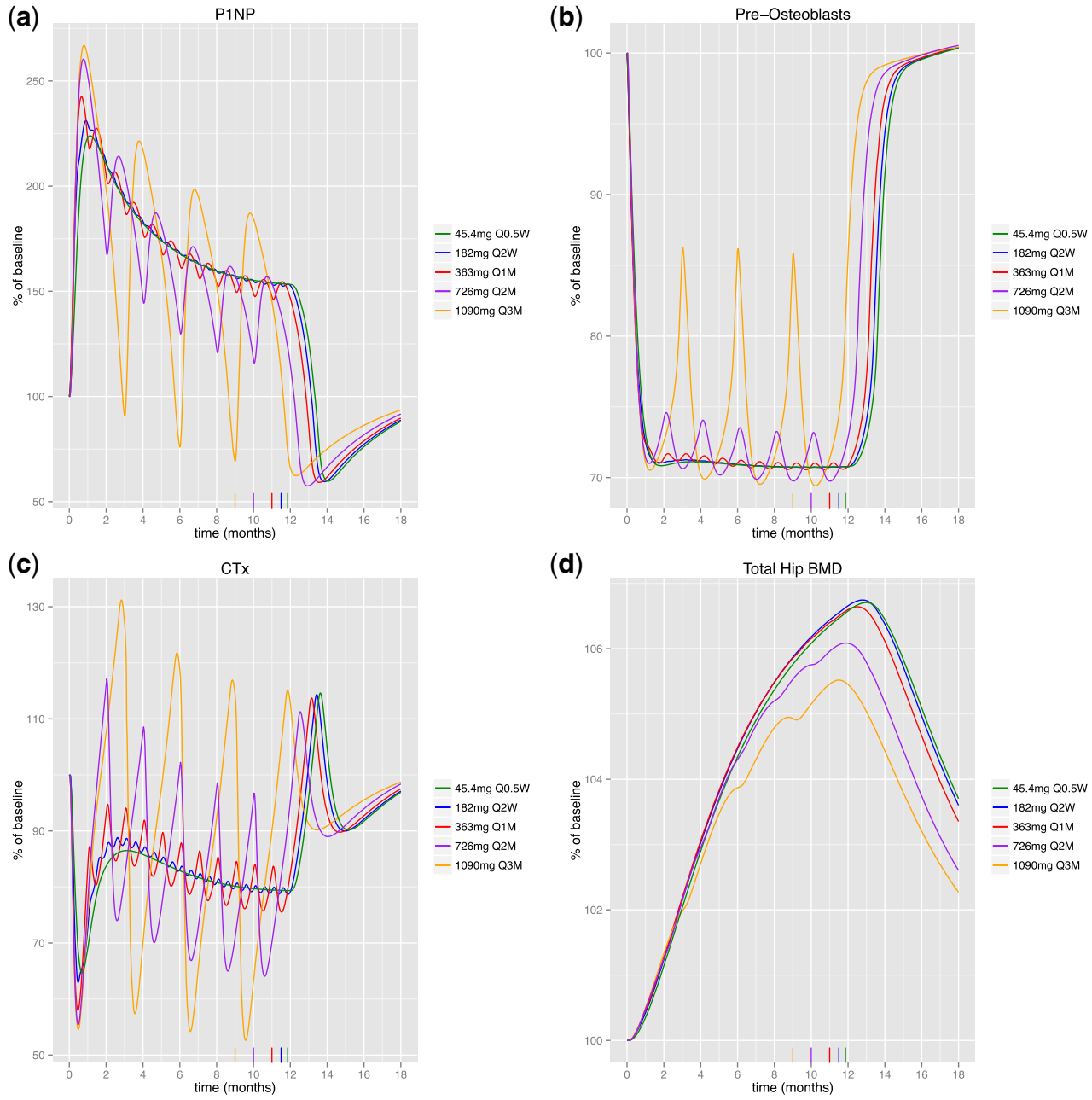

Figure 4 Simulations of dose-equivalent sclerostin mAb administered at different dosing intervals demonstrate that changing the dosing interval may alter clinical outcomes. P1NP (**a**), osteoblast precursors (**b**), CTx (**c**), total hip BMD (**d**). Colored marks indicate the final dose in each arm.

markers were consistent with what was reported in previous work.[10] The model also predicts a significant increase in circulating PTH, after sclerostin mAb administration, which is consistent with clinical reports.[12,14]

CONCLUSION

A previously published multiscale model of bone function, control, and health was extended to include OCY, sclerostin, and effects of the upregulated Wnt signaling pathway elicited by sclerostin mAb administration. The model was used to simulate P1NP, CTX, and BMD profiles that resembled those in clinical studies with sclerostin mAb treatment. The utility of the model to explore biological implications of Wnt pathway modification and the role of the OCY in bone remodeling was demonstrated. Model simulations point to differential effects of osteocyte-driven feedback-driven increases in resorption activity and suggest possible benefits of shorter dosing intervals in future clinical trials with sclerostin mAbs. The model also suggests osteoporosis patients may benefit from combination therapy to mitigate these feedback effects.

The extended model offers a broader *in silico* model-based platform to explore therapeutic target modification towards the goal of more efficiently addressing clinical development considerations and improving long-term outcomes.

Author Contributions. R.J.E. and M.M.R. wrote the manuscript; R.J.E., M.R.G., and M.M.R. designed the research; R.J.E. performed the research; R.J.E. analyzed the data; K.T.B. contributed new reagents/analytical tools.

Conflict of Interest. The authors have no conflicts of interest to declare.

1. Padhi, D., Jang, G., Stouch, B., Fang, L. & Posvar, E. Single-dose, placebo-controlled, randomized study of AMG 785, a sclerostin monoclonal antibody. *J. Bone Min. Res.* **26**, 19–26 (2011).
2. Van Bezooijen, R.L. *et al.* Sclerostin is an osteocyte-expressed negative regulator of bone formation, but not a classical BMP antagonist. *J. Exp. Med.* **199**, 805–814 (2004).
3. Peterson, M.C. & Riggs, M.M. A physiologically based mathematical model of integrated calcium homeostasis and bone remodeling. *Bone* **46**, 49–63 (2010).
4. Raposo, J.F., Sobrinho, L.G. & Ferreira, H.G. A minimal mathematical model of calcium homeostasis. *J. Clin. Endocrinol. Metab.* **87**, 4330–4340 (2002).
5. Lemaire, V., Tobin, F.L., Greller, L.D., Cho, C.R. & Suva, L.J. Modeling the interactions between osteoblast and osteoclast activities in bone remodeling. *J. Theor. Biol.* **229**, 293–309 (2004).
6. Bellido, T. *et al.* Proteasomal degradation of Runx2 shortens parathyroid hormone-induced anti-apoptotic signaling in osteoblasts. A putative explanation for why intermittent administration is needed for bone anabolism. *J. Biol. Chem.* **278**, 50259–50272 (2003).
7. Graham, J.M., Ayati, B.P., Holstein, S.A. & Martin, J.A. The role of osteocytes in targeted bone remodeling: a mathematical model. *PLoS One* **8**, e63884 (2013).
8. Carew, E.O. A semi-empirical cell dynamics model for bone turnover under external stimulus. *J. Biomech. Eng.* **134**, 24503 (2012).
9. Baiotto, S. & Zidi, M. Theoretical and numerical study of a bone remodeling model: the effect of osteocyte cells distribution. *Biomech. Model. Mechanobiol.* **3**, 6–16 (2004).
10. Peterson, M.C. & Riggs, M.M. Predicting nonlinear changes in bone mineral density over time using a multiscale systems pharmacology model. *CPT Pharmacometrics Syst. Pharmacol.* **1**, e14 (2012).
11. Padhi, D. *et al.* Multiple doses of sclerostin antibody romosozumab in healthy men and postmenopausal women with low bone mass: a randomized, double-blind, placebo-controlled study. *J. Clin. Pharmacol.* **54**, 168–178 (2013).
12. McColm, J., Hu, L., Womack, T., Tang, C.C. & Chiang, A.Y. Single- and multiple-dose randomized studies of blosozumab, a monoclonal antibody against sclerostin, in healthy postmenopausal women. *J. Bone Miner. Res.* **29**, 935–943 (2013).
13. McClung, M.R. *et al.* Romosozumab in postmenopausal women with low bone mineral density. *N. Engl. J. Med.* **370**, 412–420 (2014).
14. Recker, R. *et al.* A randomized, double-blind phase 2 clinical trial of blosozumab, a sclerostin antibody, in postmenopausal women with low bone mineral density. *J Bone Miner. Res.* **30**, 216–224 (2014).
15. Ahn, J.E. & French, J.L. Longitudinal aggregate data model-based meta-analysis with NONMEM: approaches to handling within treatment arm correlation. *J. Pharmacokinet. Pharmacodyn.* **37**, 179–201 (2010).
16. Akaike, H. A new look at the statistical model identification. *IEEE Trans. Autom. Control* **19**, 716–723 (1974).
17. R Core Team. R: A language and environment for statistical computing. <http://www.r-project.org/> (2014).
18. Eddelbuettel, D. & Fran, R. Rcpp: Seamless R and C ++ integration. *J. Stat. Softw.* **40**, 1–18 (2011).
19. Bates, D., Mullen, K.M., Nash, J.C. & Varadhan, R. minqa: derivative-free optimization algorithms by quadratic approximation. <http://cran.r-project.org/package=minqa> (2014).
20. Bone, H.G. *et al.* Effects of denosumab on bone mineral density and bone turnover in postmenopausal women. *J. Clin. Endocrinol. Metab.* **93**, 2149–2157 (2008).
21. Leder, B.Z. *et al.* Two years of denosumab and teriparatide administration in postmenopausal women with osteoporosis (The DATA Extension Study): a randomized controlled trial. *J. Clin. Endocrinol. Metab.* **99**, 1694–1700 (2014).
22. Lewiecki, E.M. *et al.* Two-year treatment with denosumab (AMG 162) in a randomized phase 2 study of postmenopausal women with low BMD. *J. Bone Miner. Res.* **22**, 1832–1841 (2007).
23. Lin, T. *et al.* Comparison of clinical efficacy and safety between denosumab and alendronate in postmenopausal women with osteoporosis: a meta-analysis. *Int. J. Clin. Pract.* **66**, 399–408 (2012).
24. Bonnick, S. *et al.* Comparison of weekly treatment of postmenopausal osteoporosis with alendronate versus risedronate over two years. *J. Clin. Endocrinol. Metab.* **91**, 2631–2637 (2006).
25. Agoram, B. Evaluating systems pharmacology models is different from evaluating standard pharmacokinetic-pharmacodynamic models. *CPT Pharmacometrics Syst. Pharmacol.* **3**, e101 (2014).
26. Glass, D.A. 2nd *et al.* Canonical Wnt signaling in differentiated osteoblasts controls osteoclast differentiation. *Dev. Cell.* **8**, 751–764 (2005).
27. Kramer, I. *et al.* Osteocyte Wnt/beta-catenin signaling is required for normal bone homeostasis. *Mol. Cell. Biol.* **30**, 3071–3085 (2010).
28. Li, X. *et al.* Inhibition of sclerostin by monoclonal antibody increases bone formation, bone mass, and bone strength in aged male rats. *J. Bone Miner. Res.* **25**, 2647–2656 (2010).
29. Wu, A.C., Kidd, L.J., Cowling, N.R., Kelly, W.L. & Forwood, M.R. Osteocyte expression of caspase-3, COX-2, IL-6 and sclerostin are spatially and temporally associated following stress fracture initiation. *BoneKEy Rep.* **3** (2014).
30. Honma, M. *et al.* RANKL subcellular trafficking and regulatory mechanisms in osteocytes. *J. Bone Miner. Res.* **28**, 1936–1949 (2013).
31. Holmen, S.L. *et al.* Essential role of beta-catenin in postnatal bone acquisition. *J. Biol. Chem.* **280**, 21162–21168 (2005).
32. Kamiya, N. *et al.* BMP signaling negatively regulates bone mass through sclerostin by inhibiting the canonical Wnt pathway. *Development* **135**, 3801–3811 (2008).
33. Bellido, T. Osteocyte-driven bone remodeling. *Calcif. Tissue Int.* **94**, 25–34 (2014).
34. Li, L. *et al.* Influence of exercise on bone remodeling-related hormones and cytokines in ovariectomized rats: a model of postmenopausal osteoporosis. *PLoS One* **9**, e112845 (2014).

Supplementary information accompanies this paper on the *CPT: Pharmacometrics & Systems Pharmacology* website (http://www.wileyonlinelibrary.com/psp4)

Supplementary Figures

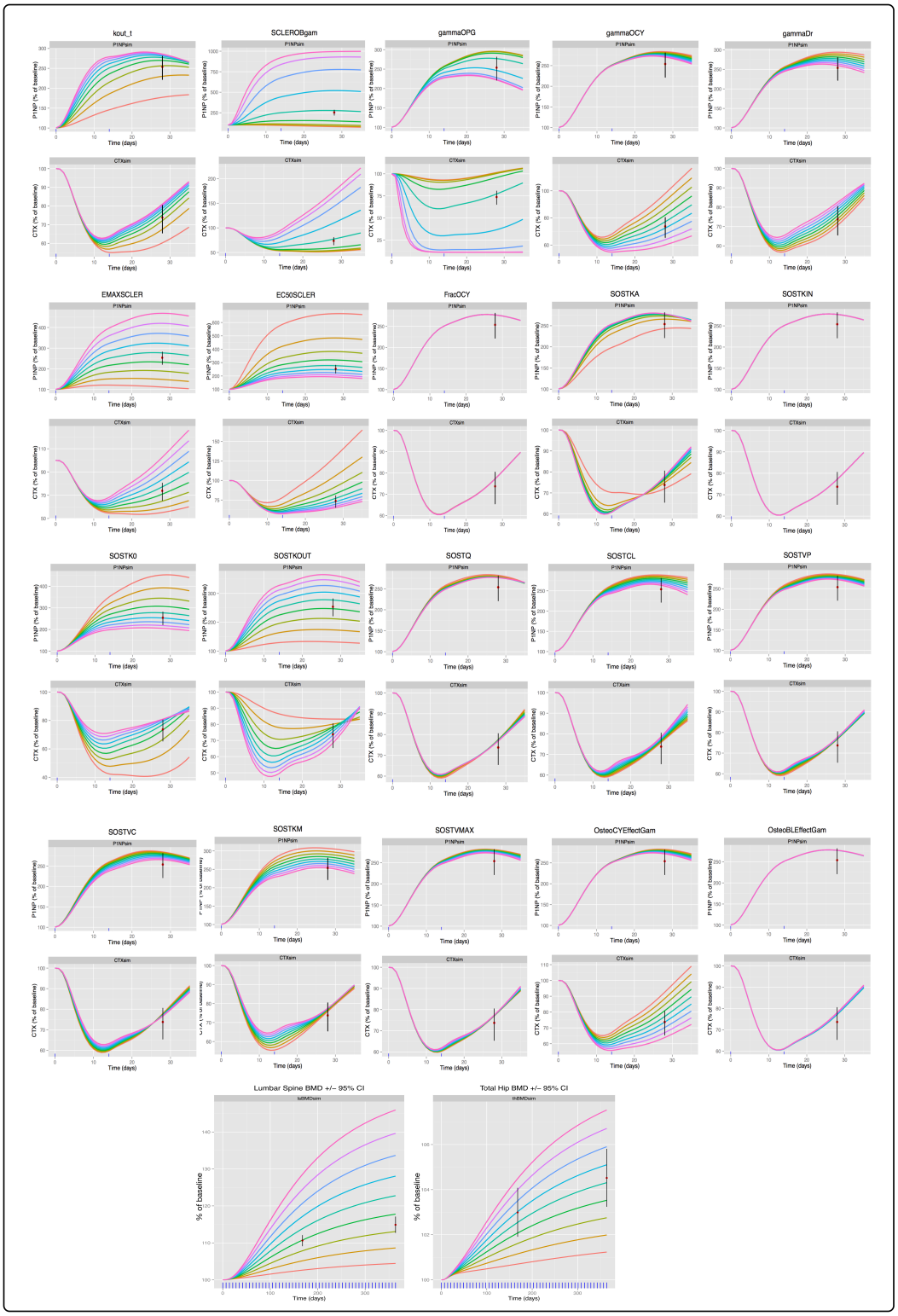

Supplementary Figure 1. Sensitivity analysis showing the impact of perturbing each individual parameter by +/- 0.8*estimated parameter value, on P1NP, CTX, LSBMD, and THBMD

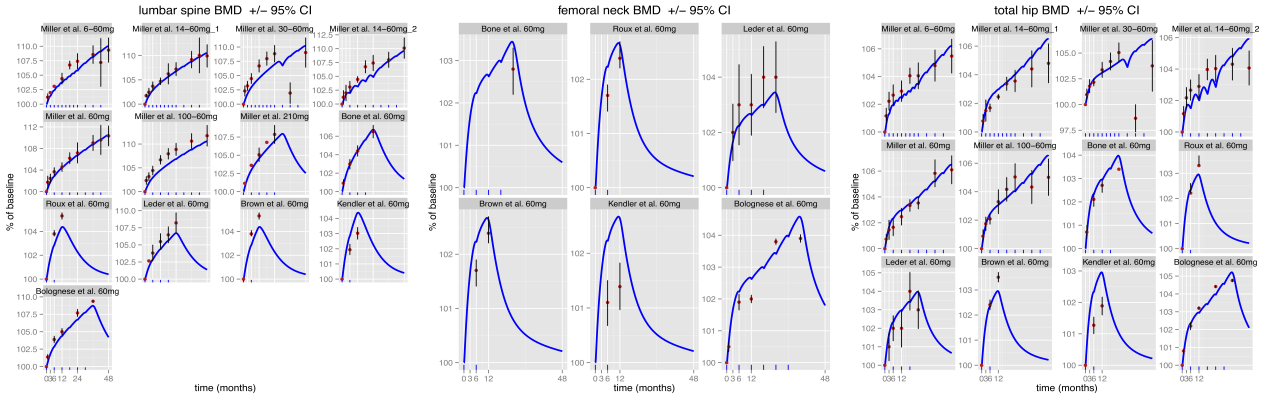

Supplementary Figure 2. For model qualification, several doses of denosumab were simulated along with data from 7 clinical studies. Simulations show good agreement with clinical data

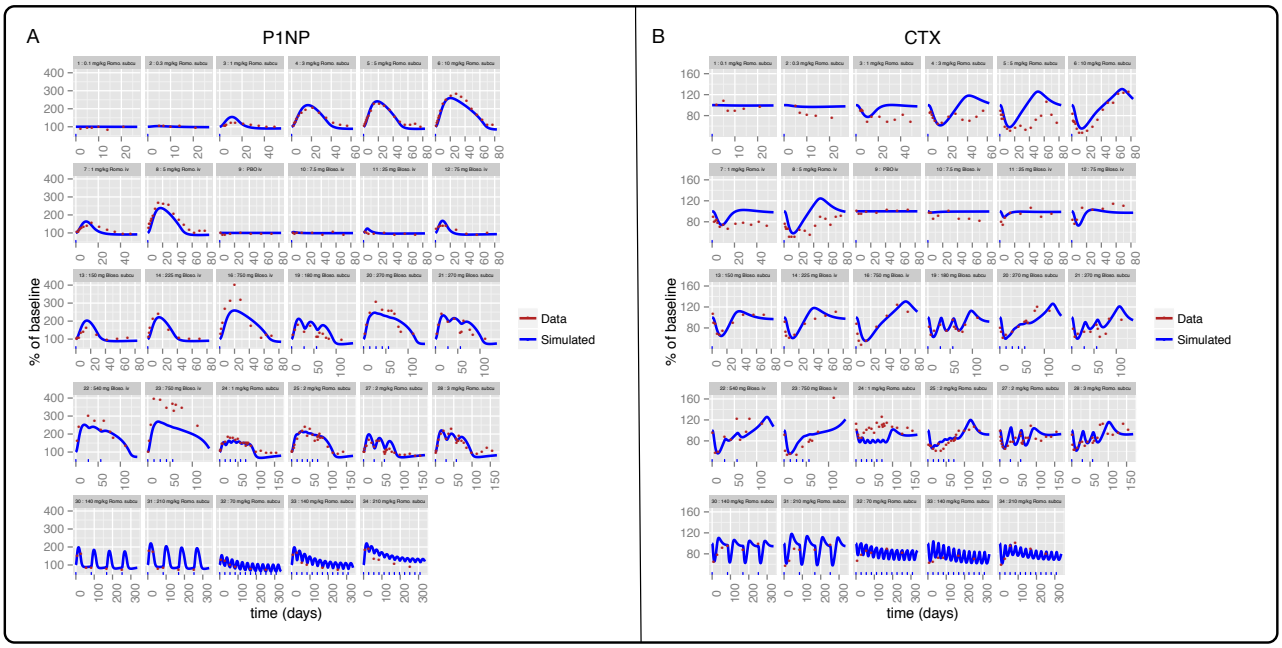

Supplementary Figure 3. Simulated turnover markers plotted overlaying actual data from 5 clinical studies with romosozumab and blosozumab

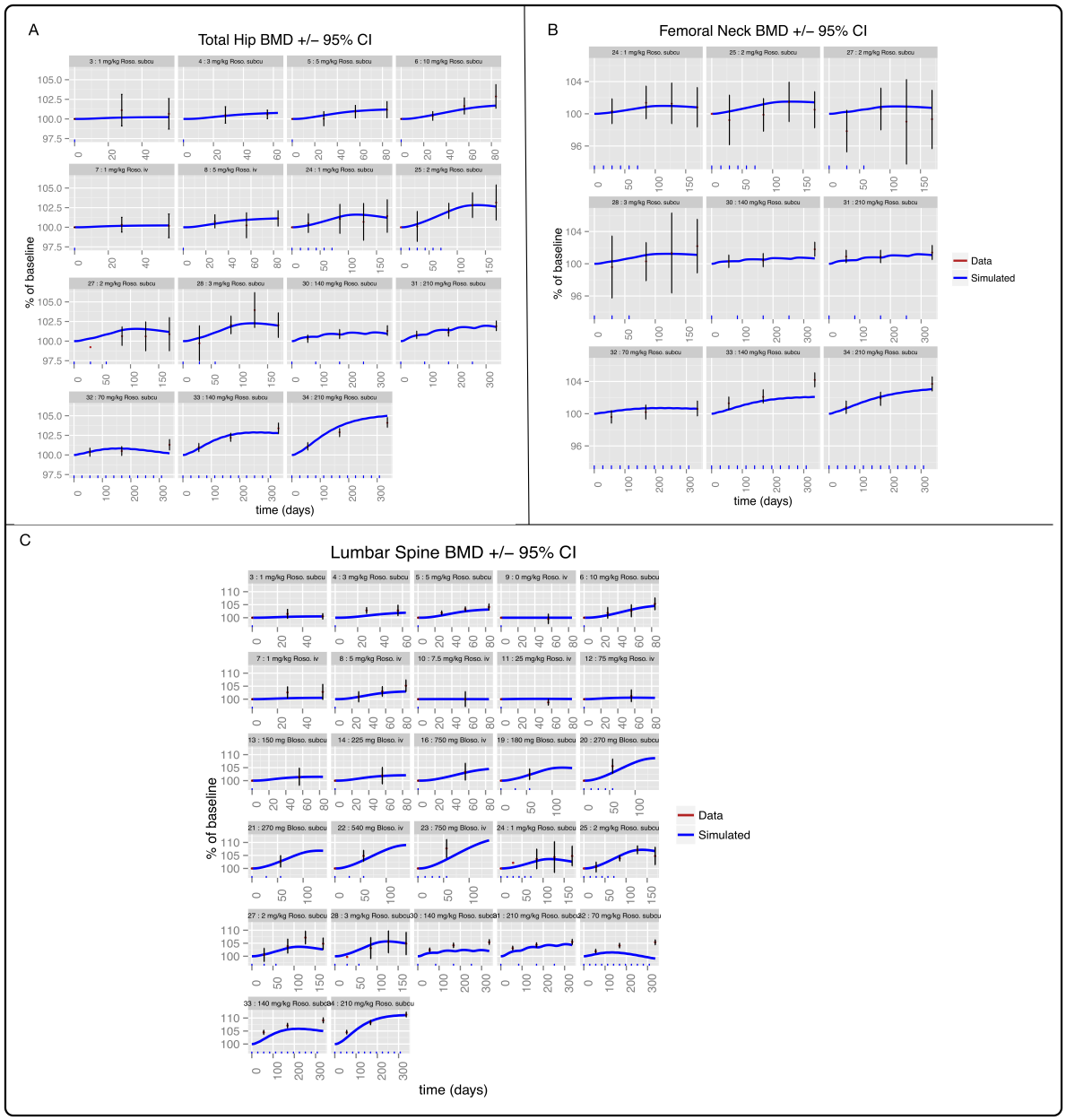

Supplementary Figure 4. Simulated regional changes in BMD plotted overlaying available BMD data from 5 clinical studies with romosozumab and blosozumab. Numbered labels correspond to the same arms from Supplementary Figure 3

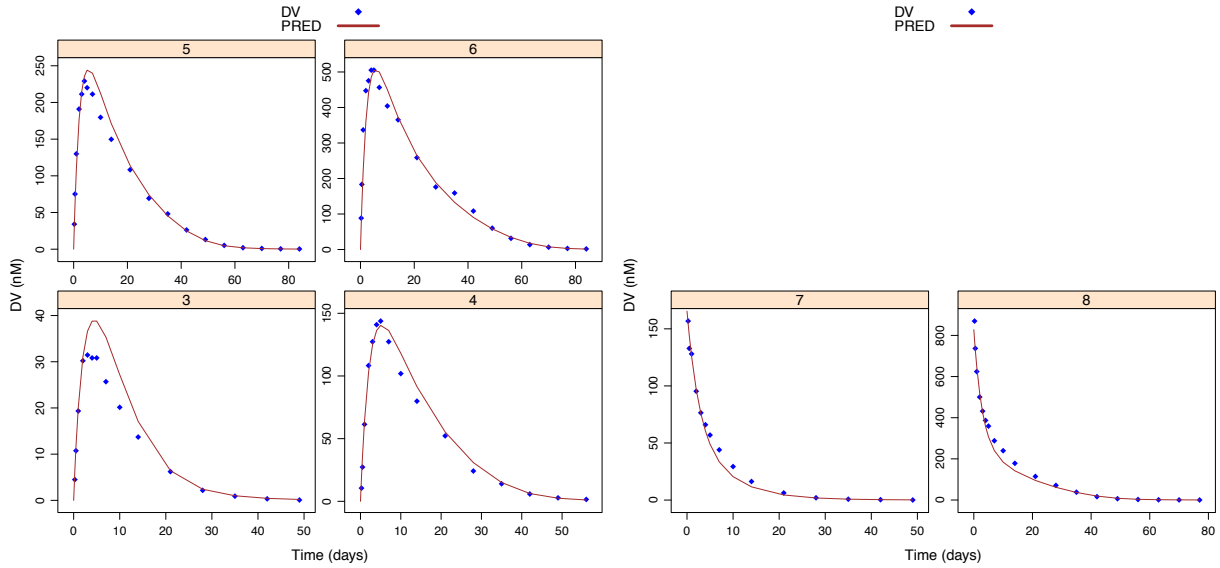

Supplementary Figure 5: PK predictive checks for romosozumab data, grouped by 1, 3, 5, and 10 mg/kg sc (IDs 3-6), and 1 and 5 mg/kg iv (IDs 7,8) dosing arms. Clinical data is show in blue, simulations in red

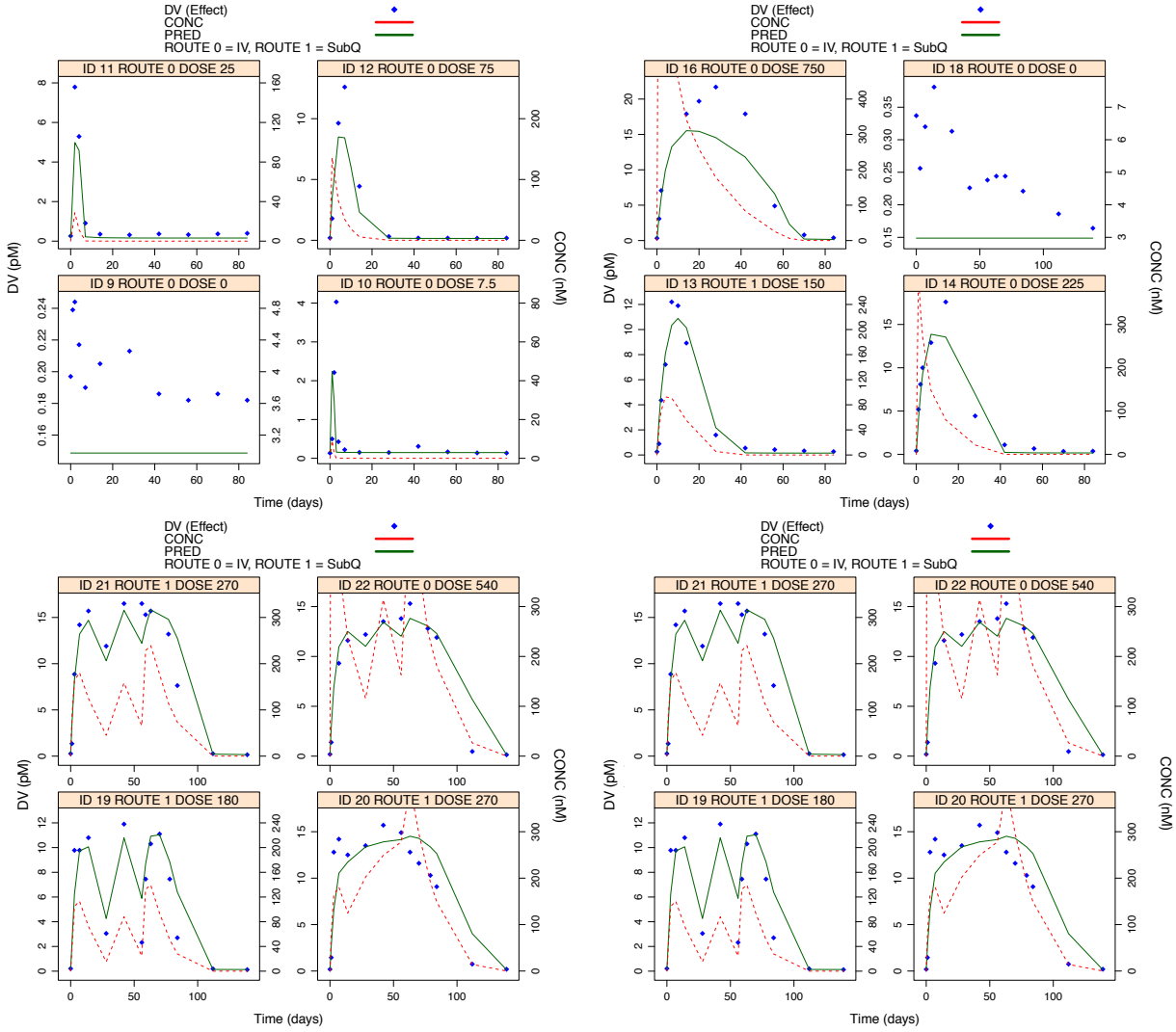

Supplementary Figure 6: PD predictive checks from clinical trial with blosozumab, grouped by dosing arm and route. Clinical data for sclerostin is show in blue, simulations of sclerostin in green (left axis); simulations for sclerostin mAb concentration are shown in red (right axis)

Appendix

Model Assumptions:
1.) An average 70kg individual body weight was assumed so that a 1 mg/kg dose is equivalent to a 70 mg dose of the same drug.

2.) The PK profiles of sclerostin antibodies and resulting effects on sclerostin are the same in healthy women and those with osteoporosis. This assumption was made because only phase 1 data of Romosozumab exposure was available in healthy women and all other data used to build the model was taken from studies in women with osteoporosis.

3.) The pharmacokinetics are very similar between the two mAbs (romosozumab and blosozumab), so that the PK parameters estimated for romosozumab can be carried into the PD model for blosozumab. Romosozumab and blosozumab are both igG iosotypes and mAbs of this isotype have been shown to have very similar PK properties, but have variable binding properties, defined by parameters Km and Vmax [1]. The number of receptors available to bind with the target molecule is described by the Vmax parameter. In the case of sclerostin antibodies, the number of receptors available for binding is common between the two therapies, thus this is a shared parameter in the model, and only the Km was re-estimated for blosozumab in the PD model. Having mAb-matched free drug and total target profiles would improve model predictions, as the model could then be adjusted for relative potencies of the different mAbs, but in the absence of these data, these assumptions are required. We know that OCY are terminally-differentiated bone cells derived from mesenchymal osteoblast lineage, but there is much uncertainty around the fraction of OB that become OCY, or the rate at which they become embedded in the matrix. Bellido (2013) states that anywhere from 5-20% of mature osteoblasts become OCY and that OCY make up more than 90% of bone cells within the matrix. In our model, we fixed the rate of osteocyte production at 0.5 * OB population, and set the initial condition of osteocyte compartment equal to approximately 90% of starting population of total bone cells. We assume apoptosis rate of OCY is dependent on sclerostin antibody concentration, so that when circulating sclerostin is increased, as a result of sclerostin mAb administration, osteocyte activity decreases accordingly.

5.) Changes in BMD in this model are functions of changes in OB and OC activity, which are derived from changes in biomarkers P1NP and CTx. In reality there is more complexing around the dynamics occurring at localized sites in the bone that govern changes in BMD. For example, it is said that PTH treatment, which increases P1NP and CTx, simulates intracortical bone remodeling and can increase porosity at the endocortical surface, but could be offset by increasing cortical thickness [2]. The result is in an increase in hip BMD but not necessarily bone strength, because it is not certain if anabolic or catabolic activity prevails in the optimal endocortical and periosteal proportions. The assumption is that a larger anabolic window is desirable for increased bone strength and fracture prevention but the bone modeling and remodeling activity must also occur in the correct regional proportions to properly strengthen bone. This model cannot yet be used to predict changes in endocortical or periosteal composition.

6.) A zero-placebo response was assumed, which is consistent with the placebo arms in the clinical data not deviating significantly from baseline for either marker or BMD. The model does include disease progression in the context of menopause transition which has been used to model effects of

estrogen loss[3] but in the context of sclerostin, disease progression or modification was not considered, given the lack of a discernable signal in the available placebo data. [4–22]

Appendix References

1. Dirks, N. Le. POPULATION PHARMACOKINETICS OF THERAPEUTIC MONOCLONAL ANTIBODIES: EXAMPLES AND ESTIMATION METHOD PERFORMANCE DIFFERENCES. (University of Tennessee, 2010).

2. Burr, D. B. Does early PTH treatment compromise bone strength? The balance between remodeling, porosity, bone mineral, and bone size. *Curr Osteoporos Rep* **3,** 19–24 (2005).

3. Riggs, M. M., Bennetts, M., van der Graaf, P. H. & Martin, S. W. Integrated Pharmacometrics and Systems Pharmacology Model-Based Analyses to Guide GnRH Receptor Modulator Development for Management of Endometriosis. *CPT pharmacomet. syst. pharmacol.* **1,** e11– (2012).

4. Alvarez, L. *et al.* Long-term biochemical response after bisphosphonate therapy in Paget's disease of bone. Proposed intervals for monitoring treatment. *Rheumatology* **43,** 869–874 (2004).

5. B. Abrahamsen P. Eiken, R. E. Subtrochanteric and diaphyseal femur fractures in patients treated with alendronate: A register-based national cohort study. *J Bone Min. Res* **24,** 1095–1102 (2009).

6. Blumsohn, A. *et al.* Early changes in biochemical markers of bone turnover and their relationship with bone mineral density changes after 24 months of treatment with teriparatide. in *Osteoporosis International* **22,** 1935–1946 (2011).

7. Bonnick, S. *et al.* Comparison of weekly treatment of postmenopausal osteoporosis with alendronate versus risedronate over two years. *J. Clin. Endocrinol. Metab.* **91,** 2631–2637 (2006).

8. Boonen, S. *et al.* Efficacy and safety of a once-yearly intravenous zoledronic acid 5 mg for fracture prevention in elderly postmenopausal women with osteoporosis aged 75 and older. *J. Am. Geriatr. Soc.* **58,** 292–299 (2010).

9. Carneiro, R. M. *et al.* Lactation and bone turnover: A conundrum of marked bone loss in the setting of coupled bone turnover. *J. Clin. Endocrinol. Metab.* **95,** 1767–1776 (2010).

10. Covic, A. *et al.* A comparison of calcium acetate/magnesium carbonate and sevelamer-hydrochloride effects on fibroblast growth factor-23 and bone markers: Post hoc evaluation from a controlled, randomized study. *Nephrol. Dial. Transplant.* **28,** 2383–2392 (2013).

11. Cusano, N. E. *et al.* Therapy of hypoparathyroidism with PTH(1-84): A prospective four-year investigation of efficacy and safety. *J. Clin. Endocrinol. Metab.* **98,** 137–144 (2013).

12. Eastell, R. *et al.* Effect of an aromatase inhibitor on bmd and bone turnover markers: 2-year results of the Anastrozole, Tamoxifen, Alone or in Combination (ATAC) trial (18233230). *J. Bone Miner. Res.* **21,** 1215–1223 (2006).

13. Ettinger, B., San Martin, J., Crans, G. & Pavo, I. Differential effects of teriparatide on BMD after treatment with raloxifene or alendronate. *J. Bone Miner. Res.* **19,** 745–751 (2004).

14. Goss, P. E. *et al.* Effects of steroidal and nonsteroidal aromatase inhibitors on markers of bone turnover in healthy postmenopausal women. *Breast Cancer Res.* **9,** R52 (2007).

15. Greenspan, S. L. *et al.* Skeletal health after continuation, withdrawal, or delay of alendronate in men with prostate cancer undergoing androgen-deprivation therapy. *J. Clin. Oncol.* **26,** 4426–4434 (2008).

16. Haskelberg, H. *et al.* Changes in bone turnover and bone loss in HIV-infected patients changing treatment to tenofovir-emtricitabine or abacavir-lamivudine. *PLoS One* **7,** (2012).

17. Jodar-Gimeno, E. Full length parathyroid hormone (1-84) in the treatment of osteoporosis in postmenopausal women. *Clin. Interv. Aging* **2,** 163–174 (2007).

18. Kenny, A. M. *et al.* NIH Public Access. *Heal. (San Fr.* **58,** 1134–1143 (2011).

19. Moore, A. E. B. *et al.* Changes observed in radionuclide bone scans during and after teriparatide treatment for osteoporosis. *Eur. J. Nucl. Med. Mol. Imaging* **39,** 326–336 (2012).

20. Panico, A. *et al.* Teriparatide vs. alendronate as a treatment for osteoporosis: changes in biochemical markers of bone turnover, BMD and quality of life. *Med. Sci. Monit.* **17,** CR442–R448 (2011).

21. Starke, A. *et al.* Correction of metabolic acidosis with potassium citrate in renal transplant patients and its effect on bone quality. *Clin. J. Am. Soc. Nephrol.* **7,** 1461–72 (2012).

22. Undale, A. *et al.* NIH Public Access. **47,** 83–92 (2011).

Chapter 9

PAPER III

Title: Development of a Hazard Model of Fracture to Explore the Impact of Different Therapeutic Mechanisms on Clinical Outcomes in Patients with Osteoporosis

Author List: Rena J. Eudy[1,2], Matthew M. Riggs[3] , Marc R. Gastonguay[1,2,3] , William Gillespie[3]

(1) Department of Biomedical Engineering, University of Connecticut, Storrs, Connecticut, USA
(2) Metrum Institute, Tariffville, Connecticut, USA
(3) Metrum Research Group, LLC, Tariffville, Connecticut, USA

Corresponding Author's Name:
Rena J. Eudy
Department of Biomedical Engineering, University of Connecticut
Metrum Institute
2 Tunxis Road, Suite 112
Tariffville, CT 06081

Keywords: Bone mineral density, fracture, osteoporosis, hazard model

Abstract

A hazard model of fracture was developed using individual-level data from the NHANES (2005-2008) database and summary-level data from an aggregate dataset. The aggregate dataset was build by performing a comprehensive and systematic literature search of clinical studies published from 1995-2015, recording fracture rate and bone mineral density (BMD) during and after various treatments. Eight candidate models were evaluated by deviance information criteria (DIC) and posterior predictive check (PPC). The model with covariates for change from baseline (CFB) lumbar spine (LS) BMD, baseline LS BMD, and patient body mass index (BMI), years post-menopause, fracture measure method (clinical or radiological) and additional drug effects outperformed other models with different representations of BMD and those without additional drug effects. The approximated hazard ratio relative to placebo for fracture for each drug class was 0.544 for bisphosphonates, 0.412 for PTH/teriparatide, 0.485 for denosumab, 0.180 for calicitonin, 0.511 for growth hormone secretogogue MK-677, and 0.760 for strontium ranelate. Similar to the FRAX® tool [1], this model is useful for predicting the 10-year probability of fracture for a patient with osteoporosis but represents an expandable and open-source framework for generating these predictions.

1. Introduction

The aging global population has lead to significant increases in osteoporosis diagnoses. Patients with progressed form of this disease suffer significant loss of quality of life due to bone fragility leading to fracture. Various classes of therapies have demonstrated efficacy in terms of increasing bone mineral density (BMD) at various skeletal sites as well as long-term reduction in the rate of fracture. As newer therapies are developed, it is important to establish the relationship between changes in BMD, which can be measured in early-phase clinical trials, and fracture outcomes that develop over longer periods of time. It is also essential to identify those patient characteristics that are most significantly implicated in the occurrence of fracture.

Much work has already been done to establish risk factors associated with fracture. The FRAX® [1] online calculator was developed by the World Health Organization (WHO) and is used to calculate the 10-year probability of fracture using information about individual-level patient demographics, physical traits, family history, glucocorticoid use, whether or not the patient has experienced a previous fracture, smoking habits and alcohol consumption. Unfortunately the algorithm is not published and there is no published method detailing how these patient characteristics are used to calculate fracture risk.

The work outlined here involves the development of a time-to-event (TTE)/hazard model using a compilation of historic clinical data recording fracture incidence in osteoporosis patients. This model-based meta-analysis (MBMA) approach is an attempt to make inferences about fracture based on a large body of evidence available from published works. MBMAs are well-suited for inferences regarding comparative effects of interventions. The objectives of this work were to leverage this large body of data to compare marketed therapies and to better understand how BMD enters the model, along with the patient covariates that have already been established as influential, in order to link short-term clinical outcomes like BMD with fracture outcomes. It also specifies a measure of sensitivity of fracture probability to specific patient characteristics.

2. Material and Methods

2.1 Data

2.1.1 Data Collection

A subset of individual-level data from the NHANES database was used to build the first portion of the model. These observational data were collected from 2005-2008 and the selected patients fulfilled the following criteria:

- Post-menopausal women above 20 years of age
- Patients who had BMD measurements taken at the time of the interview
- Patients who were at least 2 years post-menopause at screening

Only fracture data that were recorded either 2 years post-menopause or 10 years prior to screening (whichever was less) were recorded. The fracture incidence was assessed retrospectively and reported as the year in which it occurred. Fractures that occurred in the same year as screening were not recorded. After filtering, there were 1925 total patients in the NHANES dataset.

To the extent possible, PRISMA guidelines [2] were used to construct an aggregate dataset for the fracture model. Data were compiled from a Pubmed search conducted on or around June 1, 2015 using keywords “fracture”,“prevent”,“risk”,“occur”,“humans“,“clinical trial”,“randomized controlled trial”, “osteoporosis”, “zoledronic acid”, “teriparatide”, “alendronate”, risedronate”, denosumab”, “HRT”, MK-677”, “intransal salmon calcitonin”, “strontium ranelate” published from 1995 to 2015. 42 Studies were selected from 172 screened studies in Pubmed. Trials included were randomized, blinded and open-label, prospective and retrospective. Patient inclusion criteria were men with osteoporosis or post-menopausal women with osteoporosis greater than 50 years of age. Interventions included in the final dataset included denosumab, any bisphosphonate, teriparatide, PTH, calcitonin, MK-677 or strontium ranelate. Graphical presented data from these publications were digitized using GraphClick (v3.0 Arizona

Software). These data are summarized in Supplementary Table 1. Because vertebral fractures were the dominant type of measured fracture in most of the clinical trials, studies that did not include vertebral fractures were excluded from the dataset. If non-vertebral and vertebral fractures were reported as separate measures, these were combined and recorded as total fracture events. Fracture events were reported as percentage of patients experiencing fracture or number of categorical fracture (vertebral, nonvertebral, clinical or morphological, for example). Time-dependent changes in lumbar spine (LS) BMD were reported as change from baseline, percentage change from baseline (PCFB), g/cm^2 or t-score and converted to PCFB. Baseline mean or median LS BMD were reported in units of g/cm^2 or t-score and were converted to g/cm^2. Studies that did not include at least one post-baseline measurement of LS BMD were excluded from the dataset. Patient baseline characteristics including age, race, body mass index (BMI), years post-menopause, height, weight, prior fracture, and current smoking status were also recorded. Whether or not vertebral fractures were routinely evaluated via radiograph or classified as 'clinical vertebral fractures' was indicated in the dataset. Study extensions were recorded as independent trials, because the extension population typically had its own set of baseline characteristics. Supplementary Figure 1 shows longitudinal changes in LS BMD for each study included in the aggregate dataset (A), and the corresponding rate of fracture for each study arm (B).

2.1.2 Data Standardization and Missing Data Imputation

In the NHANES dataset, BMD measurements were taken at screening and thus had to be imputed at the time of a fracture event. The following equation was used to impute BMD, stratified by baseline quartiles, wherein coefficients were estimated by linear multiple regression:

$$BMD = \beta_0 + \beta_1\,(post\ menopausal\ age - 20) + \beta_2\,(age\ at\ last\ menstrual\ period - 51.7) + \beta_3(BMI - 27.1) + \beta_4 I_{\,afro-american} \quad [1]$$

For both NHANES and aggregate datasets, missing BMI (kg/m^2) was computed from weight and height. If neither BMI nor height and weight were reported, BMI was imputed with a multiple linear regression model where the coefficients were estimated separately for each dataset:

$$BMI_i = \beta_0 + \beta_1 * (age_{\ i} - \widetilde{age}) \quad [2]$$

for the *i*th individual (NHANES) or *i*th treatment arm (aggregate dataset)

In the NHANES dataset, all BMD measures were reported as T-scores. These, and the values of BMD in the aggregate data reported as a T scores were converted to units of g/cm^2 using the reference BMD and standard deviation (SD) parameters for a white female [47].

$$BMD_{g/cm\hat{}2} = 0.106 * BMD_{T-Score} + 1.064 \quad [3]$$

If post-menopausal age was not reported in the aggregate dataset, it was computed by subtracting a weighted average of post-menopausal ages of the treatment arms from the average age of the reported treatment arm.

2.3 Development of Hazard Model of Fracture

While the MBMA approach is useful for distinguishing effects of assigned intervention across summary-level treatment arms, it is less useful for quantifying the effects of patient characteristics on outcome. To address this, separate hazard model structures were used to fit the NHANES data and the published aggregate data, respectively. A Bayesian approach as implemented in OpenBUGS v. 3.2.2 was used to fit both models simultaneously and the majority of parameters were shared between the models. The NHANES dataset represented a single trial, as did each of the studies in the aggregate dataset. The covariates included in both models were preselected based upon the those examined in the FRAX project [1] and those available in the literature. It was determined from a previous analysis that LS BMD was more predictive of

fracture outcomes than either total hip or femoral neck BMD (data not shown). No formal covariate selection process was conducted. Inter-trial variation for both models was applied to the baseline hazard and BMD –related parameter(s) in the respective hazard model. For the population-level simulations, values for these parameters were randomly selected from a multivariate normal distribution with mean, θ and variance, Ω.

Markov Chain Monte Carlo (MCMC) simulations generated vectors of parameters from the approximate distribution. Four chains of 100,000 iterations are generated, with the first 50,000 being discarded and every 50th sample retained, resulting in 4000 samples for statistical inference. Weakly informative prior distributions for covariate parameters and variance parameters were used in all versions of the model to allow the data to influence parameter estimation. Model selection was based on values of mean deviance, DIC (deviance information criteria), and posterior predictive checks (PPCs). Under the assumption the BMD and drug effect parameters in the model are independent, an approximate hazard ratio for each class of drug in the model was calculated using the mean area under the curve (AUC) for BMD, calculated by trapezoidal rule (eq 14) for each drug class and the estimated drug effect:

$$Hazard\ ratio = \exp\left(\widehat{BMD_{time-ave}} + \left[E_{Drug}\right]\right)/\exp\left(\widehat{BMD_{time-ave-PBO}}\right) \quad [4]$$

$$\text{Where } BMD_{time-ave} = 0.5 * \Sigma((BMD_t + BMD_{t-1}) * (t - (t-1)), \quad [5]$$

where t is the elapsed time since previous BMD measurement and (t - 1) is the time of the previous BMD measurement for each treatment arm.

3. Results

3.1. Final Hazard Model Structure

3.1.1 Time-to-Event Model for NHANES dataset

The likelihood for the time to first fracture in the *i*th patient ($t_{frac,i}$) took the form:

$$L\left(\theta\middle|t_{frac,i,}censor_i, X_i\right) = \begin{cases} h_i\left(t_{frac,i}\middle|\theta, X_i\right)e^{-\int_0^{t_{frac,i,}} h_i(u|\theta,X_i)du}, & \text{Fracture observed} \\ e^{-\int_0^{t_{frac,i,}} h_i(u|\theta,X_i)du} & \text{Fracture right-censored} \end{cases} \quad [6]$$

where censor_i =1 indicates fracture is right censored (no fracture occurred during the duration of the trial) and 0 otherwise. X_i corresponds to the covariate to be estimated. If fracture is right censored, t_{frac} corresponds to the time of last observation during the observation period. h_i represents the hazard equation. Observation period was defined as beginning 10 years before the interview or 2 years post-menopause, whichever occurred last

The hazard equation (h_i) for the NHANES model took the form:

$$\begin{gathered} h_i = h_{0j} \exp\left(\beta_{BMD,j} * \log\left(\text{BMD}_{pred,i}/\widehat{BMD}\right)\right. \\ +\beta_{postMenoAge}\left(time_i + postMenoage_{0,i} + \widehat{postMenoAge}\right) \\ \left. + \beta_{BMI}\left(BMI_i - \widehat{BMI}\right)\right. \end{gathered} \quad [7]$$

in the *i*th treatment arm of the *j*th trial and *time* is the duration of observation in trial

The BMD portion of the hazard is log-transformed to ensure only BMD predictions that are positive enter the model for hazard. The effect of BMD on hazard is also more interpretable in this context; as long as the percentage increase in BMD from baseline is fixed, one would expect the same amount of decrease in the hazard for fracture.

3.1.2 Hazard Model for the Aggregate Dataset

The number of patients experiencing a fracture from the aggregate dataset followed a binomial distribution with probability of fracture, $p_{frac,ij}$ for n_{ij} patients at risk for fracture, where

$$p_{frac,ij} = 1 - e^{-\int_0^t h_{ij}(u|\theta,X_{ij})du} \quad [8]$$

in the *i*th treatment arm of the *j*th trial, X_{ij} represent the model covariates, h_{ij} represents the hazard

equation and t is the duration of observation in trial.

Four different hazard models, which were variations of a Cox regression (eq 7), were evaluated on the basis of the LS BMD representation which best predicted the proportion of patients experiencing fracture in the aggregate dataset. Each candidate model was also analyzed with and without an additional set of covariates, where each covariate represented a additional effect specific to each class of therapy in the dataset ($E_{Drug,k}$).

$$h(t) = h_0 \, e^{[\Sigma \beta_{x_i}(x_i - \hat{x_i})]} \quad [9]$$

where each x_i is a covariate and h_0 is the baseline hazard

Covariates consistent across all the model candidates included post-menopausal age, method of vertebral fracture identification ($I_{radFracture}$ = 1 if measured radiologically, and 0 if identified as clinical fractures), and body mass index (BMI).

The four candidate model structures for the BMD covariate(s) were as follows:

1.) Time-dependent

$$COV_{BMD} = \beta_{BMD,j} \log\left(\frac{BMD_{ij}(t)}{\widehat{BMD}}\right) \quad [10]$$

2.) Time-dependent + change from baseline BMD

$$COV_{BMD} = \beta_{BMD,j} \log\left(\frac{BMD_{ij}(t)}{\widehat{BMD}}\right) + \beta_{BMD\ CFB,j} BMD_{spine\ CFB,ij}(t) \quad [11]$$

3.) Baseline + change from baseline BMD

$$COV_{BMD} = \beta_{BMD\ BASE,j} \log\left(\frac{BMD_{0,ij}}{\widehat{BMD_0}}\right) + \beta_{BMD\ CFB,j} BMD_{spine\ CFB,ij}(t) \quad [12]$$

4.) Time-dependent + baseline BMD

$$COV_{BMD} = \beta_{BMD,j} \log\left(\frac{BMD_{ij}(t)}{\widehat{BMD}}\right) + \beta_{BMD\ BASE,j} \log\left(\frac{BMD_{0,ij}}{\widehat{BMD_0}}\right) \quad [13]$$

for ith arm and jth trial.

The hazard model took the form:

$$h_{ij} = h_{0j} \exp\left(COV_{BMD} + \beta_{postMenoAge}\left(postMenoAge_{ij}(t) - \widehat{postMenoAge}\right) + \beta_{radFracture} I_{radFracture,ij} + \beta_{BMI}\left(BMI_{ij} - \widehat{BMI}\right) + \left[E_{Drug,k}\right]\right) \quad [14]$$

for *i*th arm, *j*th trial, and *k*th drug class (1=placebo, 2=bisphosphonates, 3=PTH/teriparatide, 4=denosumab, 5=calcitonin, 6=growth secretagogue MK-677, 7=strontium ranelate)

3.2 Covariate Structures and Parameter Estimates

Each model was tested with and without a drug effect and yielded the following results for DIC:

Table 1. Model structures and DIC results

BMD Covariate Structure	**DIC**
Time Dependent BMD	2765.227
Time Dependent BMD + Add'l Drug Effect	**2631.669**
Time-dependent + change from baseline BMD	2716.229
Time-dependent + change from baseline BMD + Add'l Drug Effect	2640.619
Baseline + change from baseline BMD	2714.463
Baseline + change from baseline BMD + Add'l Drug Effect	2639.259
Time-dependent + baseline BMD	2731.056
Time-dependent + baseline BMD + Add'l Drug Effect	2633.337

The model that yielded the lowest DIC score included the time-dependent BMD measurement and additional drug effect. The mean parameter estimates for this model are shown in Table 2. Figure 1 shows both individual-level and population-level post-predictive checks (PPC) of the TTE model, with the NHANES data and predictions stratified by baseline BMD. Figure 2 shows PPCs of the aggregate data-driven hazard model at both the individual and population levels.

Table 2. Parameter estimates and 95% CI around the mean

Parameter	**Mean**	**95% CI**
$\boldsymbol{h_0}$ (1/years)	0.0583	(0.0447; 0.0749)
$\boldsymbol{\beta_{BMD}}$ (1/gm/cm^2)	1.33	(-1.78; 4.29)

$\boldsymbol{\beta_{radFracture}}$ (unitless)	-0.204	(-0.386; -0.0275)
$\boldsymbol{\beta_{postMenoAge}}$ (1/years)	0.0269	(0.0139; 0.0405)
$\boldsymbol{\beta_{bisphosphonates}}$(unitless)	-0.631	(-0.745; -0.513)
$\boldsymbol{\beta_{PTH/teriparatide}}$ (unitless)	-0.889	(-1.18; -0.616)
$\boldsymbol{\beta_{denosumab}}$ (unitless)	-0.750	(-1.21; -0.579)
$\boldsymbol{\beta_{calcitonin}}$ (unitless)	-1.68	(-5.0; 0.470)
$\boldsymbol{\beta_{MK-677}}$ (unitless)	-0.689	(-2.68; 0.838)
$\boldsymbol{\beta_{strontium\ ranelate}}$ (unitless)	-0.289	(-0.886; 0.327)
Ω_{h0}	0.69	(0.527; 0.898)
Ω_{BMD}	6.87	(4.63; 9.95)

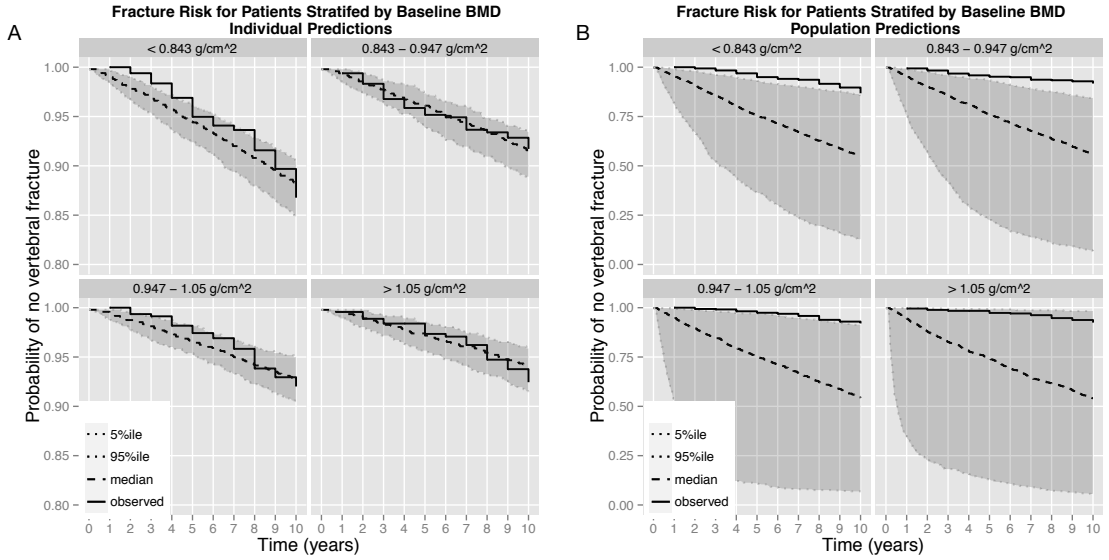

Figure 1: Individual (A) and population-level (B) PPCs for the NHANES dataset, stratified by baseline BMD. Individual-level predictions estimate fracture probability in the same trial with the same patient covariates. Predictions at the population-level reflect probability of fracture in a new trial, but same patient covariates.

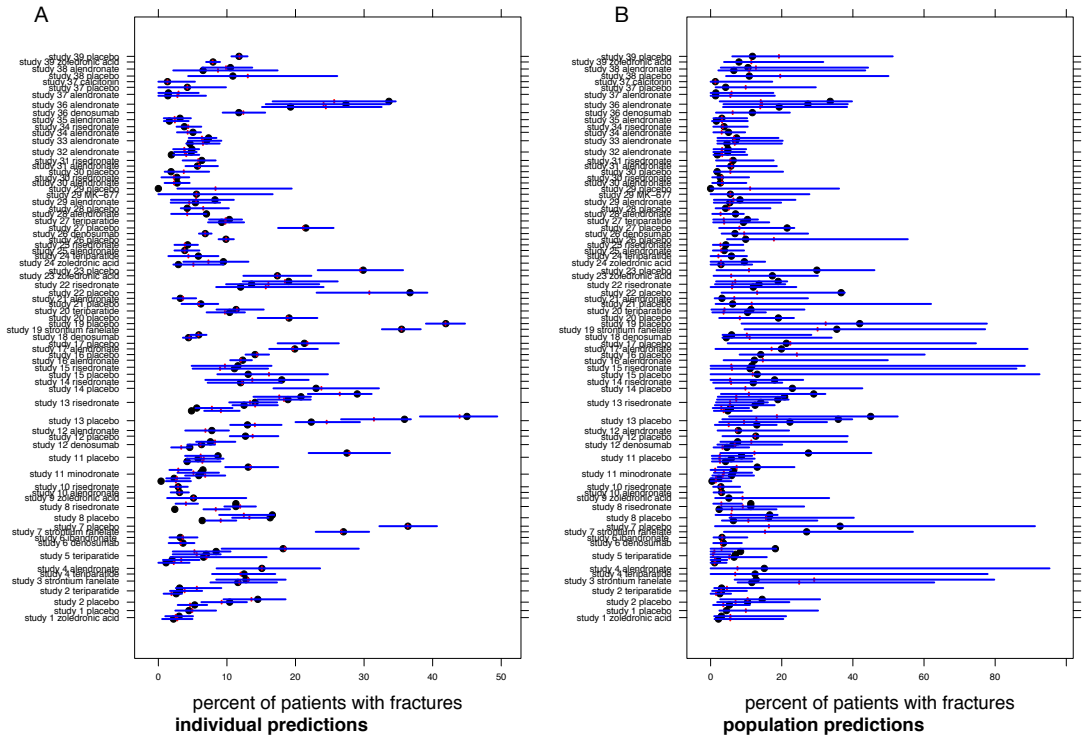

Figure 2: Individual (A) and population (B) -level PPCs for the aggregate dataset, grouped by study arm. The • indicates the mean percentage of patients with fracture from the clinical data, the red line indicates predicted median, and blue lines indicate 90% CI around the prediction. Individual-level predictions estimate fracture probability in the same trial with the same patient covariates. Predictions at the population-level reflect probability of fracture in a new trial, but same patient covariates.

4. Discussion

Prior to the development of this hazard model of fracture, there was no published model relating changes in LS BMD to probability of fracture in patients with osteoporosis. This work leverages a large amount of summary-level metadata, as well as an individual- patient level (NHANES) dataset with BMD and fracture in order to provide a framework for linking short-term changes in BMD to long term fracture outcomes. The model with best performance was the simplest model with a single covariate for BMD and a covariate for the additional drug effect.

The final model greatly over-predicted the probability of fracture over time in patients in the NHANES dataset at the population level (Figure 1B), but estimated individual-level fracture rate at a greater level of accuracy (Figure 1). This outcome could indicate high levels of inter-trial

variability at the level of the baseline hazard, (h_0). It is also important to note that the information contained in the NHANES dataset originates from an observational study and is reflective of a highly heterogeneous population. Fracture events recorded in this dataset were assessed by patient interview and subject to errors in human memory. This is in contrast to the metadata set that was made up of mostly prospective trials conducted in-house and subject to a greater level of control. Population-level estimates for the aggregate dataset were also more variable, again for the reason that inter-trial variability for the baseline hazard and BMD covariates was high. Precision around some of the parameter estimates was poor (C.I. included the null in some cases; see Table 2). In the case of the BMD covariate, this is likely due to this measure being highly variable across treatment arms and trials. Areal BMD is typically measured with a DEXA scanners but there have been documented discrepancies in measurements taken with the different types of scanners (Hologic, Lunar, Norland) [48].

Hazard models with and without an additional covariate for an independent drug effect were compared. It was determined that there is an additional beneficial effect of some classes of therapies, which is independent of the contribution of changes in BMD elicited by the therapy, on fracture reduction. One reason for this is that different drug mechanisms have differential effects on regional areal BMD (aBMD, the type measured here), as well as on bone microarchitecture. BMD and bone microarchitecture are loosely associated. For example, changes in 1/3rd radius BMD are linked to changes in the cortical bone compartment and distal radius BMD is descriptive of changes at intracortical sites[49]. However, development of this model supports the widely-held notion that BMD only tells part of the story of the association between bone composition, strength and probability of fracture. A study by Sornay-Rendu et al. [50], demonstrated that changes in microarchitecture associated with fracture are partially independent of changes in aBMD, as measured at the radius and hip. Given the results of this study and the findings that the measures of trabecular number, trabecular distribution and separation of distribution were the significant measures distinguishing osteoporotic women with and without

fracture, one could make the argument that measuring changes in bone microarchitecture would be more clinically useful in measuring bone strength and should be more routinely used. However in this study, the authors did not consider lumbar spine or femoral neck BMD, two of the routinely examined sites in clinical efficacy studies.

There is much evidence for different classes of therapy having differential effects on bone microarchitecture in the published literature. Seeman, et al. [51] published a study looking at the differences between denosumab and alendronate effects on bone microarchitecture. The authors speculated that treatment-specific changes in total and cortical BMD might point to drug mechanisms at the level of the bone multicellular unit (BMU). Because denosumab inhibits osteoclast synthesis there is a rapid reduction in newly excavated resorption cavities and simultaneous filling of existing cavities, in contrast with alendronate, which does not elicit the same CTX response at comparable doses. It has also been suggested that the anti-resporptive effect of bisphosphonates is mediated by the distribution of the drug, because the strong affinity of bisphosphonates for hydroxyappetite and bone mineral may limit distribution [49]. It is possible that osteoclasts may not commence remodeling activity until the entire matrix containing the bisphosphonate is resorbed. This process may not be linear or uniform throughout the skeleton.

In contrast to anti-resorptive therapies, teriparatide has been shown to decrease cortical thickness in the tibia and radius while increasing cortical porosity and significantly increasing trabecular number in the tibia [52]. The authors conjecture that the anabolic mechanism of action of PTH is to accelerate intracortical and endosteal remodeling. Zolerdronic acid was used as a comparator in this study and did not have an impact on cortical porosity, but did increase cortical thickness, consistent with bisphosphonate activity seen in the Seeman, et al. study. Considering the variable effects of different agents on microarchitecture, the influence of an independent, drug-effect on probability of fracture may stem from differential effects in bone composition that are not fully represented by regional areal BMD measures.

Future development of the model may include investigation of the relationship between BMD and fractures at specific sites. The major limitation to this endeavor is a lack of clinical trials reporting site-specific fracture events. Coupling MBMA developed by a comprehensive, systematic literature search with individual-level data from the NHANES database allowed for a comparison of effects of different drug classes on probability of fracture, and demonstrated the influence of patient characteristics on this probability. Still, more clinical data at the level of the individual patient is also desired in order to describe effects of patient characteristics on fracture risk more precisely.

5. Conclusion

In the development of a hazard model of fracture, the best predictions came from a model that included time-dependent BMD. In addition to these BMD changes elicited by therapy, there is a significant contribution of an additional class-specific drug effect that contributes to hazard reduction beyond effects on BMD. This additional drug effect likely reflects changes in the bone microarchitecture that are not being represented by areal BMD endpoints typically measured in a clinical trial. This fracture model is a public and expandable framework for quantifying the extent to which patient characteristics and patient response to therapy contribute to fracture reduction. As more clinical data become available and therapies with different mechanisms of action are developed, the model can be updated. Another feature of this model that distinguishes it from the FRAX model is it can be used to make inferences about how variability affects outcome in a clinical population. This utility for prediction into a clinical study paradigm is relevant for development of new therapies for osteoporosis.

References

1. World Health Organization Collaborating Centre for Metabolic Bone Diseases, University of Sheffield U. FRAX: WHO Fracture Risk Assessment Tool [Internet]. 17.10.14 Release (FRAX v3.9). 2014 [cited 2015 Jan 1]. Available from: http://www.sheffield.ac.uk/FRAX

2. Moher D, Liberati a, Tetzlaff J, Altman DG, Grp P. Preferred Reporting Items for Systematic Reviews and Meta-Analyses: The PRISMA Statement (Reprinted from Annals of Internal Medicine). Phys. Ther. [Internet]. 2009;89:873–80.

3. McClung M, Miller P, Recknor C, Mesenbrink P, Bucci-Rechtweg C, Benhamou C-L. Zoledronic acid for the prevention of bone loss in postmenopausal women with low bone mass: a randomized controlled trial. Obstet. Gynecol. 2009;114:999–1007.

4. Nakamura T, Sugimoto T, Nakano T, Kishimoto H, Ito M, Fukunaga M, et al. Randomized Teriparatide {[}human parathyroid hormone (PTH) 1-34{]} Once-Weekly Efficacy Research (TOWER) trial for examining the reduction in new vertebral fractures in subjects with primary osteoporosis and high fracture risk. J Clin Endocrinol Metab. 2012;97:3097–106.

5. Oswald AJ, Berg J, Milne G, Ralston SH. Teriparatide treatment of severe osteoporosis reduces the risk of vertebral fractures compared with standard care in routine clinical practice. Calcif Tissue Int. 2014;94:176–82.

6. Fujita T, Fukunaga M, Itabashi A, Tsutani K, Nakamura T. Once-Weekly Injection of Low-Dose Teriparatide (28.2 mug) Reduced the Risk of Vertebral Fracture in Patients with Primary Osteoporosis. Calcif Tissue Int. 2014;94:170–5.

7. Recknor C, Czerwinski E, Bone HG, Bonnick SL, Binkley N, Palacios S, et al. Denosumab compared with ibandronate in postmenopausal women previously treated with bisphosphonate therapy: a randomized open-label trial. Obs. Gynecol. 2013;121:1291–9.

8. Meunier PJ, Roux C, Ortolani S, Diaz-Curiel M, Compston J, Marquis P, et al. Effects of long-term strontium ranelate treatment on vertebral fracture risk in postmenopausal women with osteoporosis. Osteoporos. Int. 2009;20:1663–73.

9. Watts NB, Chines A, Olszynski WP, McKeever CD, McClung MR, Zhou X, et al. Fracture risk remains reduced one year after discontinuation of risedronate. Osteoporos Int. 2008;19:365–72.

10. Harris ST, Watts NB, Genant HK, McKeever CD, Hangartner T, Keller M, et al. Effects of risedronate treatment on vertebral and nonvertebral fractures in women with postmenopausal osteoporosis: A randomized controlled trial. JAMA [Internet]. 1999;282:1344–52.

11. Recker RR, Kendler D, Recknor CP, Rooney TW, Lewiecki EM, Utian WH, et al. Comparative effects of raloxifene and alendronate on fracture outcomes in postmenopausal women with low bone mass. Bone. 2007;40:843–51.

12. Hagino H, Shiraki M, Fukunaga M, Nakano T, Takaoka K, Ohashi Y, et al. Three years of treatment with minodronate in patients with postmenopausal osteoporosis. J Bone Min. Metab. 2012;30:439–46.

13. Matsumoto T, Hagino H, Shiraki M, Fukunaga M, Nakano T, Takaoka K, et al. Effect of daily oral minodronate on vertebral fractures in Japanese postmenopausal women with established osteoporosis: a randomized placebo-controlled double-blind study. Osteoporos Int. 2009;20:1429–37.

14. Nakamura T, Matsumoto T, Sugimoto T, Hosoi T, Miki T, Gorai I, et al. Clinical Trials Express: fracture risk reduction with denosumab in Japanese postmenopausal women and men with osteoporosis: denosumab fracture intervention randomized placebo controlled trial (DIRECT). J Clin Endocrinol Metab. 2014;99:2599–607.

15. Sugimoto T, Matsumoto T, Hosoi T, Miki T, Gorai I, Yoshikawa H, et al. Three-year denosumab treatment in postmenopausal Japanese women and men with osteoporosis: results from a 1-year open-label extension of the Denosumab Fracture Intervention Randomized Placebo Controlled Trial (DIRECT). Osteoporos Int. 2015;26:765–74.

16. Reginster J, Minne HW, Sorensen OH, Hooper M, Roux C, Brandi ML, et al. Randomized trial of the effects of risedronate on vertebral fractures in women with established postmenopausal osteoporosis. Vertebral Efficacy with Risedronate Therapy (VERT) Study Group. Osteoporos. Int. 2000;11:83–91.

17. Sorensen OH, Crawford GM, Mulder H, Hosking DJ, Gennari C, Mellstrom D, et al. Long-term efficacy of risedronate: A 5-year placebo-controlled clinical experience. Bone. 2003;32:120–6.

18. Mellström DD, Sörensen OH, Goemaere S, Roux C, Johnson TD, Chines a. a. Seven years of treatment with risedronate in women with postmenopausal osteoporosis. Calcif. Tissue Int. 2004;75:462–8.

19. Fogelman I, Ribot C, Smith R, Ethgen D, Sod E, Reginster JY. Risedronate reverses bone loss in postmenopausal women with low bone mass: results from a multinational, double-blind, placebo-controlled trial. BMD-MN Study Group. J. Clin. Endocrinol. Metab. 2000.

20. Hooper MJ, Ebeling PR, Roberts a P, Graham JJ, Nicholson GC, D'Emden M, et al. Risedronate prevents bone loss in early postmenopausal women: a prospective randomized, placebo-controlled trial. Climacteric. 2005;8:251–62.

21. Black DM, Cummings SR, Karpf DB, Cauley J a., Thompson DE, Nevitt MC, et al. Randomised trial of effect of alendronate on risk of fracture in women with existing vertebral fractures. Lancet. 1996;348:1535–41.

22. Ensrud KE, Barrett-Connor EL, Schwartz A, Santora AC, Bauer DC, Suryawanshi S, et al. Randomized trial of effect of alendronate continuation versus discontinuation in women with low BMD: results from the Fracture Intervention Trial long-term extension. J. Bone Miner. Res. 2004;19:1259–69.

23. Cummings SR, Black DM, Thompson DE, Applegate WB, Barrett-Connor E, Musliner T a, et al. Effect of alendronate on risk of fracture in women with low bone density but without vertebral fractures: results from the Fracture Intervention Trial. JAMA. 2012;280:2077–82.

24. Reginster J-Y, Kaufman J-M, Goemaere S, Devogelaer JP, Benhamou CL, Felsenberg D, et al. Maintenance of antifracture efficacy over 10 years with strontium ranelate in postmenopausal osteoporosis. Osteoporos Int. 2012;23:1115–22.

25. Reginster JY, Felsenberg D, Boonen S, Diez-Perez A, Rizzoli R, Brandi ML, et al. Effects of long-term strontium ranelate treatment on the risk of nonvertebral and vertebral fractures in postmenopausal osteoporosis: Results of a five-year, randomized, placebo-controlled trial. Arthritis Rheum. 2008;58:1687–95.

26. Lindsay R, Miller P, Pohl G, Glass E V., Chen P, Krege JH. Relationship between duration of teriparatide therapy and clinical outcomes in postmenopausal women with osteoporosis. Osteoporos. Int. 2009;20:943–8.

27. Devogelaer JP, Broll H, Correa-Rotter R, Cumming DC, De Deuxchaisnes CN, Geusens P, et al. Oral alendronate induces progressive increases in bone mass of the spine, hip, and total body over 3 years in postmenopausal women with osteoporosis. Bone. 1996;18:141–50.

28. Bai H, Jing D, Guo A, Yin S. Randomized controlled trial of zoledronic acid for treatment of osteoporosis in women. J. Int. Med. Res. [Internet]. 2013;41:697–704. Available from: http://www.ncbi.nlm.nih.gov/pubmed/23669294

29. Cosman F, Eriksen EF, Recknor C, Miller PD, Guañabens N, Kasperk C, et al. Effects of intravenous zoledronic acid plus subcutaneous teriparatide [rhPTH(1-34)] in postmenopausal osteoporosis. J. Bone Miner. Res. 2011;26:503–11.

30. Reid DM, Hosking D, Kendler D, Brandi ML, Wark JD, Marques-Neto JF, et al. A comparison of the effect of alendronate and risedronate on bone mineral density in postmenopausal women with osteoporosis: 24-Month results from FACTS-International. Int. J. Clin. Pract. 2008;62:575–84.

31. Reid DM, Hosking D, Kendler D, Brandi ML, Wark JD, Weryha G, et al. Alendronic acid produces greater effects than risedronic acid on bone density and turnover in postmenopausal women with osteoporosis: Results of FACTS1-International. Clin. Drug Investig. 2006;26:63–74.

32. Devogelaer JP, Brown JP, Burckhardt P, Meunier PJ, Goemaere S, Lippuner K, et al. Zoledronic acid efficacy and safety over five years in postmenopausal osteoporosis. Osteoporos Int. 2007;18:1211–8.

33. Cummings SR, San Martin J, McClung MR, Siris ES, Eastell R, Reid IR, et al. Denosumab for prevention of fractures in postmenopausal women with osteoporosis. N. Engl. J. Med. 2009;361:756–65.

34. Bone HG, Chapurlat R, Brandi ML, Brown JP, Czerwiński E, Krieg MA, et al. The effect of three or six years of denosumab exposure in women with postmenopausal osteoporosis: Results from the FREEDOM extension. J. Clin. Endocrinol. Metab. 2013;98:4483–92.

35. Neer RM, Arnaud CD, Zanchetta JR, Prince R, Gaich G a, Reginster JY, et al. Effect of parathyroid hormone (1-34) on fractures and bone mineral density in postmenopausal women with osteoporosis. N. Engl. J. Med. 2001;344:1434–41.

36. Lindsay R, Cosman F, Lobo R a, Walsh BW, Harris ST, Reagan JE, et al. Addition of alendronate to ongoing hormone replacement therapy in the treatment of osteoporosis: a randomized, controlled clinical trial. J. Clin. Endocrinol. Metab. 1999;84:3076–81.

37. Murphy MG, Weiss S, McClung M, Schnitzer T, Cerchio K, Connor J, et al. Effect of alendronate and MK-677 (a growth hormone secretagogue), individually and in combination, on markers of bone turnover and bone mineral density in postmenopausal osteoporotic women. J. Clin. Endocrinol. Metab. 2001;86:1116–25.

38. Hosking D, Adami S, Felsenberg D, Andia JC, Välimäki M, Benhamou L, et al. Comparison of change in bone resorption and bone mineral density with once-weekly alendronate and daily risedronate: a randomised, placebo-controlled study. Curr. Med. Res. Opin. 2003;19:383–94.

39. Rizzoli R, Greenspan SL, Bone G, Schnitzer TJ, Watts NB, Adami S, et al. Two-year results of once-weekly administration of alendronate 70 mg for the treatment of postmenopausal osteoporosis. J. Bone Miner. Res. 2002;17:1988–96.

40. Schnitzer T, Bone HG, Crepaldi G, Adami S, McClung M, Kiel D, et al. Therapeutic equivalence of alendronate 70 mg once-weekly and alendronate 10 mg daily in the treatment of osteoporosis. Alendronate Once-Weekly Study Group. Aging (Milano). 2000.

41. Rosen CJ, Hochberg MC, Bonnick SL, McClung M, Miller P, Broy S, et al. Treatment with once-weekly alendronate 70 mg compared with once-weekly risedronate 35 mg in women with postmenopausal osteoporosis: a randomized double-blind study. J. Bone Miner. Res. 2005;20:141–51.

42. Kendler DL, Roux C, Benhamou CL, Brown JP, Lillestol M, Siddhanti S, et al. Effects of denosumab on bone mineral density and bone turnover in postmenopausal women transitioning from alendronate therapy. J. Bone Miner. Res. 2010;25:72–81.

43. Bone HG, Hosking D, Devogelaer J-P, Tucci JR, Emkey RD, Tonino RP, et al. Ten Years' Experience With Alendronate for Osteoporosis in Postmenopausal Women. Obstet. Gynecol. Surv. 2004;59:597–8.

44. Adami S, Passeri M, Ortolani S, Broggini M, Carratelli L, Caruso I, et al. Effects of oral alendronate and intranasal salmon calcitonin on bone mass and biochemical markers of bone turnover in postmenopausal women with osteoporosis. Bone. 1995;17:383–90.

45. Miller PD, Bolognese M a., Lewiecki EM, McClung MR, Ding B, Austin M, et al. Effect of denosumab on bone density and turnover in postmenopausal women with low bone mass after long-term continued, discontinued, and restarting of therapy: A randomized blinded phase 2 clinical trial. Bone. 2008;43:222–9.

46. Black DM, Delmas PD, Eastell R, Reid IR, Boonen S, Cauley JA, et al. Once-yearly zoledronic acid for treatment of postmenopausal osteoporosis. N. Engl. J. Med. 2007;356:1809–22.

47. Ott S. opbmdtz @ courses.washington.edu [Internet]. "T Z scores Osteoporos. Bone Physiol. 2015 [cited 2015 Jun 12]. Available from: http://courses.washington.edu/bonephys/opbmdtz.html

48. Faulkner KG, Roberts LA, McClung MR. Discrepancies in normative data between Lunar and Hologic DXA systems. Osteoporos. Int. ENGLAND; 1996;6:432–6.

49. Baron R, Ferrari S, Russell RGG. Denosumab and bisphosphonates: Different mechanisms of action and effects. Bone. 2011. p. 677–92.

50. Sornay-Rendu E, Boutroy S, Munoz F, Delmas PD. Alterations of cortical and trabecular architecture are associated with fractures in postmenopausal women, partially independent of decreased BMD measured by DXA: the OFELY study. J. Bone Miner. Res. 2007;22:425–33.

51. Seeman E, Delmas PD, Hanley DA, Sellmeyer D, Cheung AM, Shane E, et al. Microarchitectural deterioration of cortical and trabecular bone: differing effects of denosumab and alendronate. J. Bone Miner. Res. 2010;25:1886–94.

52. Hansen S, Hauge EM, Beck Jensen JE, Brixen K. Differing effects of PTH 1-34, PTH 1-84, and zoledronic acid on bone microarchitecture and estimated strength in postmenopausal women with osteoporosis: An 18-month open-labeled observational study using HR-pQCT. J. Bone Miner. Res. 2013;28:736–45.

Supplementary Material

Fracture Metadataset

ID	Trial	Endpoint	Total Patients (N)	Study Length	Treatment(s)	Covariate Information	Year Published	Reference
1		% Patients experiencing fracture (uncatagorized)	581	2 years	placebo zolerdronic acid 5 mg/y	bmi caucasian years post-menopause clinical fracture	2009	[3]
2	TOWER	% Patients experiencing non-vertebral or vertebral fracture	542	1.5 years	placebo teriparatide 56.4 mcg/w	bmi previous vertebral fracture years_post-menopause radiologic fracture	2012	[4]
4		% Patients experiencing non-vertebral or vertebral fracture	323	2.8 years	teriparatide 20 ug/d alendronate 70 mg/w	bmi previous vertebral fracture previous non-vertebral fracture previous fracture years post-menopause smoking clinical fracture	2014	[5]
5		% Patients experiencing vertebral fractures	599	1.5 years	teriparatide 28.2 ug/w teriparatide 1.4 ug/w	bmi asian years post-menopause previous vertebral fracture radiologic fracture	2014	[6]
6		% Patients experiencing non-vertebral or vertebral fracture	253	1 year	denosumab 60 mg/6mo ibandronate 150 mg/mo	bmi caucasian years post-menopause previous vertebral fracture previous non-vertebral fracture previous fracture clinical fracture	2013	[7]

						bmi caucasian years post-menopause previous vertebral fracture		
7		% Patients experiencing vertebral fractures	1254	4 years	placebo strontium ranelate 2g/d	radiologic fracture	2009	[8]
8, 9	VERT North America	% Patients experiencing vertebral fractures	base study: 1329 extension: 759	3 years 1 year extension	placebo risondronate 4 mg/y; discontinued during extension	height years post-menopause previous vertebral fracture weight radiologic fracture	1999, 2008	[9,10]
10	EVA	% Patients experiencing non-vertebral or vertebral fracture	1418	0.85 years	alendronate 10 mg/d risendronate 60 mg/d	bmi caucasian years post-menopause radiologic fracture	2007	[11]
11		% Patients experiencing non-vertebral or vertebral fracture	base study:618 extension: 420	2 years 1 year extension	placebo minodronate 1 mg/d	asian bmi years post-menopause previous vertebral fracture radiologic fracture	2009, 2012	[12,13]
12	DIRECT	% Patients experiencing non-vertebral or vertebral fracture	base study: 1156 extension: 525	2 years 1-year extension	placebo denosumab 60 mg/6 mo alendronate 35 mg/w denosumab-only extension	asian bmi previous vertebral fracture radiologic fracture	2014, 2015	[14,15]
13, 22	VERT International	% Patients experiencing non-vertebral or vertebral fracture	base study: 1226 extension 1: 260 extension 2: 164	3 years 2 2-year extensions	placebo risendronate 2.5 mg/d risendronate 5 mg/d	height years-post menopause previous vertebral fracture radiologic fracture	2000, 2003,2004	[16–18]
14		% Patients experiencing non-vertebral or vertebral fracture	355	2 years	placebo risendronate 2.5 mg/d risendronate 5 mg/d	height years-post menopause previous vertebral fracture smoking weight clinical fracture	2000	[19]
15		% Patients experiencing vertebral fracture	296	2 years	placebo risendronate 2.5 mg/d risendronate 5 mg/d	years-post menopause smoking clinical fracture	2005	[20]

16, 17	FIT/FLEX	% Patients experiencing non-vertebral or vertebral fracture	base study: 3236 extension: 1099	5 years 5-year extension	placebo alendronate 5 mg/d	bmi caucasian previous fracture previous vertebral fracture smoking clinical fracture	1996,2004, 2012	[21–23]
19, 3	SOTI / TROPOS	Number of vertebral and non-vertebral fractures	Tropos core study: 3646 sub- study: 237	Tropos: 5 years sub-study: 10 years	placebo strontium ranelate 2g/d	bmi previous vertebral fracture previous non-vertebral fracture years_post-menopause radiologic fracture	2008, 2012	[24,25]
20	Fracture Prevention Trial	% Patients experiencing non-vertebral or vertebral fracture	1006	1.5 years	placebo teriparatide 20 or 40 ug/d	bmi years post-menopause previous vertebral fracture clinical fracture	2009	[26]
21		% Patients experiencing vertebral fracture	881	3 years	placebo alendronate 5,10, or 20 mg/d	bmi years post-menopause previous vertebral fracture radiological fracture	1996	[27]
23		% Patients experiencing fracture of the spine, femoral neck, trochanter	483	2 years	placebo zolerdronic acid 5 mg/y	asian bmi years-post menopause radiologic fracture	2013	[28]
24		Number of patients experiencing any fracture	412	1 year	placebo zolerdronic acid 5 mg/y zolerdronic acid 5 mg/y + teriparatide 20 mcg/d	bmi caucasian years post-menopause previous vertebral fracture previous fracture clinical fracture	2011	[29]
25, 31	FACTS International	% Patients experiencing fracture (uncatagorized)	base study: 936 extension: 798	1 year 1 year extension	alendronate 70mg/w risedronate 35 mg/w	bmi caucasian years post-menopause clinical fracture	2006, 2008	[30,31]

25		% Patients experiencing fracture (uncatagorized)	78	3 years	zolerdronic acid 4mg/y	caucasian height weight clinical fracture	2007	[32]
26, 18	FREEDOM Trial	% Patients experiencing non-vertebral or vertebral fracture	base study: 7808 extension: 4550	3 years 3 year extension	placebo denosumab 60 mg/6mo denosumab only during extension	bmi years post-menopause previous fracture clinical Fracture	2009, 2013	[33,34]
27		% Patients experiencing non-vertebral or vertebral fracture	1637	1.6 years	placebo teriparatide 20 mcg/d teriparatide 40 mcg/d	bmi years post-menopause previous fracture radiologic Fracture caucasian smoking	2001	[35]
28		Total fractures	428	1 year	placebo alendronate 10 mg/d	caucasian years post-menopause clinical fracture	1999	[36]
29		% Patients experiencing fracture (uncatagorized)	292	1.5 years	placebo alendronate 10 mg/d MK-677 25 mg/d	bmi clinical fracture	2001	[37]
30		% Patients experiencing non-vertebral or vertebral fracture	549	1 year	alendronate 70 mg/w risendronate 5 mg/d	bmi caucasian years post-menopause previous fracture clinical fracture	2003	[38]
33, 34		% Patients experiencing non-vertebral or vertebral fracture	1258	1 year 1 year extension	alendronate 10 mg/d, 35mg/0.5w, or 70 mg/w	bmi years post-menopause clinical fracture	2000, 2002	[39,40]
34		Number of any kind of fracture	1053	1 year	alendronate 70 mg/w risendronate 35 mg/w	asian black bmi hispanic other race years-post menopause clinical fracture	2005	[41]

35	STAND	% Patients experiencing fracture (uncatagorized)	502	1 year	alendronate 70 mg/w denosumab 60 mg/mo	years post-menopause previous non-vertebral fracture clinical fracture	2010	[42]
36		Total fractures	base study: 597 extension: 644	3 year 3 extension periods	placebo alendronate 5 or 10 mg/d	bmi years post-menopause previous fracture radiologic Fracture	2004	[43]
37		% Patients experiencing fracture (uncatagorized)	286	2 years	placebo alendronate 10 mg/d alendronate 20 mg/d calcitonin 100IU/d	bmi caucasian years post-menopause clinical fracture smoking	1995	[44]
38		% Patients experiencing fracture (uncatagorized)	406	4 years	placebo alendronate 10 mg/d	bmi caucasian black hispanic years post-menopause clinical fracture	2008	[45]
39		Number. of any clinical fracture	3876	3 year	placebo zolerdronic acid 5 mg/y	bmi years post-menopause clinical fracture	2007	[46]

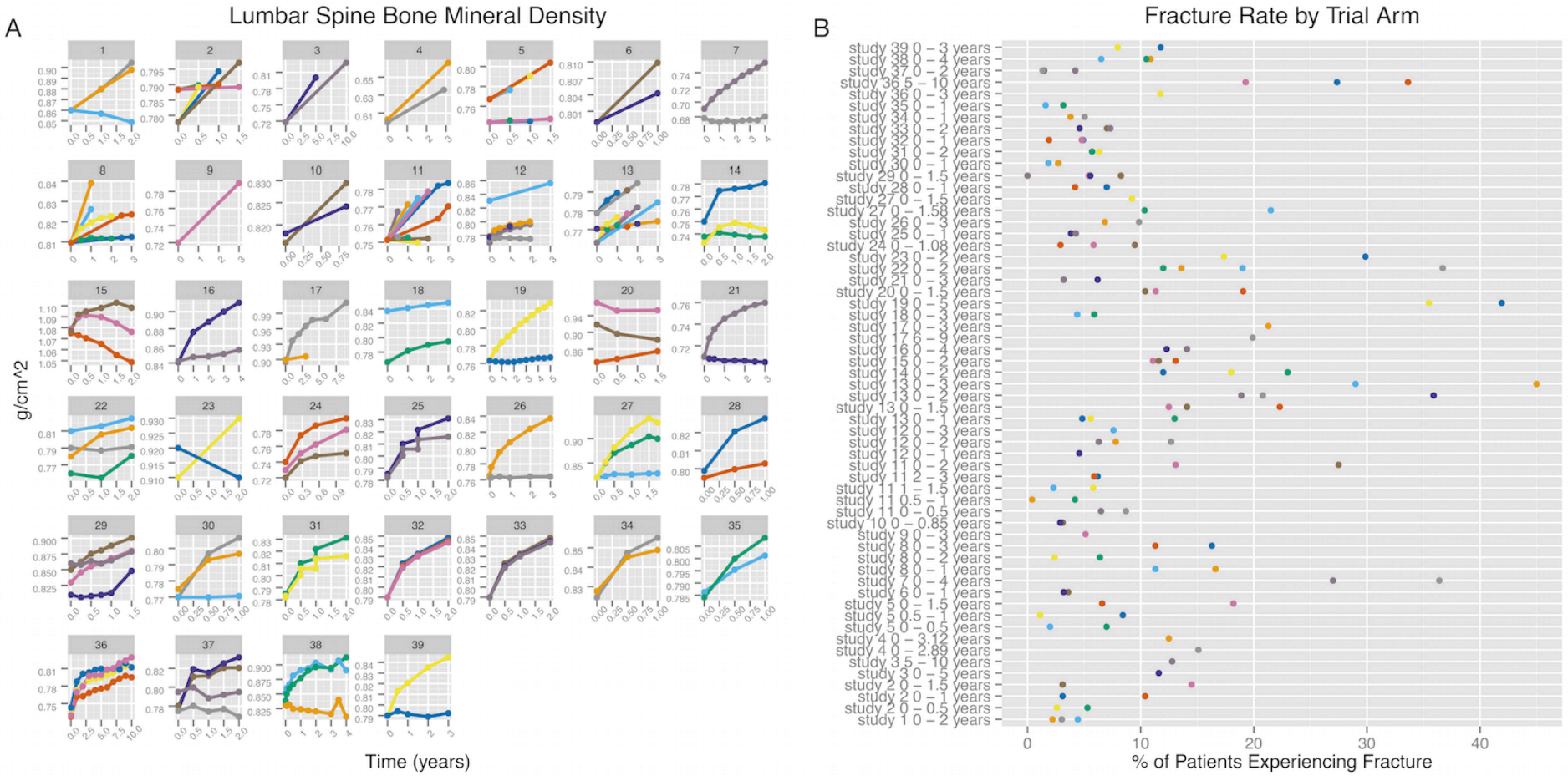

Supplementary Figure 1: Longitudinal changes in lumbar spine bone mineral density and percentage of patients experiencing fracture from the aggregate dataset by trial. Different colors represent trial arms

Appendix A

Example DAISY Input, ADC Equations, Code for Profile Likelihood and Sensitivity Analysis for Combination Arm

Example DAISY Input for a full TMDD with subcutaneous dose, when only information about the central compartment (drug concentration) is known.

```
WRITE "IDENTIFIABILITY of TMDD"$  % Feb 25, 2014 RJE

% B_ is a reserved name used to indicate the vector (non constant) input, output and state variables.
% (where I=u, x1/V=y1,C=x1, R=x2, DR=x3, A2=x4)

        B_:={y1, x1, x2, x3, x4}$

% The following instruction defines the components of vector B_ as time-depending variables:

        FOR EACH EL_ IN B_ DO DEPEND EL_,T$

% Please note: It is necessary that the known variables be always listed before the unknown variables and in the following order: input variables, output variables and known state variables.

% Please note: Constant inputs must not be listed in vector B_, but directly included in the model equations.

% B1_ is a reserved name used to indicate the vector of unknown parameters.

        B1_:={kdeg, kon, koff, kel, k12, k21,d,R_0, kint}$ %(R_0=ksyn/kdeg)

% NX_ and NY_ are reserved to indicate the number of states and outputs respectively.

        NX_:=4$

        NY_:=1$

% C_ is a reserved variable name used to indicate the system of differential polynomials (both rational and not) that describe the model. For this example, i.v. bolus dose = 5

        C_:={

        df(x1, t)= -(kel+k12)*x1-kon*x2*x1+koff*x3+(k21*x4)/(5/d),

        df(x2, t)= -kon*x2*x1+koff*x3+(R_0-x2)*kdeg,

        df(x3, t)= kon*x2*x1-(koff+kint)*x3,

        df(x4, t)= k12*x1*(5/d)-k21*x4,
```

```
y1=x1

}$
```

% Choose an integer value (seed_). The subroutine *random* will choose, in a random way in the interval [1, seed_], the numerical values corresponding to each component (model unknown parameter) of vector B1_.

```
SEED_:=100$
```

% Invoke the procedure that calculates characteristic the set:

```
DAISY()$
```

% This is the end of the input file in the case when initial conditions need not to be considered. No comment lines can be written at the end of the file.

% Initial conditions: if the user knows some or all the initial conditions of the model, these can be included in the identifiability analysis. In this case, the (numerical or symbolic) values can be inserted at the end of the input file with instructions such as *IC:=* and the subroutine CONDINIZ has to be called. The complete instruction is:

% If the user knows only some of the initial conditions, DAISY will automatically provide the missing initial conditions of the state variables xi by assigning them the unknown symbolic value xi_0.

```
IC_:={ x1=d,x2=R_0, x3=0, x4=0}$

CONDINIZ()$

END$
```

Antibody-Drug Conjugate (ADC) TMDD for One ADC Component

$$\frac{dC_1}{dt} = \frac{k_{tp}A_{t1} + In(t)}{Vc} - (k_{el1} + k_{pt})C_1 - k_{on}C_1 \cdot R + k_{off}RC_1 + k_{dec2}C_2 \tag{1}$$

$$\frac{dC_2}{dt} = \frac{k_{tp}A_{t2}}{Vc} - (k_{el2} + k_{pt})C_2 - k_{on}C_2 \cdot R + k_{off}RC_2 - k_{dec2}C_2 \tag{2}$$

$$\frac{dA_{t1}}{dt} = k_{pt}C_1Vc - k_{tp}A_{t1} \tag{3}$$

$$\frac{dA_{t2}}{dt} = k_{pt}C_2Vc - k_{tp}A_{t2} \tag{4}$$

$$\frac{dR}{dt} = k_{syn} - k_{deg}R - k_{on}(C_1 + C_2) \cdot R + k_{off}(RC_1 + RC_2) \tag{5}$$

$$\frac{dRC_1}{dt} = k_{on}C_1 \cdot R - (k_{int} + k_{off})RC_1 \tag{6}$$

$$\frac{dRC_2}{dt} = k_{on}C_2 \cdot R - (k_{int} + k_{off})RC_2 \tag{7}$$

$$\frac{dA^T}{dt} = Vc(k_{dec2}C_2 + k_{el2}C_2 + k_{int}RC_2) - k_{el}^T A^T \tag{8}$$

$$\begin{gathered} C_1(0) = 0; \quad C_2(0) = 0; \quad A_{t1}(0) = 0; \quad A_{t2}(0) = 0; \\ R(0) = \frac{k_{syn}}{k_{deg}}; \quad RC_1(0) = 0; \quad RC_2(0) = 0; \quad A^T(0) = 0 \end{gathered} \tag{9}$$

Equations from: L. Gibiansky and E. Gibiansky. Target-mediated drug disposition model and its approximations for antibody-drug conjugates. *J Pharmacokinet Pharmacodyn*, 41(1):35-47, Feb 2014.

```
setwd("/data/svn-renae/PI/First_Run")
.libPaths("../../script/lib")
library(metrumrg)
library(nlme)
library(ggplot2)

## Read in simulated data ###################################
tab2<-read.table(file="./2.TAB", header=T, as.is=T, skip=1)
head(tab2)


### Wipe out C1 and DV Columns#####
tab2$C<-NA
tab2$CMT<-NA
tab2<-tab2[,c("C","ID",'TIME',"AMT","RATE","EVID","CMT","DOSE","DV")]
tab2$AMT[tab2$AMT==0]<-NA
tab2$DV[tab2$EVID==1]<-NA

tab2$CMT[tab2$EVID==1]<-1

write.table(tab2, file="./bosentan_sim.csv",na='.',sep=",",row.names=FALSE,
    quote=FALSE)

############## Estimate ############################################################
NM72 <- '/opt/NONMEM/nm72/nmqual/autolog.pl'
NONR(
  run = 3,
  command=NM72,
  grid=TRUE,
  diag=TRUE,
  grp= c('DOSE'),
  par.list=c("KEL", "KON", "KOFF", "RMAX", "VCENT", "KTP", "KPT", "KM")
)

tab<-read.table(file="./3.TAB", header=T, as.is=T, skip=1)
p <- ggplot(data=tab, mapping=aes(x=TIME, y=IPRED, group=DOSE))
p + geom_line(aes(x=TIME,y=DV,colour=factor(DOSE)))
p + geom_point(aes(x=TIME,y=IPRED,colour=factor(ID)))+ geom_line(aes(y=IPRED,
    colour=factor(DOSE)), lwd=0.5) + facet_wrap(~ID, scales=c("free"))

############## Full TMDD MODEL
    ################################################

NM72 <- '/opt/NONMEM/nm72/nmqual/autolog.pl'
NONR(
  run = 4,
  command=NM72,
  grid=TRUE,
  diag=TRUE,
  grp= c('DOSE'),
  par.list=c("KEL", "KON", "KOFF", "RMAX", "VCENT", "KTP", "KPT", "KM")
)
```



```
tab<-read.table(file="./4.TAB", header=T, as.is=T, skip=1)
p <- ggplot(data=tab, mapping=aes(x=TIME, y=IPRED, group=DOSE))
p + geom_point(aes(x=TIME,y=IPRED,colour=factor(ID)))+ geom_line(aes(y=PRED,
```

```
    colour=factor(DOSE)), lwd=0.5) + scale_y_log10()


+ facet_wrap(~ID, scales=c("free")) + scale_y_log10()

p + scale_y_log10()
#### Get par estimates ############################
rlog(run=c(1:4),append=F,purge=F, file=filename("./",'CombRunLog_est.csv'))


est <- read.table("./CombRunLog_est.csv",sep=",",as.is=TRUE, skip=4)
head(est)
##Clean up the table so that it only includes information you will use for LLP.
##Delete unnecessary columns
est<-est[,c(6:14,29,60)]

names(est)
    [names(est)==c("V6","V7","V8","V9","V10","V11","V12","V13","V14","V29","V60")
    ]<-
  c("TH1","TH2","TH3","TH4","TH5","TH6","TH7","TH8","TH9","OM5","SG")

head(est)

#The table now consists of only PEs of the fixed and random effects parameters,
    and
#the RSEs. We want the SEs so we have to calculate the SE from RSE:


SE=function(RSE, PE){
  (RSE/100)*PE}

est[3,]<-SE(est[2,], est[1,])
head(est)

##The table now consists of point estimates, RSE, and SE values arranged in a
    single column for each parameter.
##We want to create a vector of fixed values for each LL profile: +/-4*SE and
    divide the high and low values by 10
est[4,]<-3*(est[3,])
est[5,]<-est[1,]+est[4,]
est[6,]<-est[1,]-est[4,]

head(est,7)
Finalest<-est

llpth1<-signif(c(seq(from=Finalest[6,"TH1"], to=Finalest[5,"TH1"],
    length.out=10), Finalest[1,"TH1"]),3)
llpth2<-signif(c(seq(from=Finalest[6,"TH2"], to=Finalest[5,"TH2"],
    length.out=10), Finalest[1,"TH2"]),3)
llpth3<-signif(c(seq(from=Finalest[6,"TH3"], to=Finalest[5,"TH3"],
    length.out=10), Finalest[1,"TH3"]), 3)
llpth4<-signif(c(seq(from=Finalest[6,"TH4"], to=Finalest[5,"TH4"],
    length.out=10), Finalest[1,"TH4"]),3)                                    122
llpth5<-signif(c(seq(from=Finalest[6,"TH5"], to=Finalest[5,"TH5"],
    length.out=10), Finalest[1,"TH5"]), 3)
llpth6<-signif(c(seq(from=Finalest[6,"TH6"], to=Finalest[5,"TH6"],
```

```
    length.out=10), Finalest[1,"TH6"]),3)
llpth7<-signif(c(seq(from=Finalest[6,"TH7"], to=Finalest[5,"TH7"],
    length.out=10), Finalest[1,"TH7"]),3)
llpth8<-signif(c(seq(from=Finalest[6,"TH8"], to=Finalest[5,"TH8"],
    length.out=10), Finalest[1,"TH8"]), 3)
llpth9<-signif(c(seq(from=Finalest[6,"TH9"], to=Finalest[5,"TH9"],
    length.out=10), Finalest[1,"TH9"]), 3)

llp<-c(llpth1, llpth2, llpth3, llpth4, llpth5, llpth6, llpth7, llpth8, llpth9)

## 10/10/14 Change kel range of values for manuscript #######

llpth1<-signif(c(seq(from=1.03, to=1.059, length.out=10), Finalest[1,"TH1"]),5)


llpth1
llpth2
llpth3
llpth4
llpth5
llpth6
llpth7
llpth8


## New LLPs ##

llpth4[1]<-0.008
llpth4[2]<-0.01
llpth4[3]<-0.04
llpth8[1]<-0.0001
llpth8[2]<-0.0008
llpth8[3]<-0.001

llp<-c(llpth1, llpth2, llpth3, llpth4, llpth5, llpth6, llpth7, llpth8, llpth9)
llp[llp<0] # check that no estimates are less than zero

llp<-signif(llp,3)
#Create control streams for each model run: 8Thetas
#with 10 fixed values per theta=90 control streams to run.

#create bootstrap control streams
#see help for resample.character

f4<-readLines("4.ctl")
pnm<-readLines("1.pnm")

nms <- 101:111

PE1 <- metaSub(
  f4,
  names=nms,
  pattern = list(
    "PROB 4",
    "(0, 0.990)"
  ),
```

123

```
  replacement = list(
    "PROB *",
    paste("(",llpth1," FIX",")",sep="")
  ),
  out = "../First_Run",
  suffix = ".ctl",
)
nms2 <- 112:122

PE2 <- metaSub(
  f4,
  names= nms2,
  pattern = list(
    "PROB 4",
    "(0, 0.633)"
  ),
  replacement = list(
    "PROB *",
    paste("(",llpth2," FIX",")",sep="")
  ),
  out = "../First_Run",
  suffix = ".ctl",
)

nms3 <- 123:133

PE3 <- metaSub(
  f4,
  names= nms3,
  pattern = list(
    "PROB 4",
    "(0, 0.344)"
  ),
  replacement = list(
    "PROB *",
    paste("(",llpth3," FIX",")",";",sep="")
  ),
  out = "../First_Run",
  suffix = ".ctl",
)
nms4 <- 134:144

PE4 <- metaSub(
  f4,
  names= nms4,
  pattern = list(
    "PROB 4",
    "(0, 7.85)"
  ),
  replacement = list(
    "PROB *",
    paste("(",llpth4," FIX",")",sep="")
  ),
  out = "../First_Run",
  suffix = ".ctl",
)
```

```
nms5 <- 145:155

PE5 <- metaSub(
  f4,
  names=nms5,
  pattern = list(
    "PROB 4",
    "(0, 5.37) "
  ),
  replacement = list(
    "PROB *",
    paste("(",llpth5," FIX",")",sep="")
  ),
  out = "../First_Run",
  suffix = ".ctl",
)
nms6 <- 156:166

PE6 <- metaSub(
  f4,
  names= nms6,
  pattern = list(
    "PROB 4",
    "(0, 2.31) "
  ),
  replacement = list(
    "PROB *",
    paste("(",llpth6," FIX",")",sep="")
  ),
  out = "../First_Run",
  suffix = ".ctl",
)
nms7 <- 167:177

PE7 <- metaSub(
  f4,
  names= nms7,
  pattern = list(
    "PROB 4",
    "(0, 1.49)"
  ),
  replacement = list(
    "PROB *",
    paste("(",llpth7," FIX",")",sep="")
  ),
  out = "../First_Run",
  suffix = ".ctl",
)

nms8 <- 178:188

PE8 <- metaSub(
  f4,
  names= nms8,
  pattern = list(
```

```
    "PROB 4",
    "(0, 0.108)"
  ),
  replacement = list(
    "PROB *",
    paste("(",llpth8," FIX",")",sep="")
  ),
  out = "../First_Run",
  suffix = ".ctl",
)

nms9 <- 189:199

PE9 <- metaSub(
  f4,
  names= nms9,
  pattern = list(
    "PROB 4",
    "(0, 0.2)"
  ),
  replacement = list(
    "PROB *",
    paste("(",llpth9," FIX",")",sep="")
  ),
  out = "../First_Run",
  suffix = ".ctl",
)


NOD <- metaSub(
  pnm,
  names=nms,
  out = "../First_Run",
  suffix = ".pnm"
)

runs<-c(98:99)

NONR(
  run = 97,
  command=NM72,
  grid=TRUE,
  diag=TRUE,
  pe= "orte 8",
  mode= "para"
)

NONR(
  run = 97,
  command=NM72,
  grid=TRUE,
  diag=TRUE
)

rlog(run=c(101:200),append=F,purge=F,file=filename("./",'CombRunLog_est2.csv'))
```

```
##because thetas 4,5,7 were fixed values, there was no runlog for these runs and
    were
##not included in the combined runlog

dropNA<-function(x){
  bad<-is.na(x)
  good<-x[!bad]
}

LLPbos<-read.table("CombRunLog_est2.csv", sep=",", quote="", as.is=TRUE,
    fill=TRUE)
nrow(LLPbos)
head(LLPbos)


#select only the lines with objective function values for runs:
OFVRes<-LLPbos[,c(2,3,5)] #results from all runs
OFVRes<-OFVRes[OFVRes$V2!="RSE",]
OFVRes$V5<-as.numeric(OFVRes$V5)
OFVRes$V2<-NULL

PEdata<-function(ThFIX,OFVs, ...){
  data.frame(ThFIX, OFVs, ...)}
llp<-c(llp,0.445)

PEdat<-PEdata(llp, OFVRes)
head(PEdat)
tail(PEdat)
# For all runs, create a column in the dataset labeling each theta:
Theta<-c(rep(1,11), rep(2,11), rep(3,11), rep(4,11), rep(5,11), rep(6,11), rep(7,
    11), rep(8,11), rep(9,11),3)
length(Theta)

#create the dataset that includes the OFVs, theta labels, and the Fixed parameter
    values
llpdat<-PEdata(llp, OFVRes, Theta)
head(llpdat)
row.names(llpdat)<-NULL
llpdat$V2<-NULL
# To order the Thetas sequentially and name fixed effect parameters:

llpdat<-llpdat[order(llpdat$Theta, llpdat$ThFIX),]
llpdat$THETA<-factor(paste("Theta", llpdat$Theta))

# Remove runs that didn't run or compile correctly
colnames(llpdat)<-c("ThFIX","ERR","OFVRes",'Theta',"THETA")
llpdat$ERR<-as.factor(llpdat$ERR)
llpdat$ERR<-map(llpdat$ERR,c(".","0","134","136","137","error"),c(NA,0,1,2,3,NA))
llpdat2<-llpdat[!is.na(llpdat$ERR),]  ### These didn't run
llpdat3<-llpdat2[llpdat2$ERR<2,] ### These didn't compile correctly
llpdat3<-llpdat3[llpdat3$ThFIX!=1.04000,]
```



```
llpdat3$THETA<-map(llpdat3$Theta, c(1:9),
                   c("Kel", "Kon", "Koff",
                       "Ksyn","Vcent","Kpt","Ktp","Kdeg","Kint"))
```

```
add<-data.frame(
  ThFIX = c(0.99,1.010), ERR = c(0,0), OFVRes = c(6131.279,5953.5988), Theta = c
      (1,1), THETA = c("Kel","Kel"))


llpdat3<-rbind(llpdat3, add)

llpdat3<-llpdat3[order(llpdat3$Theta, llpdat3$ThFIX),]


llpdat3$flg<-with(llpdat3,ifelse(ThFIX %in% c(1.03320,1.03640),1,0))
#1.03640,1.04290,1.05260,
llpdat3<-llpdat3[llpdat3$flg==0,]

# Then rerun the plot script with index.cond according to desired arrangement

##Now we need plot reference lines for the MOFV and +3.84MOFV, which corresponds
    to the 95% CI.


my.LLPplots<-function(x,y, point.color="blue"){
  panel.xyplot(x,y,col=point.color, pch=19, cex=0.4, type="b")
  ymin<-min(y)
  panel.abline(h=ymin)
  panel.abline(h=ymin+3.84, lty=2, col="red")
}
##Need to set Y scale to read easier: USE prepanel=function(x,
    y, ...)list(xlim=range(x), ylim=c(min(y)-1, min(y)+4.84))

axisLP<-function(side, ...){
  if(side=="bottom"){
    xlim<-current.panel.limits()$xlim
    xmin<-xlim[[1]]
    xmax<-xlim[[2]]
    Major<-pretty(signif(seq(xmin, xmax, length.out=5), 2))
    Minor<-((Major[-1]+Major[-length(Major)])/2)
    labl<-as.character(Major)
    panel.axis(side="bottom", at= Minor, outside=TRUE, labels=FALSE, ticks=TRUE,
        tck=0.6, line.col="black")
    panel.axis(side="bottom", at= Major, outside=TRUE, labels=labl, ticks=TRUE,
        tck=1.2, line.col="black")
  }
  else axis.default(side, ...)}


library(lattice)
tiff(
  file="Fig4b2.tiff",
)
xyplot(
  OFVRes~ThFIX|THETA,
  llpdat3,
  layout=c(3,3),
  as.table=TRUE,
  prepanel=function(x, y, ...)list(xlim=range(x), ylim=c(min(y)-1, min(y)+4.84)),
```

```
  panel=my.LLPplots,
  scales=list(relation="free", cex=0.65),
  axis=axisLP,
  between=list(x=0, y=2),
  xlab='Fixed Parameter Value',
  ylab='Min OFV'
)
dev.off()




rlog(run=c(101:199),
     project="./",
     append=FALSE,
     extra=c("^worke")
)


##panel.axis(side="bottom", at=Major, half=FALSE, outside=TRUE, labels=labl,
    ticks=TRUE, tck=1, line.col="orange")
```

```
$PROB 97 BOSENTAN ESTIMATION FROM SIMULATED DATASET WITH FULL TMDD

$INPUT C ID TIME AMT RATE EVID CMT DOSE DV
$DATA ../bosentan_sim.csv IGNORE=C
$SUB ADVAN6 TRANS1 TOL=6

$MODEL NPAR=9 NCOMP=4 COMP=(CENTRAL) COMP=(PERIPH) COMP=(RESPONSE) COMP=(EFFECT)

$PK

KEL=THETA(1)*EXP(ETA(1))
KON=THETA(2)*EXP(ETA(2))
KOFF=THETA(3)*EXP(ETA(3))
KSYN=THETA(4)*EXP(ETA(4))
VCENT = THETA(5)*EXP(ETA(5))
KPT=THETA(6)*EXP(ETA(6))
KTP=THETA(7)*EXP(ETA(7))
KDEG=THETA(8)*EXP(ETA(8))
KINT=THETA(9)*EXP(ETA(9))

S1=VCENT/1000 ; Unit adjustment
;S3=V3

A_0(3)=KSYN/KDEG

$DES

C1=A(1)/VCENT
C2=A(2)
C3=A(3)
C4=A(4)


DADT(1)=-(KEL+KPT)*C1+KTP*(A(2)/VCENT)-KON*A(3)*C1+KOFF*A(4)
DADT(2)=KPT*C1*VCENT-KTP*A(2)
DADT(3)=KSYN-KON*A(3)*C1+KOFF*A(4)-KDEG*A(3)
DADT(4)=KON*A(3)*C1-(KOFF+KINT)*A(4)


;A_0 (3)=KSYN/KDEG


$ERROR
;Y = F+ERR(1)
Y = F*(1+ERR(1))


IPRED=F

$THETA
(1.063 FIX)   ;  THETA(1)  KEL
(0, 0.633)   ;  THETA(2)  KON
(0, 0.344)  ;  THETA(3)  KOFF
(0, 7.85)   ;  THETA(4)  KSYN
(0, 5.37)    ;  THETA(5)  VCENT
(0, 2.31)    ;  THETA(6)  KPT
```

```
(0, 1.49)     ; THETA (7) KTP
(0, 0.108) ; THETA (8) KDEG
(0, 0.2) ; THETA (9) KINT

$OMEGA
0 FIX
0 FIX
0 FIX
0 FIX
0.02
0 FIX
0 FIX
0 FIX
0 FIX

$SIGMA
0.05


$ESTIMATION MAXEVAL=9999 METHOD=1 PRINT = 5 MSF=./97.MSF NOABORT
;$COVARIANCE
$TABLE NOPRINT ONEHEADER FILE=../97.TAB
ID TIME AMT EVID CMT DOSE IPRED
$TABLE NOPRINT ONEHEADER FILE=../97par.TAB
ID DV KEL KON KOFF VCENT KTP KPT KSYN KDEG KINT
```

Sensitivity Analysis for Combination Arm

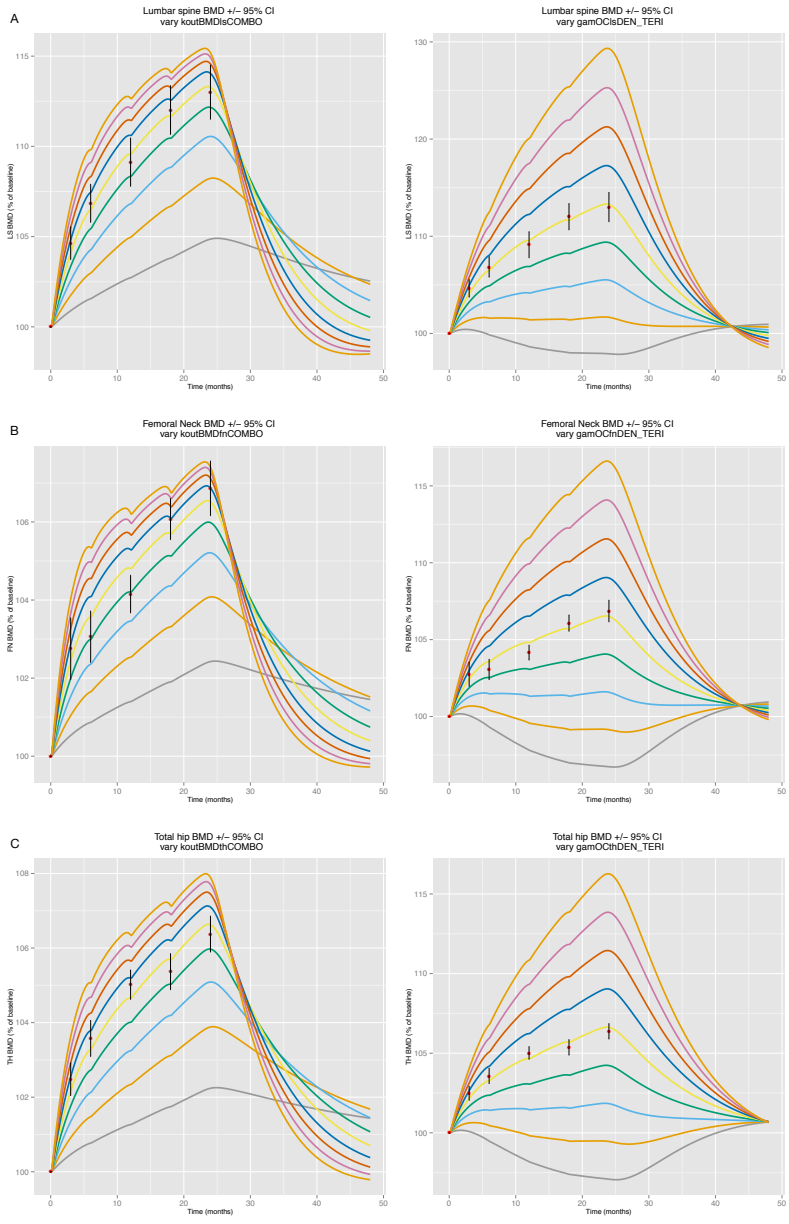

Figure A.1: Sensitivity analysis for parameters describing combination treatment. Parameters were varied between the ranges 0.8+/- estimated parameter value and plotted against the clinical data (red) +/- 95%CI

Appendix B

Model Code

```
// FINAL MODEL CODE

$GLOBAL
#define max(a,b) ((a) > (b) ? (a) : (b))
#define F11 T85
#define PicOCkin Pic0

#define SETINIT if(NEWIND <=1)


// Definitions: Initialize Compartments

#define Q0 Q_0
#define RNK0 RNK_0
#define L0 L_0
#define ROB10 ROB1_0
#define Qbone0 Qbone_0
#define O0 O_0
#define RX20 RX2_0
#define CREB0 CREB_0
#define M0 M_0
#define TGFBact0 TGFBact_0
#define TGFB0 TGFB_0
#define PREPTH0 PREPTH_0
#define PTH0 PTH_0
#define OBfast0 OBfast_0
#define OC0 OC_0
#define P0 P_0
#define T0 T_0
#define BMDfn0 BMDfn_0
#define BMDls0 BMDls_0
#define BMDlsDEN0 BMDlsDEN_0
#define EST0 EST_0
#define GFR0 GFR_0
#define OBslow0 OBslow_0
#define OCY0 OCY_0
#define TOL0 TOL_0

#define PKCP (PKCENT/PKVC)
#define DENCP (DENCENT/DENVC)

#define CaConc0 (P0/V1)
#define PTHconc0 (PTH0/V1)
#define OB (OBfast*trans + OBslow)

#define PTHconc (PTH/V1)
#define CaConc (P/V1)
#define C1 (P/V1)
#define C2 (ECCPhos/V1)
#define C8 (B/V1)
#define D  ROB1
#define Osteoclast OC
#define OB0 (OBfast0 + OBslow0)
#define Osteoblast (OBfast*trans + OBslow)
#define Calcitriol0 (B_0/V1)
```

```
#define BMDlsSCLER0 BMDlsSCLER_0
#define BMDfnSCLER0 BMDfnSCLER_0
#define BMDthSCLER0 BMDthSCLER_0

#define BMDlsTERI0 BMDlsTERI_0
#define BMDfnTERI0 BMDfnTERI_0
#define BMDthTERI0 BMDthTERI_0

#define BMDlsDEN0 BMDlsDEN_0
#define BMDfnDEN0 BMDfnDEN_0
#define BMDthDEN0 BMDthDEN_0


  // denosumab concentration (mol)
#define DENMOL (DENCENT/DENVC/150000)*1000*1000

 // sclerostin (nmol/L) and sclerostin ab concentration (nmol)
#define SOSTCP (SOSTCENT/SOSTVC)

// Parameter Declaration

 double E0PicOBkb;
 double EmaxPicOBkb;
 double EC50PicOBparenKb ;
 double EC50PicOBkb ;
 double PicOBkb;
 double E0RUNX2kbEff;
 double PicOBkbEff ;
 double kbprime ;
 double kbslow ;
 double kbfast ;
 double RUNkbMax;
 double INparen ;
 double RUNkb50;
 double RUNX2kbPrimeEff ;
 double KIN_P;
 double SCLEREFF;
 double BSAP;
 double E0PicROB;
 double EC50PicROBparen;
 double EC50PicROB;
 double Dr;
 double PicROB;
 double ROBin;
 double bigDb;
 double koutOCY;
 double kin_TOL;
 double PhosEffect;
 double J48;
 double J27;
 double RUNX2;
 double KPT;
 double kin_T;
 double kin_BMDdel;
```

```
 double kin_BMDdelTERI;
 double kin_BMDdelTERIth;
 double SCLER_TOL;
 double SC50;
 double SCLEREFF_TOL;
 double EC50SCLER;
 double fracOBEffect;
 double Hazard;
 double Survival;
 double lsBMD;
 double SclerBMDpred;
 double DenoBMDpred;
 double TeriBMDpred;
 double ComboBMDpred;
 double damp;
 double drug;

// PARAMETER VALUES

$PARAM
  OBtot0 = 0.00501324  // initial OB compartment concentration
  k1 = 0.00000624  // binding affinity RANKL-OPG
  k2 = 0.112013 // dissassociation rate RANKL
  k3 = 0.00000624 // binding affinity RANK-RANKL
  k4 = 0.112013 // dissassociation rate RANK
  V1= 14 // volume of distribution: CA compartment (L)
  FracJ14 = 0.107763 // extracellular CA flux
  J14OCmax = 0.543488 // de-mineralization of CA
  J14OCgam = 1.6971 // de-mineralization of CA
  FracJ15 = 0.114376 // extracellular CA flux
  kinRNKgam = 0.151825 //TGF-B on RANKL effect
  koutRNK = 0.00323667 // RANK degradation
  MOCratioGam = 0.603754 // RANK-RANKL complex effect on OB
  Da = 0.7/24 // OC formation rate
  OBtgfGAM = 0.0111319 // OB influence on latent TGF-b
  koutTGF0 = 0.0000298449 // degradation rate TGF-b
  koutTGFGam = 0.919131 // TGF-b scaling effect on degredation
  OCtgfGAM = 0.593891 // scaling effect on latent TGF-b
  EmaxPicROB = 3.9745 // emax effect of TGF on responding OB
  PicROBgam = 1.80968 // gamma term on TGF on responding OB
  FracPicROB =  0.883824 // fraction of responding osteoblast
precursors contributing to mature osteoblasts
  PicOBgam = 0.122313 // gamma on active TGF-beta
  FracPicOB = 0.000244818 // fraction of osteoblast precursors
contributing to mature osteoblasts
  EmaxPicOB = 0.251636 // emax on OB compartment
  E0Meff = 0.388267 // RANK-RANKL Complex and Latent TGF-Beta effect
  EmaxMeffOC = 3.15667 // Max effect of  RANK-RANKL Complex on
osteoclasts
  kinOCgam = 8.53065 // gamma on RANK-RANKL complex
  EmaxPicOC = 1.9746 // Max effect of active TGF-Beta, osteoclasts
  FracPicOC = 0.878215 // Fraction of osteoclast precursors
contributing to differentiation
  PicOCgam = 1.0168 // Active TGF-Beta effect on osteoclasts
  E0RANKL = 3.80338 // SS initial condition for RANKL
```

```
  EmaxL = 0.469779 // max effect of RANKL on osteoclasts
  T16 = 1.06147 // PTH-sensitive calcium reabsorption in kidney
  T64 = 0.05 //1-alpha hydroxylase degredation rate
  T65 = 6.3 // extracellular phosphate concentration input rate
  T67 = 1.54865 // alpha hydroxylase effect on PTH excretion
  AlphOHgam =  0.111241 // 1-alpha hydroxylase effect on PTH
  k14a =  0.0000244437 // rate of non-immediately exchangeable calcium-
immediately exchangely bone calcium
  HApMRT = 3.60609 //endogenous hydroxy-apatite formation
  koutL = 0.00293273 // degradation rate of RANKL
  TotOsteoEffectGam = 0.173833 // Fractionated effect on RANKL
  TESTPOWER = 1 // not used currently - can be used to increase the
effect of PTH
  opgPTH50 = 3.85 // EC50 term of PTH effect on OPG
  IO = 0 // additional OPG substrate
  RX2Kout0 = 0.693 // RunX2 effect on extracellular PTH
  E0rx2Kout = 0.125 // RunX2 to extracellular PTH
  EmaxPTHRX2x = 5 // Max effect of PTH on calcium flux from plasma into
bone
  E0crebKin = 0.5 // Creb formation rate
  EmaxPTHcreb = 3.39745 // max effect of PTH on creb
  crebKout = 0.00279513 // creb degratation rate
  bcl2Kout = 0.693 // degradation rate of Bcl-2
  ScaEffGam = 0.9 // effect of calcium ratio on calcium excretion via
kidney
  PhosEff0 = 1.52493 // baseline extracellular phosphate effect on 1-
alpha hydroxylase
  PhosEff50 = 1.3021 // EC50 term for phosphate effect on 1-alpha
hydroxylase
  PhosEffGam = 8.25229 // gamma term for phosphate effect on 1-alpha
hydroxylase
  PO4inhPTHgam = 0 // effect of phosphate on PTH
  T69 = 0.10 // degradation rate of circulating calcitriol
  Reabs50 = 1.57322 // EC50 term for PTH-sensitive calcium reabsorption
in kidney
  T7 = 2 //  effect of circulating calcitriol to extracellular calcium
  T9 = 90 // effect of circulating calcitriol to extracellular calcium
and excretion
  T70 = 0.01 // effect on PTH leaving PTH gland pool
  T71 = 0.03 // effect of PTH gland on calcium reabsorbtion
  T33 = 0.003 // effect of circulating calcitriol on calcitriol-
dependent calcium absorption into gut
  T34 = 0.037 // effect of circulating calcitriol on calcitriol-
dependent calcium absorption out of gut
  T35 = 90 // EC50 term for circulating calcitriol on calcitriol-
dependent calcium absorption
  CaPOgam = 1 // gamma term on effect for circulating calcitriol on
calcitriol-dependent calcium absorption
  T46 = 1.142 // rate of phosphate renal excretion
  T52 =  0.365 // rate of oral phosphate absorbtion
  OralPhos = 10.5/24 // rate of oral phosphate absorbtion into gut
  F12 = 0.7  // availability of oral phosphate
  T49 = 51.8 // rate of extracellular phosphate to intracellular
phosphate
  T55 = 0.019268 // intracellular phosphate to extracellular phosphate
```

```
  PicOBgamkb = 2.92375 //  TGF-beta effects on Osteoblast and clast
differentiation
  MultPicOBkb = 3.11842 // fraction of ROB contributing to TGF-beta
effect on OB differentation
  FracPic0kb = 0.764028 // fraction of osteoblast precursors that
contribute to differentiation in TGF beta
  E0RUNX2kbEffFACT = 1.01 // osteoblast apoptosis as affected by PTH
  RUNkbGAM = 3.81644 // gamma term on RUNX2 effect of osteoblast
apoptosis
  RUNkbMaxFact = 0.638114 // emax term of RUNX2 effect of osteoblast
apoptosis
  RUNX20 = 10 // RUNX2 baseline effect on EC50 for RUNX2
  Frackb = 0.313186 // degradation rate of fast/slow osteoblasts
  T81 = 0.75 // effect of calcitriol-dependent calcium absorption on
oral calcium.
  T87 = 0.0495 // rate of calcium movement to/from gut
  T28 = 0.9 // EC50 term for calcium movement to/from gut
  OralCa = 24.055/24 // calcium intake via gut per day
  T310 = 0.105929 // fraction of oral calcium being absorbed
  T77 = 0.909359 //effect on extent of absorption of orally-
administered calcium dose
  T80 = 4 // gamma term for calcitriol-dependent calcium absorption
  CtriolPTgam = 12.5033 // gamma term on calcitriol for PT gland
capacity
  CtriolMax = 4.1029 // max effect of calcitriol for PT gland capacity
  CtriolMin = 0.9 // min effect of calcitriol for PT gland capacity
  PTout = 0.0001604 // flux out of PT gland
  kout = 100/14 // degredation rate of PTH
  T58 = 6249.09 // max PTH-related calcium flux
  T59 = 11.7387 // gamma term for PTH-related calcium flux
  T61 = 96.25 // min PTH-related calcium flux
  IPTHint = 0 // intravenous PTH
  IPTHinf = 0 // infused PTH
  Pic0 = 0.228142 //  baseline of osteoblast precursors
  EmaxLpth = 1.30721 // Emax PTH effect on RANKL
  kO = 15.8885 // formation rate OPG
  kb = 0.000605516 // conversion rate of preosteoblasts to osteoblasts
  LsurvOCgam =3.09023 // effect of RANKL on osteoclasts
  FracOBfast = 0.797629 //fraction of osteoblast pool that are quickly
differentiated

  // Teriparatide PK parameters
  TERIKA = 10.4, TERIVC = 94.4, TERIVD  = 7, TERICL = 62.2, TERIF =
0.95

  //Generic PK parameters
  PKKA = 0, PKVC = 10, PKQ1 = 0, PKQ2 = 0
  PKVP1 = 1, PKVP2 = 1, PKCL = 0, PKVMAX=0, PKKM=1

  kdenosl = 1.98411e-06 // denosumab effect on RANKL
  E2scalePicB1 = 0.0000116832 //effect of estrogen on osteoblast
apoptosis
  FracOBE = 20 // max of OB contribution to effect on RANKL

  // Denosumab PK parameters from Peterson, et al.The AAPS Journal,
```

```
24(6 Abstract W4340), 2004 //
  DENVMAX = 3110, DENKM = 188, DENVC = 2340
  DENVP = 1324  // = Q/K(12,11)
  DENCL = 2.75
  DENQ = 18.67 // = K(12,11) * VC
  DENKA = 0.00592, DENF = 0.729

  ESTON = 0 // estrogen effect (switch)
  koutEST=0.05776227 // degredation rate of estrogen
  menoDUR=as.hour(as.year(1.66)) // duration of menopause
  ageGAM = -2.3 // age effect on estrogen effect
  age50 = 0.64 // EC50 of age effect on estrogen
  ageENTER = as.hour(as.year(41)) // Ave age at meno onset
  ageDONE = as.hour(as.year(51)) // Ave age at meno end
  tgfbGAM = 0.0374 // TGF-b effect on estrogen
  tgfbactGAM = 0.045273 // active TGF-b effect on estrogen
  robGAM = 0.16 // estrogen effect on responding osteoblasts
  maxTmESTkid = 0.923737 // maximum fractional calcium reabsorption in
the kidney
  GFRtau=10  // years over which GFR declines
  GFRdelta=0  // change in GFR

  // Sclerostin PK Parameters //
  SOSTVMAX = 5.87/24, SOSTKM = 0.453, SOSTVC = 2.9, SOSTVP = 3.29
  SOSTCL = 0.254/24, SOSTQ = 0.467/24, SOSTKA = 0.187/24, SCLERF=0.904

  // Sclerostin PD Parameters //
  SOSTKIN=3.725/24, SOSTKOUT= 25/24, SOSTK0 = 0.197/24

  // Sclerostin effects //
  FracOCY = 0.5 // Fraction of OB becoming OCY
  EMAXSCLER = 4.670795836
  gammaDr = 0.044584465 // sclerostin effect on ROB
  gammaOCY = 0.276280938 // sclerostin effect on OCY apoptosis
  gammaOPG = 1.597073748 // sclerostin effect on OPG (via Wnt
signaling)
  SCLEROBgam =  0.162250232 // sclerostin effect
  SMAX = 8.690800116 // max sclerostin effect
  kout_T = 0.006073441 // translation compartment rate constant (for
sclerostin effect on OB)
  kout_TOL = 0.001901105 // tolerance compartment rate constant (for
sclerostin effect on RANKL)

  TYPE = 2 // Allows for simultaneous fit of P1NP and CTx

  // Denosumab BMD Parameters

  koutBMDls = 0.000397
  koutBMDlsDEN = 7.374996e-05
  koutBMDfnDEN = 0.0001186424
  koutBMDthDEN = 0.0001080459
  gamOB = 0.0793
  gamOCls = 0.14
  gamOClsDEN = 7.912201e-02
  gamOCfnDEN = 0.0514712439
```

```
  gamOCthDEN = 0.0552337198

  // Sclerostin BMD Parameters

  koutBMDSCLER = 0.000145
  gamOBSCLERls =  0.75766752
  gamOCSCLER = 0.06530286
  gamOBSCLERth = 0.22459622
  gamOBSCLERfn = 0.13145334
  gamOBSCLER = 0.099
  kout_BMDdel = 0.00245716

  // Teriparatide BMD Parameters

  kout_BMDdelTERI = 0.001
  koutBMDlsTERI =  0.00055370
  koutBMDthTERI =  0.0001394248
  koutBMDfnTERI =  0.000066284
  gamOCfnTERI =   0.21199
  gamOClsTERI = 0.016916
  gamOCthTERI = 0.13118
  gamOBTERIfn =  0.495529
  gamOBTERIls =  0.271226
  gamOBTERIth =  0.29803

 // Combination (teriparatide and denosumab) Arm BMD Parameters

  koutBMDlsCOMBO = 0.0001368262
  koutBMDthCOMBO = 0.0001048986
  koutBMDfnCOMBO = 0.0001275736

  gamOClsDEN_TERI = 0.1015274694
  gamOCthDEN_TERI = 0.0704668698
  gamOCfnDEN_TERI = 0.0671132952

 // Placeholder for Hazard Model Covariates (these are supplied by the
dataset) //
  baseHazard = 0.058265425
  HazBMDCov = 1.3259
  HazpostMenoAgeCov = 0.02690102025
  HazradFracCov = -0.20419
  HazBMICov = -0.021603069564
  agepostmeno= 20
  radFracInc= 0
  BmdbaseRef = 0.783
  postMenoAgeRef = 20
  ageLastMenPeriodRef = 51.7
  bmiRef = 27.1
  lsBMDbase = 0.8

  // addtional drug effect //
  betaDrug_DENO=-1.73
  betaDrug_TERI=-0.898
  betaDrug_COMBO=-1.213  //combo ave deno&bisphos = avoid using this
```

```
 // Used to determine which BMD data to table out //

Scler_BMD_type=0,Deno_BMD_type=0,Teri_BMD_type=0,DEN_TERI_COMBO=0,Combo
_BMD_type=0, SCLER_DEN_SEQ=0


////////////////////////////////


// Link compartment number to subcu compartment name
$CMTN
SOSTSC, DENSC, TERISC

// INITIAL CONDITIONS

$INIT

    PTH = 53.90     // (pmol)
    S = 0.5         // PTH gland pool
    PTmax = 1.00    // PT gland max capacity
    B = 1260.0      // Circulating calicitriol (pmol)
    SC = 0.0        // Subcu PTH compartment (pmol)
    P = 32.90       // Extracellular calcium (mmol)
    ECCPhos = 16.8  // Extracellular phosphate (mmol)
    T = 1.58471     // Oral calcium (mmol)
    R = 0.50        // Calcitriol dependent ca absorption
    HAp = 1.00      // Hydroxyapetite conc
    PhosGut = 0.839  // Oral phosphate (mmol)
    IntraPO = 3226.0 // Intracellular phosphate (mmol)
    OC = 0.00115398  // Osteoclast population
    ROB1 = 0.00104122 // Responding osteoblasts
    L = 0.4         // RANKL concentration
    RNK= 10.0       // RANK concentration
    O = 4.0         // OPG
    Q = 100.0       // Immediate-exchangeable bone calcium (mmol)
    Qbone = 24900.0 // Non-immediate exchangeable bone calcium (mmol)
    RX2 = 10.0      // RunX2
    CREB = 10.0     // Creb
    BCL2 = 100.0    // Bcl-2
    TERISC = 0, TERICENT=0   // Teriparatide PK
    PKGUT=0, PKCENT=0, PKPER1 = 0, PKPER2 = 0  // Generic PK
    DENCENT=0, DENPER = 0,  DENSC=0 //Denosumab PK
    UCA=0           // Urine Calcium (pmol)
    VALUE1=0        // Indicator 1
    VALUE2=0        // Indicator 2
    VALUE3=0        // Indicator 3
    TGFB=0          // Latent TGF beta
    TGFBact=0       // Active TGF beta
    OBfast=0        // Fast differentiating osteoblasts
    OBslow=0        // Slow differentiating Osteoblasts
    M=0             // RANK-RANKL complex
    N=0             // OPG-RANKL complex
    AOH=126         // 1-alpha hydroxylase (pmol)
    EST  = 1        // estrogen
    BMDls = 1       // lumbar spine BMD for combination therapy
```

```
    BMDfn = 1       // femoral neck BMD
    GFR = 100/16.667  // GFR
    SOSTSC = 0, SOSTCENT=0, SOSTPER=0 //Sclerostin Ab PK
    SCLER = 0.149         // Sclerostin compartment  (nmol/L)
    OCY = 0.0709 //0.0117          // Osteocytes
    trans = 1 // translation compartment

    BMDlsSCLER = 1       // Sclerostin lumbar spine BMD
    BMDfnSCLER = 1       // Sclerostin femoral neck spine BMD
    BMDthSCLER = 1       // Sclerostin total hip BMD

    BMDlsDEN = 1     // Denosumab lumbar spine BMD
    BMDfnDEN = 1    // Denosumab femoral neck spine BMD
    BMDthDEN = 1    // Denosumab total hip BMD

    delBMDls = 1 // delay compartment for lumbar spine BMD
    delBMDth = 1 // delay compartment for total hip BMD
    delBMDfn = 1 // delay compartment for femoral neck BMD

    BMDlsTERI = 1       // TERI lumbar spine BMD //
    BMDfnTERI = 1       // TERI femoral neck spine BMD //
    BMDthTERI = 1       // TERI lumbar spine BMD
    delBMDlsTERI = 1 // delay compartment for lumbar spine BMD with
TERI
    delBMDfnTERI = 1 // delay compartment for femoral neck BMD with
TERI
    delBMDthTERI = 1 // delay compartment for total hip BMD with TERI

    BMDlsCOMBO = 1 // DEN/TERI combo lumbar spine BMD //
    BMDthCOMBO = 1 // DEN/TERI combo total hip BMD //
    BMDfnCOMBO = 1 // DEN/TERI combo femoral neck BMD //

    TOL = 1
    cumHazard = 0


// INITIALIZING COMPARTMENTS and DEFINING BIOAVAILABILITIES

$MAIN
  TGFB_0 = Pic0*1000;
  TGFBact_0 = Pic0;
  OBfast_0 = OBtot0*FracOBfast;
  OBslow_0 = OBtot0*(1-FracOBfast);
  M_0 = k3*RNK_0*L_0/k4;
  N_0 = k1*O_0*L_0/k2;
  AOH_0 = B_0/10;
 _F(_N_SOSTSC)=SCLERF;
 _F(_N_TERISC)=TERIF;
 _F(_N_DENSC)=DENF;


// ALGEBRAIC RELATIONSHIPS and DIFFERENTIAL EQUATIONS

$ODE
```

```
  // parameters derived from SS initial conditions
  double T13 = (CaDay/24)/Q0;

  double T15 = CaDay/(CaConc0*V1*24);

  double J14OC50= exp(log((J14OCmax*pow(OC0,J14OCgam)/T13) -
pow(OC0,J14OCgam))/J14OCgam);

  double OCeqn =
(J14OCmax*pow(Osteoclast,J14OCgam))/(pow(Osteoclast,J14OCgam) +
pow(J14OC50,J14OCgam));

  double kinRNK = (koutRNK*RNK0 + k3*RNK0*L0 - k4*M0) /
pow(TGFBact0,kinRNKgam) ;

  double MOCratio = M/Osteoclast;

  double MOCratio0 = M0/OC0;

  double MOCratioEff = pow((MOCratio/MOCratio0), MOCratioGam);

  double J14OCdepend = OCeqn*Q0*FracJ14*MOCratioEff;

  double J14 = T13*Q0*(1-FracJ14) + J14OCdepend;


  // CALCIUM FLUX from PLASMA into BONE
  double J15 = (T15*P*(1-FracJ15) + T15*P*FracJ15*HAp);


  //  CREB-RELATED EQUATIONS

  double EC50PTHcreb = ((EmaxPTHcreb*PTHconc0)/(1-E0crebKin)) -
PTHconc0;

  double crebKin0= crebKout*CREB0;

  double crebKin = crebKin0* (E0crebKin +
EmaxPTHcreb*PTHconc/(PTHconc+EC50PTHcreb));

  double bcl2Kin = RX2*CREB*bcl2Kout;


  // CALCITRIOL-DEPENDENT CALCIUM ABSORPTION EQUATIONS

  double T36 = T33 + (T34-T33)*(pow(C8,CaPOgam)/(pow(T35,CaPOgam)+
pow(C8,CaPOgam)));

  double T37 = T34 - (T34-T33)*(pow(C8,CaPOgam)/(pow(T35,CaPOgam)+
pow(C8,CaPOgam)));

 // CALCIUM - FILTRATION- RELATED EQUATIONS

  double CaFilt = 0.6*0.5*GFR*CaConc;
```

```
  // Maximum calcium reabsorption in the kidney - PTH sensitive
  double mtmEST = (1-maxTmESTkid)/(1-0.1);  //(1-maxEST)/(1-minEST)
  double tmEST = 1 - mtmEST + mtmEST*EST;

  double ReabsMax = tmEST * (0.3*GFR*CaConc0 - 0.149997)*(Reabs50 +
CaConc0) / CaConc0;

  // Effect of PTH on calcium reabsorption
  double T17 = PTHconc0*T16 - PTHconc0;

  double ReabsPTHeff = (T16*PTHconc)/(PTHconc + T17);

  // PTH-sensitive calcium reabsorption in kidney

  double CaReabsActive =  (ReabsMax*C1/(Reabs50 + C1))*ReabsPTHeff;

  double T20 = CaFilt - CaReabsActive;

  double T10 = T7*C8/(C8+T9);

  // Temporary calcium excretion rate
  double J27a = (2-T10)*T20;

  // J27 will be the flux of calcium out of the plasma via the kidney
  if (J27a<0)  J27 = 0 ; else  J27 = J27a;

  double ScaEff = pow( (CaConc0/CaConc), ScaEffGam);

  double T72 = 90 * ScaEff;

  double T73 = T71 * (C8 - T72);

  double T74 = (exp(T73) - exp(-T73)) / (exp(T73) + exp(-T73));

  double T75 = T70 * (0.85 * (1 + T74) + 0.15) ;

  double T76 = T70 * (0.85 * (1 - T74) + 0.15);



//  PHOSPHATE-RELATED EQUATIONS

double PO4inhPTH = pow((C2/1.2),PO4inhPTHgam); // C2 is extracellular
phosphate concentration

double PhosEffTop = (PhosEff0 - 1)*( pow(1.2, PhosEffGam) +
pow(PhosEff50, PhosEffGam));

double PhosEffBot =PhosEff0 * pow(1.2, PhosEffGam);

double PhosEffMax =  PhosEffTop / PhosEffBot;

double PhosEff = PhosEff0 - (PhosEffMax*PhosEff0 * pow(C2, PhosEffGam)
/(pow(C2, PhosEffGam)  + pow(PhosEff50, PhosEffGam)));
```

```
if (C2 > 1.2) PhosEffect = PhosEff ; else PhosEffect = 1;

double T68 = T66*pow(PTHconc, AlphOHgam)/(pow(T67,
AlphOHgam)*PO4inhPTH+pow(PTHconc, AlphOHgam)) ;

double SE = T65*T68*PhosEffect;

 // ORAL ABSORBTION
  double J53 = T52*PhosGut;

  double J54 = T49*C2;

  double J56 = T55*IntraPO;

 // EXTRACELLULAR PHOSPHATE EQUATION (MMOL)
 // J14 = calcium flux from bone into plasma
 // J15 = calcium flux from plasma into bone
 // J27 = calcium flux from plasma to urine
 // J40 = calcium flux from gut to plasma
  dxdt_ECCPhos = J41  - J42 - J48 + J53 - J54 + J56;

 // PHOSPHATE EQUATIONS (DIETARY, INTRACELLULAR)

  dxdt_PhosGut = OralPhos *F12 - J53;

  dxdt_IntraPO = J54 - J56;

 // PHOSPHATE RENAL EXCRETION
  double T47 = T46*0.88*GFR;

  double J48a = 0.88*GFR*C2 - T47;

  if (J48a < 0) J48 = 0 ; else J48 = J48a;


 // TGF-B - RELATED EFFECTS on OSTEO -BLASTS and -CLASTS

bigDb = (kb*OB0*Pic0/ROB10);

double kinTGF = koutTGF0*TGFB0;

double koutTGF = koutTGF0*(pow((TGFB/TGFB0),koutTGFGam));

double koutTGFact = koutTGF0*1000;

double koutTGFeqn = koutTGF*TGFB*(pow((Osteoclast/OC0), OCtgfGAM));

E0PicROB = (FracPicROB*Pic0);

EC50PicROBparen = (EmaxPicROB*pow(TGFBact0,PicROBgam) / (Pic0 -
E0PicROB)) - pow(TGFBact0,PicROBgam);

EC50PicROB = (exp(log(EC50PicROBparen)/PicROBgam));

Dr = (kb*OB0/Pic0) ;
```

```
PicROB = (E0PicROB +
EmaxPicROB*pow(TGFBact,PicROBgam)/(pow(TGFBact,PicROBgam) +
pow(EC50PicROB,PicROBgam)));

ROBin = (Dr*PicROB);

double E0PicOB = FracPicOB*Pic0;

double EC50PicOBparen = (EmaxPicOB*pow(TGFBact0,PicOBgam)/(Pic0 -
E0PicOB)) - pow(TGFBact0,PicOBgam);

double EC50PicOB = exp(log(EC50PicOBparen)/PicOBgam);

double PicOB = E0PicOB + EmaxPicOB*pow(TGFBact,PicOBgam) /
(pow(TGFBact,PicOBgam) + pow(EC50PicOB,PicOBgam));

KPT = (bigDb/PicOB);

double EC50MeffOC = exp(log(pow(M0, kinOCgam)*EmaxMeffOC/(1-E0Meff) -
pow(M0, kinOCgam))/kinOCgam);

double MeffOC = E0Meff + (EmaxMeffOC * pow(M, kinOCgam)/(pow(M,
kinOCgam) + pow(EC50MeffOC,kinOCgam)));

double kinOC2 = Da*PicOCkin*MeffOC*OC0;

double E0PicOC = FracPicOC*Pic0;

double EC50PicOCparen = (EmaxPicOC*pow(TGFBact0, PicOCgam)/(Pic0 -
E0PicOC)) - pow(TGFBact0, PicOCgam);

double EC50PicOC = exp(log(EC50PicOCparen)/PicOCgam);

double PicOC = E0PicOC + ((EmaxPicOC*pow(TGFBact,
PicOCgam))/(pow(TGFBact, PicOCgam) + pow(EC50PicOC, PicOCgam)));

double PiL0 = (k3/k4)*L0;

double PiL = M/10;

double EC50survInPar = (E0RANKL - EmaxL)*(pow(PiL0,
LsurvOCgam)/(E0RANKL - 1)) - pow(PiL0, LsurvOCgam);

double EC50surv = exp(log(EC50survInPar)/LsurvOCgam);

double LsurvOC = E0RANKL - (E0RANKL - EmaxL)*(pow(PiL,
LsurvOCgam)/(pow(PiL, LsurvOCgam) + pow(EC50surv, LsurvOCgam)));

double KLSoc = Da*PicOC*LsurvOC;

double T66 = (pow(T67, AlphOHgam) + pow(PTHconc0, AlphOHgam)
)/pow(PTHconc0, AlphOHgam) ;

double k15a = k14a*Qbone0/Q0 ;
```

```
double J14a = k14a*Qbone;

double J15a = k15a*Q ;

E0PicOBkb = MultPicOBkb*Pic0;

EmaxPicOBkb = FracPic0kb*Pic0;

EC50PicOBparenKb = ((E0PicOBkb - EmaxPicOBkb)*pow(TGFBact0,PicOBgamkb))
/ (E0PicOBkb - Pic0)  - pow(TGFBact0,PicOBgamkb);

EC50PicOBkb = exp(log(EC50PicOBparenKb)/PicOBgamkb);

PicOBkb = E0PicOBkb - (E0PicOBkb  -
EmaxPicOBkb)*pow(TGFBact,PicOBgamkb) / (pow(TGFBact,PicOBgamkb) +
pow(EC50PicOBkb,PicOBgamkb));


// D = ROB1; RESPONDING OSTEOBLASTS
dxdt_ROB1 = ROBin * pow(1/EST,robGAM) -
pow((SCLEREFF),gammaDr)*KPT*ROB1 ;

//LATENT AND ACTIVE TGFB POOLS

dxdt_TGFB = kinTGF*(pow((Osteoblast/OB0),OBtgfGAM)) *
pow(1/EST,tgfbGAM) - koutTGFeqn * pow(EST,tgfbactGAM);

dxdt_TGFBact = koutTGFeqn * pow(EST,tgfbactGAM) - koutTGFact*TGFBact;

 // ESTROGEN-RELATED EFFECTs on OSTEOBLAST APOPTOSIS

 E0RUNX2kbEff =(E0RUNX2kbEffFACT*kb);

 PicOBkbEff = (PicOBkb/Pic0)*(1/(pow(EST,E2scalePicB1))) ;

 kbprime =  (E0RUNX2kbEff*PicOBkbEff - RUNX2kbPrimeEff);
 kbslow = (kbprime*Frackb);
 kbfast = ((kb*OB0 + kbslow*OBfast0 - kbslow*OB0) / OBfast0 );

 // PTH EFFECTS on OSTEOBLAST APOPTOSIS (CONTINUOUS vs. INTERMITTENT
DOSING)

  if (BCL2 > 105)  RUNX2 = BCL2 - 90 ; else  RUNX2 = 10;

  RUNkbMax = E0RUNX2kbEff*RUNkbMaxFact;

  INparen = (RUNkbMax * pow(RUNX20,RUNkbGAM)) / (E0RUNX2kbEff - kb) -
pow(RUNX20,RUNkbGAM);

  RUNkb50 = exp(log(INparen)/RUNkbGAM);

  RUNX2kbPrimeEff = RUNkbMax*pow(RUNX2,RUNkbGAM) / (pow(RUNX2,RUNkbGAM)
+ pow(RUNkb50,RUNkbGAM));
```

```
  // EQUATIONS RELATED TO CALCIUM FLUX TO/FROM GUT

  double T29 = (T28*T0 - T310*T0)/T310;

  double T31 = T28*T/(T+T29);

  // R is calcitriol-dependent gut Ca2+ absorption
  double T83 = R/0.5;

  // J40 = calcium flux from gut to plasma
  double J40 = T31*T*T83/(T + T81) + T87*T;

  // T85 relates to extent of absorption of orally-administered dose

  double T85Rpart = pow(R, T80)/(pow(R,T80) + pow(T81,T80));
  double T85 = T77*T85Rpart;

  // CALCITRIOL-RELATED EQUATIONS

  double INparenCtriol =((CtriolMax - CtriolMin) * pow(Calcitriol0,
CtriolPTgam)) / (CtriolMax - 1)- pow(Calcitriol0,CtriolPTgam);

  double Ctriol50 = exp(log(INparenCtriol) / CtriolPTgam) ;

  double CtriolPTeff = CtriolMax - (CtriolMax - CtriolMin) * pow(C8,
CtriolPTgam) / (pow(C8, CtriolPTgam) + pow(Ctriol50, CtriolPTgam));

  double PTin = PTout * CtriolPTeff;

  double FCTD = (S / 0.5) * PTmax;

  dxdt_B = AOH - T69 * B;

  //  PTH-RELATED CALCIUM FLUX

 double INparenCa =(T58 - T61) * pow(CaConc0, T59) / (T58 - 385) -
pow(CaConc0, T59);
 double T60 = exp(log(INparenCa) / T59) ;
 double T63 =  T58 - (T58 - T61) * pow((CaConc), T59) / (pow((CaConc),
T59) + pow(T60, T59));

 // PTH-RELATED EQUATIONS
 // production rate from precursor
  double EPTH = T63*FCTD;

 // Infused and subcutaneously administered PTH
 double IPTH= 0.693*SC + IPTHinf;

 // Total PTH input rate
 double SPTH = EPTH + IPTH;

 dxdt_PTH = SPTH - kout*PTH + TERIPKIN;

 // PT GLAND max capacity
```

```
 dxdt_PTmax = PTin - PTout * PTmax;

 // PTH GLAND pool

 dxdt_S = (1 - S) * T76 - (S* T75);

 // Subcutaneous PTH administration

 dxdt_SC = IPTHint - 0.693*SC;


 // 1- ALPHA HYDROXYLASE
////////////////////////////////////////////

 dxdt_AOH = SE - T64*AOH ;

 // CALCIUM
//////////////////////////////////////////////////////////

 dxdt_P = J14 - J15- J27 + J40;

 // ORAL CALCIUM (MMOL)
 // J40 --> flux from gut to plasma
 dxdt_T = OralCa*T85 - J40;

 // Calcitriol-dependent Ca2+ absorption
 dxdt_R = T36*(1- R) - T37*R;

//  BONE CALCIUM
// Immediately-exchangable
dxdt_Q = J15 - J14 + J14a - J15a;

// Non-immediately-exchangable
dxdt_Qbone = J15a - J14a;

// HYDROXYAPATITE

double kLShap = 1/HApMRT;

double kHApIn = kLShap/OB0;

// CALCIUM in HYDROXYAPATITE
double J41 = 0.464*J14;
double J42 = 0.464*J15;

dxdt_HAp = kHApIn*Osteoblast - kLShap*HAp;

// ESTROGEN-RELATED EQUATIONS

 double AGE = ageENTER + T_0;

 double kinEST=0 ;

 double ageONSET = ageDONE-menoDUR;
```

```
 if(AGE < ageONSET) kinEST = koutEST * pow((AGE/ageENTER),ageGAM);

 if(AGE >= ageONSET) kinEST = koutEST * pow((AGE/ageENTER),ageGAM) * (1
- age50 * (pow((AGE-ageONSET),2)/(pow((menoDUR/2),2) + pow((AGE-
ageONSET),2))));

  dxdt_EST = (kinEST - koutEST * EST)*ESTON;


 // OSTEOBLASTS:fast and slow removal rates

 double Frackb2 = kbfast/kbprime;

 dxdt_OBfast = (bigDb/PicOB)*D*FracOBfast*Frackb2  - kbfast*OBfast;

 dxdt_OBslow = (bigDb/PicOB)*D*(1-FracOBfast)*Frackb - kbslow*OBslow;


 // OC: ACTIVE OSTEOCLASTS
 dxdt_OC = kinOC2 - KLSoc*OC;


// SCLEROSTIN-RELATED EFFECTS; PROPAGATES THROUGH OSTEOCYTE APOPTOSIS
// translation compartment

kin_T = kout_T;

EC50SCLER =  (exp(log(EMAXSCLER-1)/SCLEROBgam));

SC50 = (SMAX - 1);

dxdt_trans =
kin_T*(EMAXSCLER*pow(SCLEREFF,SCLEROBgam)/(pow(EC50SCLER,SCLEROBgam)+po
w(SCLEREFF,SCLEROBgam))) - kout_T*trans;

SCLEREFF = (SCLER/SCLER_0);

SCLER_TOL = (SMAX*SCLEREFF/(SC50 + SCLEREFF));

kin_TOL = kout_TOL;

dxdt_TOL = kin_TOL*(SCLER_TOL) - kout_TOL*TOL;

 // OSTEOCYTES

 koutOCY = (OB0*FracOCY)*(pow((SCLEREFF),gammaOCY));

 dxdt_OCY = OB*FracOCY*OCY0 - koutOCY*OCY;

// RANKL-OPG AXIS

double kinLbase = koutL*L0;

fracOBEffect = FracOBE/TOL;
```

```
double OsteoEffect = pow((Osteoblast/OB0),
(TotOsteoEffectGam/fracOBEffect)) ;

double OsteoCYEffect = pow((OCY/OCY0), (TotOsteoEffectGam*(1-
(1/fracOBEffect)))) ;

double PTH50 = EmaxLpth*PTHconc0 - PTHconc0 ;

double LpthEff = EmaxLpth*(PTHconc) /
((PTH50*pow((OsteoCYEffect*OsteoEffect),TESTPOWER)) + (PTHconc)) ;

double kinL = kinLbase*(OsteoCYEffect)*(OsteoEffect)*LpthEff;

double pObase = kO*O0;

double pO =
pObase*(D/ROB10)*((PTHconc+(opgPTH50*(D/ROB10)))/(2*PTHconc))+ IO;

double RX2Kin = RX2Kout0*RX20;

double EC50PTHRX2x = ((EmaxPTHRX2x*PTHconc0)/(RX2Kout0 - E0rx2Kout)) -
PTHconc0;

double RX2Kout = E0rx2Kout + EmaxPTHRX2x*PTHconc/(PTHconc+EC50PTHRX2x);

// L: RANK-L
dxdt_L = kinL- koutL*L - k1*O*L + k2*N - k3*RNK*L + k4*M -
kdenosl*DENMOL*L;

// RNK: RANK
dxdt_RNK = kinRNK*pow(TGFBact,kinRNKgam) - koutRNK*RNK - k3*RNK*L  +
k4*M;

// M: RANK - RANK-L complex
dxdt_M = k3*RNK*L - k4*M;

// N:  - RANK-L - OPG complex
dxdt_N = k1*O*L - k2*N;

// O: OPG
dxdt_O = pO*pow((SCLEREFF),gammaOPG) - k1*O*L + k2*N - kO*O;


// DIFFERENTIAL EFFECTS of PTH ADMINISTRATION
dxdt_RX2 = RX2Kin - RX2Kout*RX2 ;

dxdt_CREB = crebKin - crebKout*CREB;

dxdt_BCL2 = bcl2Kout*CREB*RX2 - bcl2Kout*BCL2;


// FILTRATION RATE EQUATIONS
double GFRend = GFR0 - GFRdelta/16.667;

double GFRtau_ = GFRtau*8766;
```

```
double kGFR = -log(GFRend/GFR0)/GFRtau_;

dxdt_GFR = -kGFR*GFR;

// URINE CALCIUM EQUATION
dxdt_UCA = J27;


// PK EQUATIONS

// GENERAL PK COMPARTMENTS
double PKCLNL = PKVMAX/(PKKM+PKCP);

dxdt_PKGUT = -PKKA*PKGUT;

dxdt_PKCENT = PKKA*PKGUT + PKQ1*PKPER1/PKVP1 + PKQ2*PKPER2/PKVP2 -
(PKQ1+PKQ2+PKCL+PKCLNL)*PKCENT/PKVC;

dxdt_PKPER1 = PKQ1*PKCENT/PKVC - PKQ1*PKPER1/PKVP1;

dxdt_PKPER2 = PKQ2*PKCENT/PKVC - PKQ2*PKPER2/PKVP2;

// DENOSUMAB PK

double  DENCLNL =  (DENVMAX/(DENKM+DENCP));

dxdt_DENSC =  -DENKA*DENSC;

dxdt_DENCENT = DENKA*DENSC + DENQ*DENPER/DENVP -
(DENQ+DENCL+DENCLNL)*DENCENT/DENVC;

dxdt_DENPER = DENQ*DENCENT/DENVC - DENQ*DENPER/DENVP;

// TERIPARATIDE PK

double TERIPKIN = TERISC*TERICL/TERIVC;

dxdt_TERISC = -TERIPKIN;

dxdt_TERICENT  = TERIPKIN - TERICENT*TERIKA;


// SCLEROSTIN AB PK AND SCLEROSTIN

double SOSTCLNL = SOSTVMAX/(SOSTKM+SOSTCP);

dxdt_SOSTSC = -SOSTKA*SOSTSC;

dxdt_SOSTCENT = SOSTKA*SOSTSC - SOSTCLNL*SOSTCENT-(SOSTCL*(SOSTCP))-
(SOSTQ*(SOSTCP)) + (SOSTQ*(SOSTPER/SOSTVP));

dxdt_SOSTPER = (SOSTQ*(SOSTCENT/SOSTVC))-(SOSTQ*SOSTPER/SOSTVP);

dxdt_SCLER = SOSTKIN-SOSTKOUT*SCLER-(SOSTK0-
```

```
SOSTKOUT)*SCLER*(SOSTCENT/SOSTVC)/(SOSTKM+(SOSTCENT/SOSTVC));


 // BONE MINERAL DENSITY (BMD) EQUATIONS
 // Lumbar spine - generic (pbo)

 double kinBMDls =  koutBMDls*BMDls0;

 dxdt_BMDls = kinBMDls * pow(OB/OB0,gamOB) - koutBMDls *
pow(OC/OC0,gamOCls) * BMDls;

 //Lumbar spine with DENOSUMAB

 double kinBMDlsDEN =  koutBMDlsDEN*BMDlsDEN0;

 dxdt_BMDlsDEN = kinBMDlsDEN * pow(OB/OB0,gamOB) - koutBMDlsDEN *
pow(OC/OC0,gamOClsDEN) * BMDlsDEN;

 //Femoral neck with DENOSUMAB

 double kinBMDfnDEN =  koutBMDfnDEN*BMDfnDEN0;

 dxdt_BMDfnDEN = kinBMDfnDEN * pow(OB/OB0,gamOB) - koutBMDfnDEN *
pow(OC/OC0,gamOCfnDEN) * BMDfnDEN;

//Total hip with DENOSUMAB

 double kinBMDthDEN =  koutBMDthDEN*BMDthDEN0;

 dxdt_BMDthDEN = kinBMDthDEN * pow(OB/OB0,gamOB) - koutBMDthDEN *
pow(OC/OC0,gamOCthDEN) * BMDthDEN;

 //Lumbar spine for SCLEROSTIN

 double kinBMDlsSCLER =  koutBMDSCLER*BMDlsSCLER0;

 kin_BMDdel = kout_BMDdel;

 dxdt_delBMDls = kin_BMDdel * pow(OB/OB0,gamOBSCLERls) -
kout_BMDdel*delBMDls;

 dxdt_BMDlsSCLER = kinBMDlsSCLER * delBMDls - koutBMDSCLER *
pow(OC/OC0,gamOCSCLER) * BMDlsSCLER;

 //Femoral neck for SCLEROSTIN

 double kinBMDfnSCLER =  koutBMDSCLER*BMDfnSCLER0;

 dxdt_delBMDfn = kin_BMDdel* pow(OB/OB0,gamOBSCLERfn) -
kout_BMDdel*delBMDfn;

 dxdt_BMDfnSCLER = kinBMDfnSCLER * delBMDfn  - pow(OC/OC0,gamOCSCLER) *
koutBMDSCLER * BMDfnSCLER;

 //Total hip for SCLEROSTIN
```

```
 double kinBMDthSCLER =  koutBMDSCLER*BMDthSCLER0;

 dxdt_delBMDth = kin_BMDdel * pow(OB/OB0,gamOBSCLERth) -
kout_BMDdel*delBMDth;

 dxdt_BMDthSCLER = kinBMDthSCLER * delBMDth - koutBMDSCLER *
pow(OC/OC0,gamOCSCLER) * BMDthSCLER;

 //Lumbar spine for TERIPARATIDE

  double kinBMDlsTERI =  koutBMDlsTERI*BMDlsTERI0;

 kin_BMDdelTERI = kout_BMDdelTERI;

 dxdt_delBMDlsTERI = kin_BMDdelTERI * pow(OB/OB0,gamOBTERIls) -
kout_BMDdelTERI*delBMDlsTERI;

 dxdt_BMDlsTERI = kinBMDlsTERI * delBMDlsTERI - koutBMDlsTERI *
pow(OC/OC0,gamOClsTERI) * BMDlsTERI;

//Femoral neck for TERIPARATIDE

  double kinBMDfnTERI =  koutBMDfnTERI*BMDfnTERI0;

  kin_BMDdelTERI = kout_BMDdelTERI;

  dxdt_delBMDfnTERI = kin_BMDdelTERI* pow(OB/OB0,gamOBTERIfn) -
kout_BMDdelTERI*delBMDfnTERI;

  dxdt_BMDfnTERI = kinBMDfnTERI * delBMDfnTERI  -
pow(OC/OC0,gamOCfnTERI) * koutBMDfnTERI * BMDfnTERI;

//Total hip for TERIPARATIDE

  double kinBMDthTERI =  koutBMDthTERI*BMDthTERI0;

  dxdt_delBMDthTERI = kin_BMDdelTERI* pow(OB/OB0,gamOBTERIth) -
kout_BMDdelTERI*delBMDthTERI;

  dxdt_BMDthTERI = kinBMDthTERI * delBMDthTERI  -
pow(OC/OC0,gamOCthTERI) * koutBMDthTERI * BMDthTERI;


// BMD with combination therapy

// DEN/TERI COMBO
 double kinBMDlsCOMBO = koutBMDlsCOMBO;

dxdt_BMDlsCOMBO = 0;
if(DEN_TERI_COMBO==1) dxdt_BMDlsCOMBO = kinBMDlsCOMBO *
pow(OB/OB0,gamOB) - koutBMDlsCOMBO*
pow(OC/OC0,gamOClsDEN_TERI)*BMDlsCOMBO;

double kinBMDthCOMBO = koutBMDthCOMBO;
```

```
dxdt_BMDthCOMBO = 0;
if(DEN_TERI_COMBO==1) dxdt_BMDthCOMBO = kinBMDthCOMBO *
pow(OB/OB0,gamOB) - koutBMDthCOMBO*
pow(OC/OC0,gamOCthDEN_TERI)*BMDthCOMBO;

double kinBMDfnCOMBO = koutBMDfnCOMBO;
dxdt_BMDfnCOMBO = 0;
if(DEN_TERI_COMBO==1) dxdt_BMDfnCOMBO = kinBMDfnCOMBO *
pow(OB/OB0,gamOB) - koutBMDfnCOMBO*
pow(OC/OC0,gamOCfnDEN_TERI)*BMDfnCOMBO;

// FRACTURE PROBABILITY
// Reference values:
// BMDhat = 0.8 g/cm^2
// postMenoAgehat = 20 y
// BMIhat = 27.1 kg/m^2
//req dataset items = agepostmeno (at baseline), radFracInc, BMI,
lsBMDbase
// code in switches:
// DEN_TERI_COMBO = 0 : no drug
// DEN_TERI_COMBO = 1 : combinination TERI/DEN
// DEN_TERI_COMBO = 2 : TERI only
// DEN_TERI_COMBO = 3 : DEN only
// DEN_TERI_COMBO = 4 : SCLER only

double PBO_BMD = 1;
double betaDrug = 0;
if (DEN_TERI_COMBO==0) {
    PBO_BMD = BMDls;
}

double COMBO_BMD = 1;
if (DEN_TERI_COMBO==1) {
    COMBO_BMD = BMDlsCOMBO;
  betaDrug = betaDrug_COMBO;
}

double TERI_BMD = 1;
double TERI_BMDth = 1;
double TERI_BMDfn = 1;
if (DEN_TERI_COMBO==2) {
    TERI_BMD = BMDlsTERI;
  betaDrug = betaDrug_TERI;
  TERI_BMDth = BMDthTERI;
  TERI_BMDfn = BMDfnTERI;
}

double DEN_BMD = 1;
double DEN_BMDth = 1;
double DEN_BMDfn = 1;
if (DEN_TERI_COMBO==3) {
    DEN_BMD = BMDlsDEN;
  betaDrug = betaDrug_DENO;
  DEN_BMDth=BMDthDEN;
  DEN_BMDfn=BMDfnDEN;
```

```
}

double SCLER_BMD = 1;
double SCLER_BMDth = 1;
double SCLER_BMDfn = 1;

if (DEN_TERI_COMBO==4) {
    SCLER_BMD = BMDlsSCLER;
  SCLER_BMDth=BMDthSCLER;
  SCLER_BMDfn=BMDfnSCLER;
}

if(SCLER_DEN_SEQ==1){
  SCLER_BMD = BMDlsSCLER;
  SCLER_BMDth=BMDthSCLER;
  SCLER_BMDfn=BMDfnSCLER;
  DEN_BMD = BMDlsDEN;
  DEN_BMDth=BMDthDEN;
  DEN_BMDfn=BMDfnDEN;
}

double lsBMDtot = (PBO_BMD + COMBO_BMD + TERI_BMD + DEN_BMD +
SCLER_BMD)-4;

double thBMDtot = (1 + TERI_BMDth + DEN_BMDth + SCLER_BMDth)-3;

double fnBMDtot = (1 +  TERI_BMDfn + DEN_BMDfn + SCLER_BMDfn)-3;


// HAZARD MODEL EQUATIONS

drug = betaDrug;

lsBMD = lsBMDtot*lsBMDbase; //nominal BMD

double lsBMDCFB = (lsBMDtot*lsBMDbase) - lsBMDbase; //CFB BMD

double postMenoAge = agepostmeno + T_0/365.25/24;

Hazard = baseHazard*exp(HazBMDCov*log(lsBMD/lsBMDbase) +
       HazpostMenoAgeCov*(postMenoAge-postMenoAgeRef )+
       HazradFracCov*radFracInc+HazBMICov*(BMI-bmiRef) + betaDrug);

dxdt_cumHazard = Hazard / 365.25/24;

Survival = exp(-cumHazard);


// TELLS CODE WHICH DATA TO PRINT

$TABLE
table(DENMOL) = (DENCENT/DENVC/150000)*1000*1000;
table(OB) = (OBfast*trans + OBslow);
table(BSAPsim) = (OB/OB0*100);
table(P1NPsim) = ((2050 * pow((BSAP), 1.8) / ((pow(467, 1.8) +
```

```
pow((BSAP),1.8))))-20.4181);
table(SCLEREFF) = ((SCLER/SCLER_0));
table(CTXsim) = (OC/OC0*100);
table(OsteoEffect) = pow((Osteoblast/OB0),
(TotOsteoEffectGam/fracOBEffect));
table(fracOBEffect) = (FracOBE/TOL);

table(lsBMDsimSCLER) = (BMDlsSCLER*100);
table(lsBMDsimTERI) = (BMDlsTERI*100);
table(lsBMDsimDEN) = (BMDlsDEN*100);
table(thBMDsimSCLER) = (BMDthSCLER*100);
table(thBMDsimTERI) = (BMDthTERI*100);
table(thBMDsimDEN) = (BMDthDEN*100);
table(fnBMDsimSCLER) = (BMDfnSCLER*100);
table(fnBMDsimTERI) = (BMDfnTERI*100);
table(fnBMDsimDEN) = (BMDfnDEN*100);
table(BMDls)=(BMDls*100);
table(lsBMDsimCOMBO) = (BMDlsCOMBO*100);
table(thBMDsimCOMBO) = (BMDthCOMBO*100);
table(fnBMDsimCOMBO) = (BMDfnCOMBO*100);

table(Hazard) = (cumHazard*1);
table(Survival) = (Survival*1);


// ALLOW FITTING TO MULTIPLE ENDPOINTS IN A SINGLE DATASET
DV = ((2050 * pow((BSAP), 1.8) / ((pow(467, 1.8) + pow((BSAP),1.8))))-
20.4181);
if(TYPE==1) DV = (OC/OC0*100);
table(DV) = DV;

if(Scler_BMD_type==0) SclerBMDpred = (BMDlsSCLER*100);
if(Scler_BMD_type==1) SclerBMDpred = (BMDthSCLER*100);
if(Scler_BMD_type==2) SclerBMDpred = (BMDfnSCLER*100);
table(SclerBMDpred) = SclerBMDpred;

if(Deno_BMD_type==0) DenoBMDpred = (BMDlsDEN*100);
if(Deno_BMD_type==1) DenoBMDpred = (BMDthDEN*100);
if(Deno_BMD_type==2) DenoBMDpred = (BMDfnDEN*100);
table(DenoBMDpred) = DenoBMDpred;

if(Teri_BMD_type==0) TeriBMDpred = (BMDlsTERI*100);
if(Teri_BMD_type==1) TeriBMDpred = (BMDthTERI*100);
if(Teri_BMD_type==2) TeriBMDpred = (BMDfnTERI*100);

if(Combo_BMD_type==0) ComboBMDpred = (BMDlsCOMBO*100);
if(Combo_BMD_type==1) ComboBMDpred = (BMDthCOMBO*100);
if(Combo_BMD_type==2) ComboBMDpred = (BMDfnCOMBO*100);
table(ComboBMDpred) = ComboBMDpred;

// TABLE SEVERAL ENDPOINTS TOGETHER

// report("EVID/TIME/SOSTCENT", OCY, TIME, SOSTCENT);
```

Bibliography

[1] S. W. Blume and J. R. Curtis, "Medical costs of osteoporosis in the elderly medicare population.," *Osteoporos Int*, vol. 22, pp. 1835–1844, Jun 2011.

[2] A. P. Schilcher J, Michaolsson K, "Bisphosphonate use and atypical fractures of the femoral shaft.," *N Engl J Med.*, vol. 364, pp. 1728–1737, 2011.

[3] R. E. B. Abrahamsen, P. Eiken, "Subtrochanteric and diaphyseal femur fractures in patients treated with alendronate: A register-based national cohort study.," *J Bone Miner Res*, vol. 24, pp. 1095–1102, 2009.

[4] S. Boonen, R. F. Laan, I. P. Barton, and N. B. Watts, "Effect of osteoporosis treatments on risk of non-vertebral fractures: review and meta-analysis of intention-to-treat studies.," *Osteoporos Int*, vol. 16, pp. 1291–1298, Oct 2005.

[5] E. F. Eriksen, T. M. Keaveny, E. R. Gallagher, and J. H. Krege, "Literature review: The effects of teriparatide therapy at the hip in patients with osteoporosis.," *Bone*, vol. 67, pp. 246–256, Oct 2014.

[6] A. Diez-Perez, J. D. Adachi, D. Agnusdei, J. P. Bilezikian, J. E. Compston, S. R. Cummings, R. Eastell, E. F. Eriksen, J. Gonzalez-Macias, U. A. Liberman, D. A. Wahl, E. Seeman, J. A. Kanis, and C. Cooper, "Treatment failure in osteoporosis.," *Osteoporos Int*, vol. 23, pp. 2769–2774, Dec 2012.

[7] J.-P. Rey and D. L. Ellies, "Wnt modulators in the biotech pipeline" in developmental dynamics," *Developmental-Dynamics*, vol. 239, no. 1, pp. 102–114, 2010.

[8] A. G. Costa and J. P. Bilezikian, "Sclerostin: therapeutic horizons based upon its actions.," *Curr Osteoporos Rep*, vol. 10, pp. 64–72, Mar 2012.

[9] M. P. Yavropoulou, C. Xygonakis, M. Lolou, F. Karadimou, and J. G. Yovos, "The sclerostin story: from human genetics to the development of novel anabolic treatment for osteoporosis.," *Hormones (Athens, Greece)*, vol. 13, no. 4, pp. 323–337, 2014.

[10] C. H. Lin, T. Ji, C.-F. Chen, and B. H. Hoang, "Wnt signaling in osteosarcoma.," *Adv Exp Med Biol*, vol. 804, pp. 33–45, 2014.

[11] M. L. Johnson, "Unlocking the sost gene.," *J Bone Miner Res*, vol. 30, pp. 397–399, Mar 2015.

[12] A. H. Van Lierop, N. a. T. Hamdy, M. E. Van Egmond, E. Bakker, F. G. Dikkers, and S. E. Papapoulos, "Van Buchem disease: Clinical, biochemical, and densitometric features of patients and disease carriers," *Journal of Bone and Mineral Research*, vol. 28, no. 4, pp. 848–854, 2013.

[13] A. Fayez, M. Aglan, N. Esmaiel, T. E. Zanaty, M. A. Kader, and M. E. Ruby, "A Novel Loss-of-Sclerostin Function Mutation in a First Egyptian Family with Sclerosteosis," vol. 2015, 2015.

[14] J. H. Kim, X. Liu, J. Wang, X. Chen, H. Zhang, S. H. Kim, J. Cui, R. Li, W. Zhang, Y. Kong, J. Zhang, W. Shui, J. Lamplot, M. R. Rogers, C. Zhao, N. Wang, P. Rajan, J. Tomal, J. Statz, N. Wu, H. H. Luu, R. C. Haydon, and T.-C. He, "Wnt signaling in bone formation and its therapeutic potential for bone diseases.," *Ther Adv Musculoskelet Dis*, vol. 5, pp. 13–31, Feb 2013.

[15] E. Lee, A. Salic, R. Kruger, R. Heinrich, and M. W. Kirschner, "The roles of apc and axin derived from experimental and theoretical analysis of the wnt pathway.," *PLoS Biol*, vol. 1, p. E10, Oct 2003.

[16] J. H. Kim, X. Liu, J. Wang, X. Chen, H. Zhang, S. H. Kim, J. Cui, R. Li, W. Zhang, Y. Kong, J. Zhang, W. Shui, J. Lamplot, M. R. Rogers, C. Zhao, N. Wang, P. Rajan, J. Tomal, J. Statz, N. Wu, H. H. Luu, R. C. Haydon, and T.-C. He, "Wnt signaling in bone formation and its therapeutic potential for bone diseases.," *Ther Adv Musculoskelet Dis*, vol. 5, pp. 13–31, Feb 2013.

[17] N. A. Sims and N. C. Walsh, "Intercellular cross-talk among bone cells: new factors and pathways.," *Curr Osteoporos Rep*, vol. 10, pp. 109–117, Jun 2012.

[18] A. Tomkinson, J. Reeve, R. W. Shaw, and B. S. Noble, "The death of osteocytes via apoptosis accompanies estrogen withdrawal in human bone," *Journal of Clinical Endocrinology and Metabolism*, vol. 82, no. 9, pp. 3128–3135, 1997.

[19] U. I. Mödder, M. M. Roforth, K. Hoey, L. K. McCready, J. M. Peterson, D. G. Monroe, M. J. Oursler, and S. Khosla, "Effects of estrogen on osteoprogenitor cells and cytokines/bone-regulatory factors in postmenopausal women," *Bone*, vol. 49, no. 2, pp. 202–207, 2011.

[20] X. Li, M. S. Ominsky, Q.-T. Niu, N. Sun, B. Daugherty, D. D'Agostin, C. Kurahara, Y. Gao, J. Cao, J. Gong, F. Asuncion, M. Barrero, K. Warmington, D. Dwyer, M. Stolina, S. Morony, I. Sarosi, P. J. Kostenuik, D. L. Lacey, W. S. Simonet, H. Z. Ke, and C. Paszty, "Targeted deletion of the sclerostin gene in mice results in increased bone formation and bone strength.," *J Bone Miner Res*, vol. 23, pp. 860–869, Jun 2008.

[21] P. Babij, W. Zhao, C. Small, Y. Kharode, P. J. Yaworsky, M. L. Bouxsein, P. S. Reddy, P. V. N. Bodine, J. A. Robinson, B. Bhat, J. Marzolf, R. A. Moran, and F. Bex, "High bone mass in mice expressing a mutant lrp5 gene.," *J Bone Miner Res*, vol. 18, pp. 960–974, Jun 2003.

[22] X. Li, K. S. Warmington, Q.-T. Niu, F. J. Asuncion, M. Barrero, M. Grisanti, D. Dwyer, B. Stouch, T. M. Thway, M. Stolina, M. S. Ominsky, P. J. Kostenuik, W. S. Simonet, C. Paszty, and H. Z. Ke, "Inhibition of sclerostin by monoclonal antibody increases bone formation, bone mass, and bone strength in aged male rats.," *J Bone Miner Res*, vol. 25, pp. 2647–2656, Dec 2010.

[23] M. S. Virk, F. Alaee, H. Tang, M. S. Ominsky, H. Z. Ke, and J. R. Lieberman, "Systemic administration of sclerostin antibody enhances bone repair in a critical-sized femoral defect in a rat model.," *J Bone Joint Surg Am*, vol. 95, pp. 694–701, Apr 2013.

[24] D. Padhi, G. Jang, B. Stouch, L. Fang, and E. Posvar, "Single-dose, placebo-controlled, randomized study of amg 785, a sclerostin monoclonal antibody.," *J Bone Miner Res*, vol. 26, pp. 19–26, Jan 2011.

[25] M. R. McClung, A. Grauer, S. Boonen, M. A. Bolognese, J. P. Brown, A. Diez-Perez, B. L. Langdahl, J.-Y. Reginster, J. R. Zanchetta, S. M. Wasserman, L. Katz, J. Maddox, Y.-C. Yang, C. Libanati, and H. G. Bone, "Romosozumab in postmenopausal women with low bone mineral density," *New England Journal of Medicine*, vol. 370, no. 5, pp. 412–20, 2014. PMID: 24382002.

[26] J. McColm, L. Hu, T. Womack, C. C. Tang, and A. Y. Chiang, "Single- and multiple-dose randomized studies of blosozumab, a monoclonal antibody against sclerostin, in healthy postmenopausal women.," *J Bone Miner Res*, Aug 2013.

[27] K. J. Claes, L. Viaene, S. Heye, B. Meijers, P. d'Haese, and P. Evenepoel, "Sclerostin: another vascular calcification inhibitor?," *J Clin Endocrinol Metab*, vol. 98, pp. 3221–3228, Aug 2013.

[28] X. Tu, J. Delgado-Calle, K. W. Condon, M. Maycas, H. Zhang, N. Carlesso, M. M. Taketo, D. B. Burr, L. I. Plotkin, and T. Bellido, "Osteocytes mediate the anabolic actions of canonical wnt/beta-catenin signaling in bone.," *Proc Natl Acad Sci U S A*, Jan 2015.

[29] P. Divieti Pajevic, "Recent progress in osteocyte research.," *Endocrinol Metab (Seoul)*, vol. 28, pp. 255–261, Dec 2013.

[30] C. a. O'Brien, T. Nakashima, and H. Takayanagi, "Osteocyte control of osteoclastogenesis," *Bone*, vol. 54, no. 2, pp. 258–263, 2013.

[31] T. Bellido, "Osteocyte-driven bone remodeling.," *Calcif Tissue Int*, Sep 2013.

[32] T. Nakashima, M. Hayashi, T. Fukunaga, K. Kurata, M. Oh-Hora, J. Q. Feng, L. F. Bonewald, T. Kodama, A. Wutz, E. F. Wagner, J. M. Penninger, and H. Takayanagi, "Evidence for osteocyte regulation of bone homeostasis through rankl expression.," *Nat Med*, vol. 17, pp. 1231–1234, Oct 2011.

[33] S. L. Holmen, C. R. Zylstra, A. Mukherjee, R. E. Sigler, M.-C. Faugere, M. L. Bouxsein, L. Deng, T. L. Clemens, and B. O. Williams, "Essential role of beta-catenin in postnatal bone acquisition.," *J Biol Chem*, vol. 280, pp. 21162–21168, Jun 2005.

[34] L. Zhang, V. Sinha, S. T. Forgue, S. Callies, L. Ni, R. Peck, and S. R. B. Allerheiligen, "Model-based drug development: The road to quantitative pharmacology," *Journal of Pharmacokinetics and Pharmacodynamics*, vol. 33, no. 3, pp. 369–393, 2006.

[35] M. Peterson and M. Riggs, "Fda advisory meeting clinical pharmacology review utilizes a quantitative systems pharmacology (qsp) model: A watershed moment?," *CPT: Pharmacometrics and Systems Pharmacology*, vol. 4, no. 3, pp. 189–192, 2015.

[36] P. Pivonka and S. V. Komarova, "Mathematical modeling in bone biology: From intracellular signaling to tissue mechanics," *Bone*, vol. 47, no. 2, pp. 181 – 189, 2010.

[37] Y. Kogan, K. E. Halevi-Tobias, G. Hochman, A. K. Baczmanska, L. Leyns, and Z. Agur, "A new validated mathematical model of the wnt signalling pathway predicts effective combinational therapy by sfrp and dkk.," *Biochem J*, vol. 444, pp. 115–125, May 2012.

[38] G. R. Mirams, H. M. Byrne, and J. R. King, "A multiple timescale analysis of a mathematical model of the wnt/beta-catenin signalling pathway.," *J Math Biol*, vol. 60, pp. 131–160, Jan 2010.

[39] J. M. Graham, B. P. Ayati, S. A. Holstein, and J. A. Martin, "The role of osteocytes in targeted bone remodeling: A mathematical model," *PLoS ONE*, vol. 8, p. e63884, May 2013.

[40] E. O. Carew, "A semi-empirical cell dynamics model for bone turnover under external stimulus.," *J Biomech Eng*, vol. 134, p. 024503, Feb 2012.

[41] R. F. van Oers, R. Ruimerman, B. van Rietbergen, P. A. Hilbers, and R. Huiskes, "Relating osteon diameter to strain," *Bone*, vol. 43, no. 3, pp. 476 – 482, 2008.

[42] M. Colloca, R. Blanchard, C. Hellmich, K. Ito, and B. van Rietbergen, "A multiscale analytical approach for bone remodeling simulations: linking scales from collagen to trabeculae.," *Bone*, vol. 64, pp. 303–313, Jul 2014.

[43] P. R. Buenzli, "Osteocytes as a record of bone formation dynamics: a mathematical model of osteocyte generation in bone matrix.," *J Theor Biol*, vol. 364, pp. 418–427, Jan 2015.

[44] P. Pivonka, J. Zimak, D. W. Smith, B. S. Gardiner, C. R. Dunstan, N. A. Sims, T. John Martin, and G. R. Mundy, "Theoretical investigation of the role of the rank–rankl–opg system in bone remodeling," *Journal of Theoretical Biology*, vol. 262, pp. 306–316, 1 2010.

[45] J. Kaiser, T. Lemaire, S. Naili, V. Sansalone, and S. V. Komarova, "Do calcium fluxes within cortical bone affect osteocyte mechanosensitivity?," *J Theor Biol*, vol. 303, pp. 75–86, Jun 2012.

[46] D. Webster and R. Muller, "In silico models of bone remodeling from macro to nano-from organ to cell," *Syst Biol Med*, vol. 3, pp. 241–251, 2011.

[47] M. C. Peterson and M. M. Riggs, "A physiologically based mathematical model of integrated calcium homeostasis and bone remodeling.," *Bone*, vol. 46, pp. 49–63, Jan 2010.

[48] V. Lemaire, F. L. Tobin, L. D. Greller, C. R. Cho, and L. J. Suva, "Modeling the interactions between osteoblast and osteoclast activities in bone remodeling.," *J Theor Biol*, vol. 229, pp. 293–309, Aug 2004.

[49] J. F. Raposo, L. G. Sobrinho, and H. G. Ferreira, "A minimal mathematical model of calcium homeostasis.," *J Clin Endocrinol Metab*, vol. 87, pp. 4330–4340, Sep 2002.

[50] T. Bellido, A. A. Ali, L. I. Plotkin, Q. Fu, I. Gubrij, P. K. Roberson, R. S. Weinstein, C. A. O'Brien, S. C. Manolagas, and R. L. Jilka, "Proteasomal degradation of runx2 shortens parathyroid hormone-induced anti-apoptotic signaling in osteoblasts. a putative explanation for why intermittent administration is needed for bone anabolism.," *J Biol Chem*, vol. 278, pp. 50259–50272, Dec 2003.

[51] R. Recker, C. Benson, T. Matsumoto, M. Bolognese, D. Robins, J. Alam, A. Y. Chiang, L. Hu, J. H. Krege, H. Sowa, B. Mitlak, and S. Myers, "A randomized, double-blind phase 2 clinical trial of blosozumab, a sclerostin antibody, in postmenopausal women with low bone mineral density.," *J Bone Miner Res*, Sep 2014.

[52] A. G. Robling, P. J. Niziolek, L. A. Baldridge, K. W. Condon, M. R. Allen, I. Alam, S. M. Mantila, J. Gluhak-Heinrich, T. M. Bellido, S. E. Harris, and C. H. Turner, "Mechanical stimulation of bone in vivo reduces osteocyte expression of sost/sclerostin.," *J Biol Chem*, vol. 283, pp. 5866–5875, Feb 2008.

[53] D. E. Mager and W. J. Jusko, "General pharmacokinetic model for drugs exhibiting target-mediated drug disposition," *J Pharmacokinet Pharmacodyn*, vol. 28, pp. 507–532, Dec 2001.

[54] L. Gibiansky and E. Gibiansky, "Target-mediated drug disposition model: approximations, identifiability of model parameters and applications to the population pharmacokinetic-pharmacodynamic modeling of biologics.," *Expert Opin Drug Metab Toxicol*, vol. 5, pp. 803–812, Jul 2009.

[55] M. Saccomani and G. Bellu, "Daisy: An efficient tool to test global identifiability. some case studies," *16th Mediterranean Conference on Control and Automation*, pp. 1723–1728, June 2008.

[56] A. C. Hearn, *REDUCE User's Manual*. Reduce-Algebra, Santa Monica, CA, USA, 3.8 ed., Feb 2004.

[57] C. Weber, R. Schmitt, H. Birnboeck, G. Hopfgartner, S. P. van Marle, P. A. Peeters, J. H. Jonkman, and C. R. Jones, "Pharmacokinetics and pharmacodynamics of the endothelin-receptor antagonist bosentan in healthy human subjects," *Clin Pharmacol Ther*, vol. 60, pp. 124–137, Aug 1996.

[58] B. Z. Leder, J. N. Tsai, A. V. Uihlein, S.-A. M. Burnett-Bowie, Y. Zhu, K. Foley, H. Lee, and R. M. Neer, "Two years of denosumab and teriparatide administration in postmenopausal women with osteoporosis (the data extension study): a randomized controlled trial.," *J Clin Endocrinol Metab*, vol. 99, pp. 1694–1700, May 2014.

[59] S. Boonen, F. Marin, B. Obermayer-Pietsch, M. E. Simões, C. Barker, E. V. Glass, P. Hadji, G. Lyritis, H. Oertel, T. Nickelsen, E. V. McCloskey, and EUROFORS Investigators, "Effects of previous antiresorptive therapy on the bone mineral density response to two years of teriparatide treatment in postmenopausal women with osteoporosis," *J Clin Endocrinol Metab*, vol. 93, pp. 852–60, Mar 2008.

[60] "Protocol a900129: A pilot methodology study to evaluate changes in bone quality parameters following therapy with recombinant human parathyroid hormone (pth; forteo)," tech. rep., clinicalstudyresults.org, 2009.

[61] E. S. Orwoll, W. H. Scheele, S. Paul, S. Adami, U. Syversen, A. Diez-Perez, J. M. Kaufman, A. D. Clancy, and G. A. Gaich, "The effect of teriparatide [human parathyroid hormone (1-34)] therapy on bone density in men with osteoporosis," *J Bone Miner Res*, vol. 18, pp. 9–17, Jan 2003.

[62] L. G. Ste-Marie, S. L. Schwartz, A. Hossain, D. Desaiah, and G. A. Gaich, "Effect of teriparatide [rhpth(1-34)] on bmd when given to postmenopausal women receiving hormone replacement therapy," *J Bone Miner Res*, vol. 21, pp. 283–91, Feb 2006.

[63] A. Miyauchi, T. Matsumoto, T. Sugimoto, M. Tsujimoto, M. R. Warner, and T. Nakamura, "Effects of teriparatide on bone mineral density and bone turnover markers in japanese subjects with osteoporosis at high risk of fracture in a 24-month clinical study: 12-month, randomized, placebo-controlled, double-blind and 12-month open-label phases," *Bone*, vol. 47, pp. 493–502, Sep 2010.

[64] F. Cosman, E. F. Eriksen, C. Recknor, P. D. Miller, N. Guañabens, C. Kasperk, P. Papanastasiou, A. Readie, H. Rao, J. A. Gasser, C. Bucci-Rechtweg, and S. Boonen, "Effects of intravenous zoledronic acid plus subcutaneous teriparatide [rhpth(1-34)] in postmenopausal osteoporosis," *J Bone Miner Res*, vol. 26, pp. 503–11, Mar 2011.

[65] C. Deal, M. Omizo, E. N. Schwartz, E. F. Eriksen, P. Cantor, J. Wang, E. V. Glass, S. L. Myers, and J. H. Krege, "Combination teriparatide and raloxifene therapy for postmenopausal osteoporosis: results from a 6-month double-blind placebo-controlled trial," *J Bone Miner Res*, vol. 20, pp. 1905–11, Nov 2005.

[66] J. S. Hwang, S. T. Tu, T. S. Yang, J. F. Chen, C. J. Wang, and K. S. Tsai, "Teriparatide vs. calcitonin in the treatment of asian postmenopausal women with established osteoporosis," *Osteoporos Int*, vol. 17, no. 3, pp. 373–8, 2006.

[67] K. G. Saag, J. R. Zanchetta, J.-P. Devogelaer, R. A. Adler, R. Eastell, K. See, J. H. Krege, K. Krohn, and M. R. Warner, "Effects of teriparatide versus alendronate for treating glucocorticoid-induced osteoporosis: thirty-six-month results of a randomized, double-blind, controlled trial," *Arthritis Rheum*, vol. 60, pp. 3346–55, Nov 2009.

[68] T. Fujita, T. Inoue, H. Morii, R. Morita, H. Norimatsu, H. Orimo, H. E. Takahashi, K. Yamamoto, and M. Fukunaga, "Effect of an intermittent weekly dose of human parathyroid hormone (1-34) on osteoporosis: a randomized double-masked prospective study using three dose levels," *Osteoporos Int*, vol. 9, no. 4, pp. 296–306, 1999.

[69] R. M. Neer, C. D. Arnaud, J. R. Zanchetta, R. Prince, G. A. Gaich, J. Y. Reginster, A. B. Hodsman, E. F. Eriksen, S. Ish-Shalom, H. K. Genant, O. Wang, and B. H. Mitlak, "Effect of parathyroid hormone (1-34) on fractures and bone mineral density in postmenopausal women with osteoporosis," *N Engl J Med*, vol. 344, pp. 1434–41, May 2001.

[70] "Nda 21-318 medical review part 2."

[71] A. Panico, G. A. Lupoli, F. Marciello, R. Lupoli, M. Cacciapuoti, A. Martinelli, L. Granieri, D. Iacono, and G. Lupoli, "Teriparatide vs. alendronate as a treatment for osteoporosis: changes in biochemical markers of bone turnover, bmd and quality of life," *Med Sci Monit*, vol. 17, pp. CR442–448, Aug 2011.

[72] J. N. Tsai, A. V. Uihlein, H. Lee, R. Kumbhani, E. Siwila-Sackman, E. A. McKay, S.-A. M. Burnett-Bowie, R. M. Neer, and B. Z. Leder, "Teriparatide and denosumab, alone or combined, in women with postmenopausal osteoporosis: the data study randomised trial," *The Lancet*, vol. 382, pp. 50–56, 7 2013.

[73] C. Muschitz, R. Kocijan, A. Fahrleitner-Pammer, I. Pavo, J. Haschka, W. Schima, S. Kapiotis, and H. Resch, "Overlapping and continued alendronate or raloxifene administration in patients on

teriparatide: effects on areal and volumetric bone mineral density–the confors study.," *J Bone Miner Res*, vol. 29, pp. 1777–1785, Aug 2014.

[74] T. Yamamoto, M. Tsujimoto, E. Hamaya, and H. Sowa, "Assessing the effect of baseline status of serum bone turnover markers and vitamin d levels on efficacy of teriparatide 20 mug/day administered subcutaneously in japanese patients with osteoporosis.," *J Bone Miner Metab*, vol. 31, pp. 199–205, Mar 2013.

[75] M. D. Walker, N. E. Cusano, J. J. Sliney, M. Romano, C. Zhang, D. J. McMahon, and J. P. Bilezikian, "Combination therapy with risedronate and teriparatide in male osteoporosis.," *Endocrine*, vol. 44, pp. 237–246, Aug 2013.

[76] M. J. D. Powell, "Developments of newuoa for minimization without derivatives," *IMA Journal of Numerical Analysis*, vol. 28, no. 649-664, 2008.

[77] J. A. Nelder and R. Mead, "A simplex method for function minimization," *The Computer Journal*, vol. 7, no. 4, pp. 308–313, 1965.

[78] C. J. P. Belisle, "Convergence theorems for a class of simulated annealing algorithms on rd," *J. Applied Probability*, pp. 885–895, 1992.

[79] R. H. Byrd, P. Lu, J. Nocedal, and C. Zhu, "A limited memory algorithm for bound constrained optimization," *SIAM Journal on Scientific Computing*, vol. 16, no. 5, pp. 1190–1208, 1995.

[80] R. Fletcher, *Practical Methods of Optimization.* John Wiley, Chichester, second edition ed., 1987.

[81] J. Nocedal and S. J. Wright, *Numerical Optimization.* Springer-Verlag, New York, 1999.

[82] Y.Ye, "Interior algorithms for linear, quadratic, and linearly constrained non linear programming," Master's thesis, Stanford University,Department of EES, Stanford CA, https://cran.r-project.org/web/packages/Rsolnp/Rsolnp.pdf.

[83] A. D. Martin, K. M. Quinn, and J. H. Park, "Mcmcpack: Markov chain monte carlo in r," *Journal of Statistical Software*, vol. 42, pp. 1–21, 6 2011.

[84] K. M. Mullen, D. Ardia, D. L. Gil, D. Windover, and J. Cline, "Deoptim: An r package for global optimization by differential evolution," *Journal of Statistical Software*, vol. 40, pp. 1–26, 4 2011.

[85] clinicaltrials.gov, "An open-label study to evaluate the effect of treatment with amg 785 or teriparatide in postmenopausal women (structure)," July 2015.

[86] K. Baron, ""mrgsolve", url: http://metrumrg.com/opensourcetools.html." October 2015.

[87] H. Kondo, J. Guo, and F. R. Bringhurst, "Cyclic adenosine monophosphate/protein kinase a mediates parathyroid hormone/parathyroid hormone-related protein receptor regulation of osteoclastogenesis and expression of rankl and osteoprotegerin mrnas by marrow stromal cells.," *J Bone Miner Res*, vol. 17, pp. 1667–1679, Sep 2002.

[88] O.-T. Chis, J. R. Banga, and E. Balsa-Canto, "Structural identifiability of systems biology models: a critical comparison of methods.," *PLoS One*, vol. 6, no. 11, p. e27755, 2011.

[89] S. Y. A. Cheung, O. Majid, J. W. T. Yates, and L. Aarons, "Structural identifiability analysis and reparameterisation (parameter reduction) of a cardiovascular feedback model.," *Eur J Pharm Sci*, vol. 46, pp. 259–271, Jul 2012.

[90] S. Y. A. Cheung, J. W. T. Yates, and L. Aarons, "The design and analysis of parallel experiments to produce structurally identifiable models.," *J Pharmacokinet Pharmacodyn*, vol. 40, pp. 93–100, Feb 2013.

[91] T. Sugiyama, T. Torio, T. Miyajima, Y. T. Kim, and H. Oda, "Romosozumab and blosozumab: alternative drugs of mechanical strain-related stimulus toward a cure for osteoporosis.," *Front Endocrinol (Lausanne)*, vol. 6, p. 54, 2015.

[92] M. S. Ominsky, C. Libanati, R. Boyce, P. J. Kostenuik, R. Baron, R. B. Wagman, and D. W. Dempster, "Continuous modelling-based bone formation could explain sustained increases in hip bone mineral density with denosumab treatment," in *Bone Abstracts*, vol. 3, p. 335, 2014.

[93] T. Sugiyama, Y. T. Kim, and H. Oda, "Osteoporosis therapy: a novel insight from natural homeostatic system in the skeleton.," *Osteoporos Int*, vol. 26, pp. 443–447, Feb 2015.

[94] R. Zebaze and E. Seeman, "Cortical bone: a challenging geography.," *J Bone Miner Res*, vol. 30, pp. 24–29, Jan 2015.

[95] A. J. Burghardt, G. J. Kazakia, M. Sode, A. E. de Papp, T. M. Link, and S. Majumdar, "A longitudinal hr-pqct study of alendronate treatment in postmenopausal women with low bone density: Relations among density, cortical and trabecular microarchitecture, biomechanics, and bone turnover," *Journal of Bone and Mineral Research*, vol. 25, no. 12, pp. 2558–2571, 2010.

[96] E. Seeman, P. D. Delmas, D. A. Hanley, D. Sellmeyer, A. M. Cheung, E. Shane, A. Kearns, T. Thomas, S. K. Boyd, S. Boutroy, C. Bogado, S. Majumdar, M. Fan, C. Libanati, and J. Zanchetta, "Microarchitectural deterioration of cortical and trabecular bone: differing effects of denosumab and alendronate," *Journal of Bone and Mineral Research*, vol. 25, no. 8, pp. 1886–1894, 2010.

[97] K. E. S. Poole, G. M. Treece, G. R. Ridgway, P. M. Mayhew, J. Borggrefe, and A. H. Gee, "Targeted regeneration of bone in the osteoporotic human femur," *PLoS ONE*, vol. 6, p. e16190, 01 2011.

[98] T. Sugimoto, T. Matsumoto, T. Hosoi, T. Miki, I. Gorai, H. Yoshikawa, Y. Tanaka, S. Tanaka, M. Fukunaga, T. Sone, T. Nakano, M. Ito, S. Matsui, T. Yoneda, H. Takami, K. Watanabe, T. Osakabe, N. Okubo, M. Shiraki, and T. Nakamura, "Three-year denosumab treatment in postmenopausal japanese women and men with osteoporosis: results from a 1-year open-label extension of the denosumab fracture intervention randomized placebo controlled trial (direct).," *Osteoporos Int*, vol. 26, pp. 765–774, Feb 2015.

[99] A. G. Costa, J. P. Bilezikian, and E. M. Lewiecki, "The potential use of antisclerostin therapy in chronic kidney disease - mineral and bone disorder.," *Curr Opin Nephrol Hypertens*, vol. 24, pp. 324–329, Jul 2015.

[100] A. Morse, M. M. McDonald, N. H. Kelly, K. M. Melville, A. Schindeler, I. Kramer, M. Kneissel, M. C. van der Meulen, and D. G. Little, "Mechanical load increases in bone formation via a sclerostin-independent pathway," *Journal of Bone and Mineral Research*, vol. 29, no. 11, pp. 2456–2467, 2014.

[101] B. Agoram, "Evaluating systems pharmacology models is different from evaluating standard pharmacokinetic-pharmacodynamic models.," *CPT: pharmacometrics & systems pharmacology*, vol. 3, no. February, p. e101, 2014.

[102] I. Kramer, C. Halleux, H. Keller, M. Pegurri, J. H. Gooi, P. B. Weber, J. Q. Feng, L. F. Bonewald, and M. Kneissel, "Osteocyte wnt/beta-catenin signaling is required for normal bone homeostasis.," *Mol Cell Biol*, vol. 30, pp. 3071–3085, Jun 2010.

[103] M. Honma, Y. Ikebuchi, Y. Kariya, and H. Suzuki, "Regulatory mechanisms of rankl presentation to osteoclast precursors.," *Curr Osteoporos Rep*, vol. 12, pp. 115–120, Mar 2014.

[104] T. Nakashima, M. Hayashi, T. Fukunaga, K. Kurata, M. Oh-Hora, J. Q. Feng, L. F. Bonewald, T. Kodama, A. Wutz, E. F. Wagner, J. M. Penninger, and H. Takayanagi, "Evidence for osteocyte regulation of bone homeostasis through rankl expression.," *Nat Med*, vol. 17, pp. 1231–1234, Oct 2011.

[105] Y. Cui, P. J. Niziolek, B. T. MacDonald, C. R. Zylstra, N. Alenina, D. R. Robinson, Z. Zhong, S. Matthes, C. M. Jacobsen, R. A. Conlon, R. Brommage, Q. Liu, F. Mseeh, D. R. Powell, Q. M. Yang, B. Zambrowicz, H. Gerrits, J. A. Gossen, X. He, M. Bader, B. O. Williams, M. L. Warman, and A. G. Robling, "Lrp5 functions in bone to regulate bone mass.," *Nat Med*, vol. 17, pp. 684–691, Jun 2011.

[106] M. Stolina, D. Dwyer, Q.-T. Niu, K. S. Villasenor, P. Kurimoto, M. Grisanti, C.-Y. Han, M. Liu, X. Li, M. S. Ominsky, H. Z. Ke, and P. J. Kostenuik, "Temporal changes in systemic and local expression of bone turnover markers during six months of sclerostin antibody administration to ovariectomized rats," *Bone*, vol. 67, pp. 305 – 313, 2014.

[107] D. Gatti, O. Viapiana, E. Fracassi, L. Idolazzi, C. Dartizio, M. R. Povino, S. Adami, and M. Rossini, "Sclerostin and dkk1 in postmenopausal osteoporosis treated with denosumab.," *J Bone Miner Res*, vol. 27, pp. 2259–2263, Nov 2012.

[108] L. Li, X. Chen, S. Lv, M. Dong, L. Zhang, J. Tu, J. Yang, L. Zhang, Y. Song, L. Xu, and J. Zou, "Influence of exercise on bone remodeling-related hormones and cytokines in ovariectomized rats: a model of postmenopausal osteoporosis.," *PLoS One*, vol. 9, no. 11, p. e112845, 2014.

[109] M. G. Mullender and R. Huiskes, "Osteocytes and bone lining cells: which are the best candidates for mechano-sensors in cancellous bone?," *Bone*, vol. 20, pp. 527–532, Jun 1997.